

REPORT DOCUMENTATION PAGE

Public reporting burden for this collection of information is estimated to average 1 hour per response, including the time for review of the data needed, and completing and reviewing this collection of information. Send comments regarding this burden estimate or a reducing this burden to Washington Headquarters Services, Directorate for Information Operations and Reports, 1215 Jefferson Davis Highway, Suite 1204, Arlington, VA 22202-4302, and to the Office of Management and Budget, Paperwork Reduction Project (0704-0188), Washington, DC 20503.

0457

1. AGENCY USE ONLY (Leave blank)		2. REPORT DATE June 2004		3. REPORT TYPE AND DATES COVERED Final Technical Report: June 2001 to June 2004	
4. TITLE AND SUBTITLE Study of the Coupling Between Twin Single Beveled Supersonic Jets using Linear and Non-Linear Spectral Analysis Techniques				5. FUNDING NUMBERS F49620-01-1-0450	
6. AUTHOR(S) G. Raman, D.R. Williams, P. Panickar, and K. Srinivasan					
7. PERFORMING ORGANIZATION NAME(S) AND ADDRESS(ES) Illinois Institute of Technology, Fluid Dynamics Research Center, Engineering 1 Building, MMAE Department, 10 W 32nd Street, Chicago, IL 60616				8. PERFORMING ORGANIZATION REPORT NUMBER	
9. SPONSORING / MONITORING AGENCY NAME(S) AND ADDRESS(ES) Air Force Office of Scientific Research 4015 Wilson Boulevard, Room 713 Arlington, VA 22203-1954 NA				10. SPONSORING / MONITORING 20040914 018	
11. SUPPLEMENTARY NOTES					
12a. DISTRIBUTION / AVAILABILITY STATEMENT Available for Public Release				12b. DISTRIBUTION CODE DISTRIBUTION STATEMENT A Approved for Public Release Distribution Unlimited	
13. ABSTRACT (Maximum 200 Words) Twin jets emanating from closely spaced nozzles can interact quite unpredictably and give rise to high dynamic pressures in the internozzle region which can result in sonic fatigue of sensitive aircraft equipment. This project studies the interaction between two such jets from nozzles having a single beveled exit geometry. Such nozzles are finding increasing use in modern aircraft due to the thrust vectoring and performance advantages they present. The study begins by using traditional linear spectral analysis techniques to study the coupling mechanism. It goes on to reveal the limitations of such linear techniques for understanding phenomena that are as complex as the one studied in this project and uses non-linear techniques to uncover results that have hitherto gone unreported. It is hoped that the results of these techniques will be of use to nozzle designers as well as to scientists involved in the field of numerical simulation of jet noise so as to provide benchmark data for the validation of their models					
14. SUBJECT TERMS Twin Jet Coupling, Screech, Non-Linear Spectral Analysis				15. NUMBER OF PAGES 93	
				16. PRICE CODE	
17. SECURITY CLASSIFICATION OF REPORT	18. SECURITY CLASSIFICATION OF THIS PAGE	19. SECURITY CLASSIFICATION OF ABSTRACT		20. LIMITATION OF ABSTRACT	

NSN 7540-01-280-5500

Standard Form 298 (Rev. 2-89)
Prescribed by ANSI Std. Z39-18
298-102

BEST AVAILABLE COPY

Study of the Coupling Between Twin Single Beveled Supersonic Jets using Linear and Non- Linear Spectral Analysis Techniques

Authors

**G. Raman, D. R. Williams, P. Panickar and K.
Srinivasan**

**Illinois Institute of Technology
Fluid Dynamics Research Center**

DISTRIBUTION STATEMENT A
Approved for Public Release
Distribution Unlimited

**AFOSR Final Report 2004
Contract # F49620-01-0450**

TABLE OF CONTENTS

	Page
LIST OF TABLES	ii
LIST OF FIGURE CAPTIONS	iii
EXECUTIVE SUMMARY	1
1. INTRODUCTION	2
1.1 Motivation	2
1.2 Review of Relevant Literature	3
1.3 Description of Experimental Facility	6
1.4 Uncertainty of Measurements	8
1.5 Objectives	8
2. STUDY OF COUPLING USING LINEAR SPECTRAL ANALYSIS	
TECHNIQUES	10
2.1 Twin Jet Coupling Modes	10
2.2 Coupling Behavior under Dynamically Varying Test Conditions	14
2.3 Near-Field Pressure Behavior	16
2.4 Phase Averaged Measurements	17
2.5 Applicability of Tam's Waveguide Approach	18
2.6 Directivity Studies	20
2.7 Broadband Shock Noise	22
3. STUDY OF COUPLING USING HIGHER-ORDER SPECTRAL	
ANALYSIS TECHNIQUES	24
3.1 Time-Series Analysis	24
3.2 Computation of Cross-Bicoherence	27
3.3 Results of Non-Linear Spectral Analysis	31
4. CONCLUSIONS	41
5. LIST OF THESES, PAPERS AND PUBLICATIONS FROM	
THIS PROGRAM	44
7. FIGURES	45
BIBLIOGRAPHY	81

List of Table Captions

Table 2-1. Table showing spanwise frequencies for the configurations shown in figures (3a) and (4a). Microphone positions as indicated in figures (3b) and (4b). For phase locked coupling we would expect the exact same frequency to be recorded by both the microphones which is not observed for the configuration in figure (3a), indicating the absence of phase locked coupling.

Table 3-1: Description of the dynamics revealed from time-localized phase plots.

Table 3-2: Details of the major non-linear interactions occurring in the Co-directed twin jet at $M_j = 1.3$, and $s/h = 7.3$

List of Figure Captions

Figure 1.1. Schematic diagrams showing single and twin jet configurations. (a). Single jet, (b). Twin Jet: V-shaped configuration, (c). Twin Jet: Arrowhead-shaped configuration.

Figure 1.2. Spark-schlieren photographs of a jet comparing shock containing jets from uniform and spanwise beveled nozzles (from Raman [25]). (a). Uniform exit (b). Single beveled exit. Note the spanwise oblique shock cell structure.

Figure 2.1. Twin jet in the arrowhead or A-shaped configuration and spanwise phase associated with it (a). A-shaped twin jet configuration of the two single beveled nozzles, along with the coordinate axis setup, and nozzle dimension nomenclature used during the experimental study (b). Spanwise phase angle between the two jets as measured by microphones 1 and 2. The microphone locations are on the spanwise center of the individual nozzle as shown by the black rectangular strips in the schematic. This configuration showed **no** coupling as is evident from the phase chart.

Figure 2.2. Twin jet in the V-shaped configuration and spanwise phase associated with it (a). Schematic of V-shaped configuration of the two single beveled nozzles (b). Spanwise phase angle between the two jets as measured by microphones 1 and 2. The microphone locations are on the spanwise center of the individual nozzle as shown by the black rectangular strips in the schematic.

Figure 2.3. Frequency characteristics of Single Beveled Nozzles at various fully expanded Mach Numbers. The data was taken using microphone 1 for jet 1 operating individually, microphone 3 for jet 2 operating individually and microphone 2 for the twin jet operation. (—■—) Jet 1, (—●—) Jet 2, (—▲—) twin jet configuration

Figure 2.4. SPL characteristics of Single Beveled Nozzles at various fully expanded Mach Numbers. Note the augmentation in dB levels for the twin jet case at lower M_j and

the suppression in the dB levels at medium and high M_j . The data was taken using microphone 1 for all the 3 cases. (—■—) Jet 1, (—●—) Jet 2, (—▲—) twin jet configuration

Figure 2.5. Spectra illustrating the coupling modes in V-shaped twin jets. (a). Antisymmetric coupling at a fully expanded jet Mach number $M_j=1.46$ (b). Symmetric coupling at a fully expanded jet Mach number $M_j = 1.33$. Note the difference in amplitude levels for the twin jet case as compared to the individual jets. (black —) Spectra for single jet. (white) Spectra for twin jet configuration

Figure 2.6. Continuous instantaneous spectra for nozzles acquired while the internozzle distance remained fixed at $s/h = 7.4$ and the pressure changed continuously. The two modes of coupling can be seen simultaneously at the intermediate pressures at non-harmonically related frequencies. (a). Two dimensional representation of spectra showing screech frequency variation with change in NPR. The plot shows constant SPL contours. (b). Three dimensional continuous instantaneous spectra. (c). Phase variation with change in the NPR. The color bar on the left shows the phase variation and the plot on the right shows contours of constant phase.

Figure 2.7. Continuous instantaneous spectra for nozzles acquired while the internozzle distance changed continuously and the exit jet Mach number remained fixed at 1.33. (a). Two dimensional representation of spectra showing screech frequency variation with change in the internozzle separation. (b). Three dimensional continuous instantaneous spectra. (c). Phase variation with change in the nozzle separation. The color bar on the left shows the phase variation and the plot on the right shows contours of constant phase.

Figure 2.8. Inter-nozzle rms sound pressure distribution. (a), (b) and (c) show the distribution of the rms pressure in the internozzle region for the various operating conditions. (—■—) coupled jets $M_j = 1.33$, (—●—) uncoupled jets $M_j = 1.33$, (---▲---) coupled jets $M_j = 1.46$, (---★---) uncoupled jets $M_j = 1.46$ (d), (e), (f) show the timeseries data at the operating conditions circled in the graph. The solid curves (—) are for the

coupled case at $M_j = 1.33$ and the dashed curves (---) are for the uncoupled case at $M_j = 1.33$, the coupled case at $M_j = 1.46$, and the uncoupled case at $M_j = 1.46$ respectively. Data taken keeping $y/h = 0$ and $z/h = 4$.

Figure 2.9. Phase averaged sound pressure values for the twin nozzles. The values are averaged on either side of the Y-axis keeping the X and Z coordinate fixed. (a). Operating condition $M_j = 1.33$. Note the symmetry about $y/h = 0$ indicating symmetric coupling. (b). Operating condition $M_j = 1.46$. Note the antisymmetry about $y/h = 0$ indicating antisymmetric coupling. Successive curves are offset by 70 Pa and a phase difference of 15° . Line codes repeat every 60° .

Figure 2.10. Screech frequency data compared to Tam's waveguide theory. (a). Screech frequency vs. fully expanded jet Mach Number for an aspect ratio 7 rectangular exit jet. (—) curve for lowest waveguide mode ($n = 1$), (\blacktriangle) single rectangular jet, (\blacksquare) twin rectangular jets (b). Screech frequency vs. fully expanded jet Mach number for the single beveled jets used in this study. Curves show waveguide modes (—) $n = 1$, (---) $n = 2$, (---) $n = 3$, (---) $n = 4$. (\blacktriangle) single jet (\blacksquare) twin jet (\bullet) symmetrically coupled, (\blacksquare) twin jets (\blacksquare) antisymmetrically coupled.

Figure 2.11. Comparison between twin jet spectra for various angles at an arc radius of $r/h = 22.5$ in the vertical plane (XZ plane depicted in Figure 3(a)) for the arrowhead and the V-shaped configurations at $M_j = 1.33$ at $s/h = 7.4$ (a) 50° (b) 70° (c) 90° (d) 110° (e) 130° (f) 150° . Solid curves (—) are for the 'V'-shaped configuration and the dashed curves (---) are for the Arrowhead configuration.

Figure 2.12. Comparison between twin jet spectra for various angles at an arc radius of $r/h = 22.5$ in the vertical plane (XZ plane depicted in Figure 3(a)) for the arrowhead and the V-shaped configurations at $M_j = 1.46$ at $s/h = 7.4$ (a) 50° (b) 70° (c) 90° (d) 110° (e) 130° (f) 150° . Solid curves (—) are for the 'V'-shaped configuration and dashed curves (---) are for the Arrowhead configuration.

Figure 2.13. Broadband shock noise characteristics of single and twin jets at $M_j = 1.46$, $s/h = 7.4$, and arc radius of $r/h = 22.5$. (\blacktriangle) Single jet, (\bullet) twin jets in the V-shaped configuration, and (\blacksquare) twin jets in the arrowhead configuration. θ is the angle measured with respect to the jet exit axis on the XZ plane depicted in Figure 3(a).

Figure 3.1. Contour map showing the coupling zones in the parametric space comprising Mach number and inter-nozzle spacing based on the phase difference at the screech tone. Legend shows phase angles.

Figure 3.2. Schematic of phase plot generation.

Figure 3.3. Phase plots between the two microphone signals at various Mach numbers, for the co-directed twin jet at $s/h = 7.3$. Mach numbers are shown in each plot.

Figure 3.4. Cross power spectra, X-Y phase plots, and X-X phase plots, and Y-Y phase plots of microphone signals at Mach No. 1.38 for the co-directed twin jet configuration at $s/h = 7.3$. The time interval of the data is shown on top of the cross-spectrum.

Figure 3.5. Cross power spectra, X-Y phase plots, and X-X phase plots, and Y-Y phase plots of microphone signals at Mach No. 1.4 for the co-directed twin jet configuration at $s/h = 7.3$. The time interval of the data is shown on top of the cross-spectrum.

Figure 3.6. (a) Power Spectra of the test signals. (b) Cross-Bicoherence plot.

Figure 3.7. Sensitivity of cross-bicoherence to phase standard deviation between modulated test sinusoids.

Figure 3.8. Comparison of sensitivity of second order and third order statistics to the relative magnitude of non-linear component: (a,e: 50%), (b,f: 10%), (c,g: 1%), (d,h: 0.5%).

Figure 3.9. Cross-bicoherence and spectra of twin jets at $M_j = 1.33$, $s/h = 7.3$ for co-directed and contra-directed configurations. (a) Cross-bicoherence spectrum for co-directed, (b) Power spectrum for co-directed, (c) Cross-bicoherence spectrum for contra-directed, (d) Power spectrum for contra-directed.

Figure 3.10. Comparison of cross-bicoherence spectra and power spectra of co-directed twin jets and single jet. $M_j = 1.35$, Twin jet spacing: $s/h = 7.3$

Figure 3.11. Cross-bicoherence and linear spectra of co-directed twin jets at $s/h = 7.3$, at various Mach numbers. Mach numbers; (a, b: 1.3), (c, d: 1.33), (e, f: 1.40), and (g, h: 1.46).

Figure 3.12. Depiction of the clustering phenomenon. Frequencies within parentheses denote resultant frequencies, and those without parentheses denote participating frequencies. The dotted ellipses are shown to indicate clusters.

Figure 3.13. Close-up view of a cluster illustrating the sequence of interactions building it.

Figure 3.14. : Details of the evolution of non-linear interactions shown in Figure 14(b). Left hand side of the illustration shows sum interactions while the right side shows difference interactions. The modes resulting from the interactions are shown inside the circles, and the cross-bicoherence values are mentioned below them.

Figure 3.15. Cross-bicoherence and spectra of co-directed twin jets at $M_j = 1.32$, for various internozzle spacings. (a,b): $s/h = 7.3$, (c,d): $s/h = 7.5$, (e,f): $s/h = 7.7$, (g,h): $s/h = 7.9$

Figure 3.16. Cross-bicoherence spectrum of co-directed twin jets at $M_j = 1.32$, at internozzle spacing $s/h = 11.2$. Except those marked, all other interactions had a coherency of 0.3 or less.

Figure 3.17. Cross-bicoherence and spectra of co-directed twin jets at $M_j = 1.46$, for various internozzle spacings. (a,b): $s/h = 7.3$, (c,d): $s/h = 7.5$, (e,f): $s/h = 7.7$, (g,h): $s/h = 7.9$

Figure 3.18. Close-up views of rectilinearly aligned interactions. The dotted line in (a) denotes the most active participating frequency, and the dotted line in (b) denotes the most desired resultant frequency.

Figure 3.19. Interaction density variation with Mach number. (a) Threshold 0.3. (b) Threshold 0.4.

Figure 3.20. Variation of average interaction density with Mach number and internozzle spacing. (a,c) Cross-bicoherence Threshold 0.3, (b,d) Threshold 0.4.

Executive Summary

This report describes experiments that study the nature of the interaction between jets emanating from twin two-dimensional nozzles having single beveled exit geometry. Nozzles with spanwise oblique exits are increasingly being considered for modern aircraft. Although several studies have examined aspects of twin jet coupling, very little data is available on the coupling of jets from nozzles of complex geometry. Several spanwise modes can exist in such jets, and when two such jets are brought together they can interact quite unpredictably. The present study focuses on twin convergent nozzles with an aspect ratio of 6.6 with spanwise oblique exits operated over a fully expanded Mach number range from 1.3 to 1.6.

The first part of this study focused on understanding the nature of the interaction modes produced by the twin jets, in addition to understanding various other acoustic features using linear spectral analysis. A detailed description of this effort can be obtained in the Masters' Thesis work of Panickar [1] and in the forthcoming article in the Journal of Sound and Vibration by Panickar, Srinivasan and Raman [2]. The main conclusions drawn from this part of the study were: (a) Coupling of twin nozzles with a beveled exit was observed only when the beveled edges faced each other and the nozzles formed a 'V' shape in the inter-nozzle region (also referred to as the co-directed configuration). Specifically, if the two beveled edges were oriented away from each other to form an arrowhead ('A') shape (also referred to as the contra-directed configuration) no coupling was observed. (b) Despite the presence of spanwise antisymmetric, spanwise symmetric and spanwise oblique modes for the single nozzles, only the first two modes were evident in the coupling. (c) Dynamic tests conducted by moving the nozzles apart while they were operating or by continuously changing the stagnation pressure at fixed inter-nozzle spacing revealed that coupling modes could co-exist at non-harmonically related frequencies. (d) The frequency of both coupling modes agrees with the higher order waveguide modes based on Tam's theory. (e) Directivity of the tonal noise component varied according to the coupling mode for the coupled twin jet configuration ('V' shaped/co-directed) and the broadband shock noise level for the uncoupled twin jet configuration (arrowhead/contra-directed) was more than that of either the coupled twin jet configuration ('V' shaped) or the single jet.

Recognizing that jets emanating from nozzles having complex exit geometries, such as the ones used in the present study, are rich in closely spaced complex noise sources, the second part of this study used higher order spectral analysis techniques to understand the non-linear interactions occurring during the coupling process. The details of the experiments and analyses can be obtained from the AIAA conference papers by Srinivasan et. al. [3] and Panickar, Srinivasan and Raman [4]. The main conclusions from these studies can be summarized as follows: (i) some configurations that were apparently uncoupled by linear spectral analysis metrics were found to be non-linearly coupled. (ii) two types of non-linear coupling were observed – one dominated by the fundamental and its interaction with higher modes, and another that displayed clusters of interactions between a frequency component and its sidebands. (iii) a new interaction density metric was developed to quantify non-linear coupling. (iv) a second metric known as the average interaction density was shown to increase sharply during coupling mode transition.

The personnel involved in this research undertaken are:

Principal Investigator:	Dr. G. Raman
Co-Principal Investigator:	Dr. D. R. Williams
Graduate Students:	P. Panickar, R. Joshi
Visiting Research Scholar:	Dr. K. Srinivasan

1. INTRODUCTION

1.1. Motivation

Most supersonic jet aircraft exhaust systems are imperfectly expanded in flight which places an emphasis on the components of shock noise. Shock noise has two main components – the broadband component and a discrete tone. This discrete tone component is called screech. Screech, discovered by Powell [5], is caused by a feedback loop that involves the interaction of the hydrodynamic disturbances with the shock. This interaction leads to the production of pressure waves that feedback to the nozzle exit and couple with nascent hydrodynamic disturbances, thus completing the feedback loop. Raman [6] recently summarized half a century of research on screech. The presence of screech components in underexpanded jets can cause nozzle or tail plane damage.

In aircraft with twin closely spaced nozzles, the jet plumes can couple and lead to even higher dynamic pressures in the inter-nozzle region. These pressures may cause significant structural damage to the nozzle material and may also cause fatigue failure of the material. In some cases the high dynamic pressures may also cause damage to the advanced materials used on aircraft bodies (like aircraft skin). Twin nozzles of complex geometry – particularly double beveled in the case of the new F-22s – have found special use in modern aircraft because of their variable area and aspect ratio, and thrust vectoring capabilities. The proper functioning of such beveled nozzles under adverse conditions is of concern.

The first part of this project concentrated on the study of the interaction between the jets from twin nozzles of spanwise oblique geometry using linear spectral analysis techniques. The dimensions of individual nozzles were 33.58 mm in the spanwise direction and 5.08 mm in the transverse direction. Thus, the aspect ratio of the individual jets was around 6.6. A bevel angle of 30^0 was chosen due to a wealth of information in the literature on single nozzles at this angle. The schematic diagrams of the configurations studied in this paper are shown in Figure 1.1. Underexpanded single beveled nozzles can produce screech noise in spanwise oblique modes. It is presumed

that the spanwise oblique modes of screech noise are caused by the spanwise oblique shock cells, revealed in the schlieren images taken from Raman [25] and reproduced in figure 1.2.

Acoustic fields have traditionally been characterized using linear spectral analyses of single and two point measurements. These methods could provide adequate information to describe acoustic fields comprising a simple acoustic source, or, multiple sources where the spatial separation of acoustic sources is much larger than the characteristic acoustic wavelength. In the case of shock-containing jets, there could be multiple acoustic sources of comparable strengths spatially separated within a few acoustic wavelengths. There is evidence in the literature for jets with multiple screech tones, with their corresponding feedback loops. When such complexities are possible in a single jet plume, further complexity is inevitable when the shock-cells are spanwise oblique and when another such plume is located in close vicinity. For this reason, the second part of the present study focuses on the higher order (nonlinear) acoustic interactions in such jets with complex shock structures.

1.2. Review of Relevant Literature

Most of the published works on twin jets have focused on jets having circular exit geometry. Berndt [7] performed a series of wind tunnel experiments to measure the dynamic pressure fluctuations on the nozzle surfaces of a twin-jet nacelle and was able to conclude that the pattern of the highest dynamic pressures measured in the wind tunnel matched the pattern of the hardware damage that occurred during the flight test program. Seiner, Manning and Ponton [8] experimentally showed that for closely spaced supersonic jets operating at off design conditions, the dynamic pressures upstream of the jet exits can reach levels that could result in structural damage. Tam and Seiner [9] observed that the twin jet screech frequency was greater than the frequency of two jets that did not interact with each other. Morris [10] showed how an instability wave analysis can provide some insight into the interaction of twin supersonic circular jets. His analysis showed how the growth rates of instability waves or large structures in the

initial mixing region of the twin jets are affected by the jet separation. Wlezien [11] showed that the noise produced by the mutual interaction of two supersonic plumes is a strong function of nozzle spacing and the fully expanded jet Mach number. Shaw [12] examined methods to evaluate the effectiveness of several concepts in suppressing the twin-jet screech i.e. tabs, lateral spacing, axial spacing and secondary jets.

Compared to circular jets, there is a very limited amount of data available on jets with rectangular exit geometry. Moreover, of late, the focus has shifted to scarfed [13], asymmetric [14], beveled [15-17], and trailing edge modified [18, 19] nozzles. Raman and Taghavi [20] also studied the flow and acoustic features of multiple supersonic uniform exit rectangular jets with phase locked screech. Later, Raman and Taghavi [21] conducted a detailed study of the near acoustic field and the coupling mechanism of twin rectangular supersonic jets having uniform exit geometry. They found that there were two modes of coupling that prevailed - the symmetric mode that augmented the screech amplitude and the antisymmetric mode that suppressed it and both these modes were mutually exclusive. A companion study by Taghavi and Raman [22] on twin jets having straight rectangular exit geometry in various configurations found that the shock spacing did not change significantly when the jets coupled.

The coupling of twin supersonic jets of double beveled exit geometry was studied by Raman [23], and it was found that twin double beveled jets can couple and may lead to either an augmentation or suppression of sound in the inter-nozzle region depending on the fully expanded Mach number at which the jets were operating. Although previous work has illuminated some aspects of individual single beveled nozzles [24, 25], to the best of our knowledge there is no published information on the interaction of twin supersonic jets having single beveled exit geometry. In addition, the effect of varying nozzle separation while the nozzles were operating appears never to have been considered before. Note that the rectangular shock containing jets exhibit both spanwise and transverse oscillation modes. For high aspect ratio ($b/h > 5$) nozzles, the transverse oscillation mode is predominantly antisymmetric. However in the spanwise direction

symmetric, antisymmetric and oblique oscillation modes are possible. Greater detail regarding spanwise modes is provided in Chapter 2, § 2.1.

The use of higher-order spectral tools in the understanding of free shear flows has advanced the state of the art knowledge in the subject. The need for these tools emerged from the challenge posed by the extensive non-linearity in the axial evolution of shear layers. Since higher order spectral methods shed light on the non-linearity in the system, they are also referred to as non-linear spectral methods. Elementary non-linear spectral methods use triple correlations. The auto-bicoherence and the cross-bicoherence are the non-linear analogues of the auto-spectrum and cross-spectrum functions in the conventional linear spectral analyses. Some earlier work on the use of these techniques in free shear flows is presented below to serve as an example to justify the use of these techniques in the present work. Since the earlier research do not directly relate with the current work, and since only the tools used are common, we discuss earlier work without delving deep into the specific topics, simply touching upon the commonalities, with a main focus on the capabilities of the non-linear tools used therein.

Thomas and Chu [26] studied the evolution of a planar shear layer using auto- and cross-bicoherence to trace the dynamics of axial evolution of the planar shear layer. They used two hot-wire probes separated by a distance to obtain the time series for the non-linear analysis. The probe pair was placed at several axial locations and both the linear and the non-linear spectra were obtained and analyzed. These studies revealed several results concerning the use of the technique as well as the dynamics of the shear layer. They

- (i). concluded that the cross-bispectrum was more useful than the auto-bispectrum in localizing the non-linear processes,
- (ii). obtained the spectral evolution in the axial direction by identifying the relative magnitudes of various non-linear interactions,

- (iii). found that the shear layer showed a preference for difference interactions than sum interactions.

Thomas and Chu [27, 28] extended their work to unravel other interesting dynamics of the shear layer. Using higher order cumulants, they were able to quantify the dominance of non-linearity over linearity by obtaining the linear and non-linear coupling coefficients. These studies revealed the role of resonance involving subharmonics on the shear layer development.

All the studies discussed above pertained to low speed flows. To the best of our knowledge, higher order spectral analysis was first used in the study of high speed flows by Walker and Thomas [29] who conducted experiments on screeching rectangular jets. They demonstrated that while linear techniques such as spectra, SPL contours, and phase coherence provide valuable information about the gross features of a screeching jet, the inherent non-linearity can be explained only by non-linear spectral methods. They used non-linear spectra to quantify the quadratic interactions. Their results obtained from a hydrodynamic analysis were consistent with their acoustic studies, emphasizing the direct correspondence between the two. They were able to deduce the interactions between the various modes, using non-linear spectra, and trace the axial evolution of each mode. Although the present work involves screeching jets, the focus is different. We focus on twin jet coupling, and further the shock-cells are spanwise non-uniform. Therefore, rather than individual jet modes, we are interested in twin jet coupling modes.

1.3. Description of Experimental Facility

The experiments were carried out in the high speed jet facility at the Fluid Dynamics Research Center, Illinois Institute of Technology, Chicago. A detailed description of this facility is given in the Masters' thesis work of Panickar [1]. However, for the purpose of this report a brief description is warranted. This facility receives compressed air at a maximum initial pressure of approximately 1.54 MPa from storage tanks that have a total volume of approximately 198 m³. The compressor bank is made of four compressors and

serves not only to charge the storage tanks before a run, but also to extend the life of each run by supplementing their flow incrementally as the pressure falls during blow down. The settling chamber has walls covered with acoustic foam in order to reduce flow borne acoustic disturbances. Furthermore, honeycomb sections and screens provide additional flow conditioning. The compressed air system can provide a maximum momentary exit pressure ratio of 15.3 resulting in a fully expanded Mach number of 2.4 and a Reynolds number based on exit diameter of 5.4×10^6 based on an exit diameter of 25.4 mm. The jet exhausts into an anechoic chamber, equipped with multiple access panels including a set of optical windows. The jet nozzles are connected to the stagnation chamber by means of reinforced flexible tubing to facilitate positioning of the nozzles, dynamic tests, as well as to enable a quick transition between different configurations. The nozzles are mounted on a uni-axial traverse, with the lead screw having opposite threads for each nozzle. Thus, the motorized traverse can move the nozzles towards, or away from each other. The nozzle axes are kept parallel to each other for all the experiments described in this study. While this does not necessarily depict actual aircraft operating conditions, it provides a baseline where the coupling studies could begin. Further results with different axial orientations will be discussed in a forthcoming paper. The spanwise width of each nozzle was 33.58 mm and the transverse dimension was 5.08 mm, which meant that the nozzles used had an aspect ratio of 6.6. Zilz and Wlezien [32] showed that for low aspect ratio jets it was possible to have oscillation modes in the spanwise as well as the transverse directions. For large aspect ratio jets, such as the ones used in this study, the transverse oscillation modes are predominantly antisymmetric and the spanwise modes can vary. The lip thickness of the nozzles was 2.0 mm which meant that at the closest location the internozzle separation parameter $s/h = 7.4$. The nozzles were tested in the fully expanded jet Mach number range from 1.28 to 1.72. The Mach number range studied is narrow since the jets did not screech in the twin jet configuration beyond this range.

All acoustic measurements were made using 6.35 mm diameter B & K microphones. The microphones were calibrated using a B & K pistonphone calibrator. The sound pressure levels reported are in dB relative to 20 μ Pa. All the data acquisition was achieved using a PC based National Instruments data acquisition board capable of acquiring 1.6

Megasamples/second, using LabVIEW 6. Spectra were obtained by sampling at 200 kHz, dividing the time series into 50 records and taking FFT blocks of 4096 data points each. Phase data was processed using the Matlab software.

1.4. Uncertainty of Measurements

The uncertainty in the SPL measurements could be attributed to three sources, namely, the uncertainty in the fluctuating pressure data acquired by the microphone, the uncertainty due to number of records averaged for obtaining the FFT, and the uncertainty in the stagnation pressure measurements. Of all these three sources the uncertainty in the stagnation pressure measurements by the pressure transducer played the most dominant role. The uncertainty in the SPL measurements is calculated to be 1%, including repeatability factors. The error in the frequency measurements was within 2%. The fully expanded Mach number for each of the data points was obtained by considering an isentropic expansion of the jet to atmospheric conditions. Hence the uncertainty in the fully expanded Mach number value is calculated to be 0.016%. Error bars are shown on key figures. The dynamic tests performed also showed good repeatability.

1.5. Objectives

As mentioned earlier, the study was divided into two stages. The first stage concentrated on quantifying the interaction between twin jets using linear spectral analyses techniques. The specific objectives for this stage of the study were: -

- To examine the spanwise behavior of single-beveled rectangular jets in single jet and twin jet configurations ('A' and 'V' as shown in Figure 1.1) and to identify the screech modes (symmetric or antisymmetric) produced by twin jets from spanwise oblique nozzles using detailed steady and unsteady measurements in the near field.
- To study the behavior of twin jets under dynamically varying conditions, namely inter-nozzle spacing and stagnation pressure, using continuous instantaneous spectra.

- To report the various manifestations of coupling, revealed by phase averaged measurements, and acoustic pressure distribution in the inter-nozzle region. Phase averaged measurements provide an insight into the dynamic pressure loads, which is more relevant to the problem at hand rather than the mean sound pressure levels.
- To examine the applicability of Tam's waveguide theory to single and twin coupled jets from beveled geometries.
- To survey the directivity of sound pressure along the central vertical plane of the two twin jet configurations (namely, the V-shaped configuration and the arrowhead shaped (A) configuration).
- To study the differences in broadband noise emission between the two twin jet configurations.

The second stage utilized higher order spectral analyses techniques to study the nonlinear interactions occurring between the jets. Later, the authors attempt to quantify the nonlinear interactions occurring in these jets, and explore the possibility of tracing the evolution of power spectra, and explain the behavior of these complex flow systems, hitherto unknown.

2. STUDY OF COUPLING USING LINEAR SPECTRAL ANALYSIS

TECHNIQUES

In order to accomplish the objectives mentioned in the previous chapter, the authors chose three basic configurations: (i) twin jets directed towards each other (co-directed), (ii) twin jets directed away from each other (contra-directed), and (iii) single jet. The fully expanded Mach number range covered in the study was $1.28 \leq M_j \leq 1.72$ beyond which the jets did not screech. The inter-nozzle spacing was varied in the co-directed twin jet configuration in the range $7.3 \leq s/h \leq 7.9$, where s and h are nozzle center spacing and height as indicated in figure 3. The inter-nozzle spacing was not varied in the contra-directed configuration since it did not show coupling. The two microphones were placed at the respective spanwise centers of the nozzles, so as to reveal the spanwise coupling behavior. Thus, the distance between the two microphone locations was the same as the inter-nozzle distance. This microphone separation is of the order of a screech wavelength. Since our objective is to obtain the spanwise differences between the two individual jets, the pair of spanwise centers seemed to be a logical choice for locating the microphones.

2.1. Twin jet coupling modes

Before beginning to examine the data to obtain the spanwise modes, a brief definition of the spanwise modes that could be expected is presented in the following list:

1. Phase locked operation of the twin jets with the spanwise phase angle approximately 0° corresponds to a spanwise symmetric mode.
2. Phase locked operation of the twin jets with the spanwise phase angle approximately 180° corresponds to a spanwise antisymmetric mode.
3. Phase locked operation of the twin jets with the spanwise phase angle between 0° and 180° corresponds to a spanwise oblique mode.

4. Non phase locked operation (which in this case means that the frequencies recorded by the individual microphones are different).

The jet modes were examined by mounting microphones at the two spanwise extreme ends of the nozzle in the case of single jet, and at the respective nozzle centers in the case of twin jets, and in both cases, slightly upstream of the nozzle lip. This location of the microphone was chosen to capture the phase characteristics of the screech. This was done in order to investigate the characteristics of the outer cycle of the screech loop. However, previous work that recorded phase conditioned schlieren and microphone data simultaneously (Raman and Taghavi [21]), showed a clear correspondence between the phase measurements made by the microphone and the motions within the jet plume. The single beveled jets used in this study screeched in the audible range when operated individually. The parameters used in the present investigation are Mach number, and the inter-nozzle (center-to-center) spacing, ' s ' non-dimensionalized using the shorter nozzle dimension ' h ' (see figure 2.1). In the case of twin jets, at least two geometric configurations are possible, one in which the bevel planes of the individual nozzles faced each other, which is being referred to as "*V-shaped*" or co-directed configuration (figure 1.1(b)), and another in which the bevel planes do not face each other, which is referred as "*Arrowhead-shaped*" ('A') or contra-directed configuration (figure 1.1(c)). For the present study, we define coupling as follows: When two individual jets having slightly different frequencies are placed next to each other they are said to couple if their interaction produces a single frequency accompanied by the phase locking of the screech instabilities of the two jets.

Figure 2.1 shows the schematic arrangement for the arrowhead-shaped ('A') configuration (figure 2.1(a)), and a plot of the relative phase difference between the spanwise microphones (figure 2.1(b)). The inter-nozzle spacing for this plot was $s/h = 7.4$. As can be seen from figure 2.1(b), a wide variation in the phase difference exists between the two jets, across the entire Mach number range covered in the present study. This indicates the absence of phase locked coupling between the individual jets,

establishing that the single beveled nozzles do not couple in the arrowhead-shaped ('A') configuration.

In contrast, the V-shaped configuration (figure 2.2(a)) exhibits coupling behavior as shown in figure 2.2(b). In this plot, the inter-nozzle spacing was $s/h = 7.4$. It is clear from figure 2.2(b) that the coupling is symmetric (phase difference ≈ 0) at the lower Mach numbers and antisymmetric (phase difference $\approx 180^\circ$) at the mid-range and higher Mach numbers covered in this study. It was observed that there was an abrupt change of phase from 0° to 180° at a fully expanded Mach number of 1.4. After this point the phase remains antisymmetric throughout the entire Mach number range. The result here is in sharp contrast to that found by Raman and Taghavi [21] who found that for twin rectangular jets with uniform exits the jets coupled in the antisymmetric mode at low Mach numbers and in the symmetric mode at higher Mach numbers. The frequencies recorded by the individual microphones for both the twin jet configurations are given in Table 2-1. This table shows that the jets are frequency locked in the V-shaped configuration, whereas the screech frequencies are distinctly different for the arrowhead-shaped configuration.

The above observations raise the question of why one configuration couples and the other does not. It is interesting to note that Raman [23] studied double beveled jets in single and twin configurations and found that these jets exhibit both, spanwise symmetric and spanwise antisymmetric, modes even when operated individually. The arrowhead-shaped configuration is similar to an individual double beveled jet with a splitter plate inserted along the flow direction along the spanwise center. It may be reasoned that the V-shaped configuration offers a larger interaction region than in the case of the arrowhead-shaped configuration. In the V-shaped configuration, all points on a nozzle exit are in line-of sight with the corresponding point on its neighboring nozzle, whereas, this is not true for the arrowhead configuration, where only the points on the downstream edge of the nozzles see each other. Although there is no information in the literature connecting spanwise flow communication with coupling it appears that a larger interaction region encourages jet coupling. The mechanism behind this phenomenon warrants a deeper

study of the physics of the flow and is, as yet, an unresolved issue and beyond the scope of this study. In addition some clues are provided by the work of Rice and Raman [16] who showed that for convergent single beveled nozzles with a 30° bevel the flow field of the jet was deflected on account of the spanwise pressure relief. Thus in the V-shaped configuration the jets would be deflected towards each other whereas in the A-shaped configuration they would be deflected away from each other resulting in a reduced propensity to couple. The fact that the arrowhead-shaped configuration showed no spanwise symmetric or antisymmetric modes may prove to be useful in the design of nozzles having oblique geometries to be used in single or twin configuration. Note that all discussions pertaining to coupling are made only with reference to the V-shaped configuration that coupled.

The characteristics of each individual nozzle were also studied separately. The single beveled nozzle was tested and the phase difference across the spanwise direction was measured and it was found that the spanwise phase for the individual single beveled nozzle could be antisymmetric, symmetric or oblique. Both single beveled nozzles exhibited a spanwise antisymmetric mode at the lower Mach numbers from 1.28 to 1.38 and a spanwise oblique mode at the higher Mach numbers 1.48 to 1.58. One of the jets also exhibited a spanwise symmetric mode at the midrange Mach numbers from 1.4 to 1.46 and in this Mach number range the other jet exhibited spanwise oblique modes. In other words, the individual jets screech in well defined spanwise modes and these modes (and the corresponding feedback loops) are completely altered by the coupling, for the V-shaped configuration. The rest of this chapter will focus on this configuration with the exception of a comparison of directivities and broadband shock noise towards the end.

Figure 2.3 shows the tonal frequency characteristics of the single jets when operated separately, and the twin jets in V-shaped configuration, as a function of the fully expanded Mach number. This chart shows that the V-shaped configuration produced screech tones that have a frequency that can be up to about 7% different from the screech tones of either individual jet. An interesting observation is that the frequencies during symmetric mode coupling ($M < 1.4$) are higher than the frequency of either individual jet.

In contrast the frequencies during antisymmetric mode coupling are in between (and very close) to that of either jet. Raman and Taghavi [21] showed that such frequency changes during mode jumps are caused by source shifts of the equivalent screech source.

Figure 2.4 shows the SPL characteristics of single and V-shaped twin jet configurations as a function of the fully expanded jet Mach number. This plot shows the effect of coupling as follows: At the lower Mach numbers, the sound amplitudes for the twin jet are more than 6 dB higher than those of the single jets that would be expected due to source doubling. An abrupt switch from the symmetric to the antisymmetric coupling occurs at a Mach number of around 1.4, consistent with the phase plot shown in figure 2.2(b). Beyond this Mach number (around 1.4), the twin jet coupling remained antisymmetric for the entire range. Figure 2.5 shows a comparative plot of the spectra for the single jet and V-shaped twin jet configuration, for the antisymmetric ($M_j = 1.46$, $s/h = 7.4$), and symmetric ($M_j = 1.33$, $s/h = 7.4$) coupling modes. It is clear from these spectra that coupling renders the peaks sharp, with appreciable amount of power in the fundamental frequency and its harmonics. Non-harmonically related stray peaks observable in single jet spectra get suppressed in the coupling process. For example, many such non-harmonically related peaks can be seen in the spectra of single jets in figures 2.5(a) and 2.5(b). These peaks are not observable under coupled conditions.

2.2. Coupling behavior under dynamically varying test conditions

Following static tests, twin jet coupling behavior under dynamically varying test conditions was investigated. Such tests may be relevant to processes occurring during actual flight. However, no attempt is made in the present study to establish a direct correspondence with actual flight operations. The test facilities allowed two parameters to be varied dynamically while the jets operated. They were: (i) the stagnation pressure, and hence the jet Mach number, and (ii) the inter-nozzle spacing between the two nozzles. While the former variation was achieved by facility blowdown; thus allowing the

stagnation pressure to drop continuously, the latter was possible due to the traversing system used to mount the nozzles, as described in § 1.3.

The blow-down test was performed at a spacing $s/h = 7.4$. While the stagnation pressure dropped, the microphone signals were recorded. The microphones were mounted at the spanwise center of each nozzle. From these signals, spectra and relative phase difference were calculated. Figure 2.6 shows spectra for varying Mach number. Figure 2.6(a) shows a top view of the three dimensional spectra shown in Figure 2.6(b). While there is a single screech tone at the highest and lowest pressures, intermediate Mach numbers show two dominant non-harmonically related frequencies. The spanwise phase difference between the two microphones at various frequencies and Mach numbers was plotted from which the symmetric and antisymmetric coupling regions were extracted. These iso-phase regions are shown in figure 2.6(c). The frequencies in the phase plot correspond exactly to the tonal frequencies seen in the continuous spectra. This shows the coexistence of symmetric and antisymmetric coupling modes in the V-shaped twin jet under dynamically varying pressure conditions.

Continuous spectra were also taken while moving the nozzles apart at a constant rate of 3 mm/s (keeping the pressure constant) in order to check if the jets remained coupled or decoupled. The spectra obtained are shown in figures 2.7(a) and 2.7(b). The corresponding phase chart is shown in figure 2.7(c). As can be seen from these two figures, the jets remain coupled in a symmetric mode till around $s/h = 9.7$ after which they start decoupling until eventually no phase locked coupling remains at all. This goes on to show the strength of the symmetric coupling in the sense that it leads to production of composite shock cells of tremendous strength that remain structurally coupled with each other, stretching as the internozzle separation increases, before finally breaking. Although a strong interaction may be present beyond $s/h = 9.7$, frequency matching between the two jets was no longer observed which contradicts our definition of phase-locked coupling. Note that the time scale at which the nozzles moved apart differed from the time scale of the instabilities in the flow by a factor of 20000. Clearly, it is not

possible to move the nozzles apart at the time scale of instabilities in the flow. Our objective was to acquire data in the time scale commonly used to deploy nozzle flaps and/or conduct vectoring or aspect ratio change operations on aircraft.

2.3. Near-field pressure behavior

Since unsteady dynamic pressures could be severe during coupling, it seemed relevant to examine the acoustic pressure distribution in the inter-nozzle region. These near-field measurements are important to quantify the acoustic loads perceivable by the nozzle structures. The sound pressure was measured by traversing the microphone along the negative X-axis starting at $x/h = 0$ (the point of intersection of the two bevel planes in the V-shaped twin jet) and moving backwards keeping $z/h = 4$ fixed during the test. This study was conducted only for the V-shaped twin jet configuration under coupled and uncoupled conditions (since the A-shaped configuration did not couple). The fully expanded Mach numbers studied were $M_j = 1.33$ and $M_j = 1.46$ for inter-nozzle spacings ratios of $s/h = 7.4$ (where coupling was strongest) and $s/h = 10$ (where coupling was absent as verified from the continuous spectra).

Figure 2.8(a) shows the graph comparing the rms pressure at the various upstream axial locations for $M_j = 1.33$ for the symmetrically coupled case ($s/h = 7.4$) and the uncoupled case ($s/h = 10$). It is clear from this figure that the symmetric coupling produces much higher pressures in the inter-nozzle region when compared to the uncoupled case. Figure 2.8(b) shows the same two curves as in figure 2.8(a), along with the addition of the antisymmetrically coupled case at $M_j = 1.46$ ($s/h = 7.4$). It can be seen that when the jets are antisymmetrically coupled the inter-nozzle pressure is lower than that we would see even when the jets are uncoupled. The results show that symmetric coupling produces sound pressures in the inter-nozzle region that are 5.5-7.5 dB higher than those for antisymmetric coupling. Figure 2.8(c) adds the curve for the uncoupled case at $M_j = 1.46$ ($s/h = 10$) to the previous figure. This curve shows that this case produces the smallest

inter-nozzle pressures. These trends also indicate that inter-nozzle spacing strongly eases the acoustic loading on near-field structures. For example, in figure 2.8(c), between the two uncoupled cases, the higher Mach number case shows a lower pressure distribution owing to a larger inter-nozzle spacing. Another feature of Figures 2.8(a – c) is the fact that the pressures in the internozzle region do not reduce monotonically, rather they exhibit an fluctuation reduction in amplitude. This indicates that the acoustic pressure waves in the upstream internozzle region exhibit some kind of damped standing wave pattern which would explain the continuously reducing oscillatory nature of the pressure amplitude. It must be noted that due to the oscillatory nature, the detrimental effects of the enhanced pressure levels could be felt at far upstream locations in the internozzle region.

Figure 2.8(d) shows a comparison between the time series signals for the symmetrically coupled case at $M_j=1.33$ and the uncoupled case at $M_j=1.33$ at an upstream location corresponding to $x/h = -3.2$. Similarly, figure 2.8(e) and figure 2.8(f) show comparisons between the time series signals for the symmetrically coupled case at $M_j = 1.33$ and the antisymmetrically coupled case at $M_j = 1.46$, and the symmetrically coupled case at $M_j = 1.33$ and the uncoupled case at $M_j = 1.46$ respectively. In each of these figures, it can be clearly seen that the symmetrically coupled case exhibits regular peaks with greater amplitudes as compared to both the antisymmetric case and the uncoupled case. In addition, the graphs as well as the time series show that the antisymmetric coupling does not automatically imply that the pressure magnitudes are the minimum possible. The minimum possible pressure magnitudes in the inter-nozzle region were obtained when the jets were decoupled at Mach numbers that showed antisymmetric coupling at the closest inter-nozzle spacings.

2.4. Phase averaged measurements

In order to obtain the phase averaged readings, the reference microphone was placed in between the two nozzles at the coordinate axis origin and the measurement microphone was traversed in the Y direction from a location where $y/h = -10.0$ to $y/h = 10.0$, keeping

$x/h = 0.0$ and $z/h = -5.3$ constant. At each measurement location, the timeseries data for both the microphones was acquired. The reference signal was digitally filtered around the screech frequency in order to obtain a pure sinusoidal wave. The signal from the measurement microphone at each location was triggered at selected phase angles of the screech cycle from the reference signal. One screech cycle is the time period corresponding to the screech frequency, and was calculated by counting the number of peaks over a certain time period. This was done by the LabVIEW program that computed the phase-averaging. Finally, the sound pressures at the triggered phase angles were ensemble averaged, thus yielding the averaged sound pressure corresponding to that particular phase angle. Figure 2.9(a) shows the phase averaged picture along a line on which $x/h = 0$ and $z/h = -5.3$ for an inter-nozzle spacing of $s/h = 7.4$ and a fully expanded jet Mach number of 1.33. In this figure, the curves represent the pressure distribution in the spanwise direction, for a particular position (phase) in the screech cycle. Thus, 24 curves, separated at 15° intervals represent the activity over a cycle (360°) as shown in the figure. For clarity, subsequent curves are translated vertically by 70 Pa. As can be seen from figure, the pressure magnitudes are symmetric about $y/h = 0$ as expected from a symmetrically coupled jet. Figure 2.9(b) shows the phase averaged picture for a fully expanded jet Mach number of 1.46. As in the previous figure each successive curve corresponds to a 15° increment in phase angle and each curve is offset from the previous by 70 Pa. It can be seen that points on corresponding sides of $y/h = 0$ have pressures that are opposite in phase, revealing antisymmetric coupling. Thus, the coupling modes are documented not only using two point phase measurements but by spatial phase averages that cover the entire spanwise extent of the coupling.

2.5. Applicability of Tam's waveguide approach

A question that naturally arises is: Can we predict or even reconcile the frequencies of complex nozzle coupling that can occur unpredictably in practical situations? To address this question we examined Tam's waveguide mode approach that includes higher order waveguide modes. Tam et. al. [33] showed that the frequencies produced by

underexpanded jets of complex geometries could be predicted using a waveguide approach. According to Tam's formula, the predicted frequency (f_p) is given by

$$f_p = \frac{u_c \kappa}{2\pi[1 + u_c / a_\infty]} \quad (2-1)$$

where u_c is the convection velocity of the instability waves, which, for rectangular jets, was recommended (Tam and Reddy [34]) to be

$$u_c \approx 0.55u_j \quad (2-2)$$

where u_j is the jet speed. a_∞ is the ambient sound speed. κ is the wave number of the shock cell structure. Using the vortex sheet model, Tam [35] found out that for large aspect ratio jets, like the ones used in the present study, the value of κ is given by

$$\kappa = k_{n1} = \left(\frac{n^2}{b_j^2} + \frac{1}{h_j^2} \right)^{\frac{1}{2}} \frac{\pi}{(M_j^2 - 1)^{\frac{1}{2}}} \quad (2-3)$$

where M_j is the fully expanded jet Mach number. Substituting these values into (2.1), the predicted frequency is given by,

$$f_p = \frac{0.55u_j}{2\pi[1 + (0.55u_j / a_\infty)]} \left(\frac{n^2}{b_j^2} + \frac{1}{h_j^2} \right)^{\frac{1}{2}} \frac{\pi}{(M_j^2 - 1)^{\frac{1}{2}}} \quad (2-4)$$

According to this approach, for rectangular jets with a regular exit geometry, the screech frequency could be accurately predicted using the lowest order waveguide mode, i.e. $n=1$. In order to test the validity of this approach, we tested two rectangular nozzles with a regular exit geometry in the single jet and twin jet configuration and plotted the screech frequency observed and compared it to Tam's waveguide theory substituting $n=1$ in equation (2-4). Figure 2.10(a) shows the plot for the single and twin jet screech

frequencies plotted as a function of the fully expanded jet Mach number. It can be seen from this graph that the observed frequencies show reasonably good agreement with the frequencies corresponding to the lowest order waveguide mode. The observed screech frequencies for the single beveled jets were then plotted as a function of the fully expanded jet Mach number for both the single jet and V-shaped twin jet configurations (Figure 2.10(b)). Comparing the observed frequencies with Tam's waveguide modes, we can see that the symmetric coupling case corresponded to a waveguide mode of $n=3$ and the antisymmetric case corresponded to the modes $n=2$ and $n=1$. In contrast the single beveled jet corresponded to an $n=2$ mode at lower values of the fully expanded jet Mach number and $n=1$ at the higher values of the fully expanded jet Mach number. However, these predictions strongly depend on the accuracy of the convection velocity used. Since the convection velocity estimate provided by Equation (2-2) is for a uniform exit, the extent of validity of this equation for beveled exits needs to be verified by actual measurements of u_c for these jets. Although the waveguide approach cannot provide an *a priori* estimate of the frequency the agreement suggests that the tool can indicate to a nozzle designer the range of expected screech frequencies.

Having studied the V-shaped configuration to a certain amount of detail, it was disappointing to note that the A-shaped configuration was not amenable to similar analyses due to the absence of coupling. However, the possibility of looking into the differences between the two configurations is interesting. Among the several possible discrimination tools, directivity measurement was chosen for studying the differences between the two twin jet configurations. These studies are described in the following section.

2.6 Directivity studies

The directivity of sound pressure was measured along the vertical plane (the XZ plane as depicted in Figure 2.1(a)) separating the two nozzles. The focus of these studies was to gain knowledge about the differences between the various configurations. Therefore, the directivity was measured for the single jet configuration, the V-shaped twin jet

configuration, and the arrowhead-shaped twin jet configuration. The radius of the microphone arc (R) was chosen as 4.5 inches (114.3 mm), which corresponds to around 4.5 equivalent diameters, or 22.5 shorter dimensions of the rectangular nozzles, or between 3.5 and 5.3 acoustic wavelengths corresponding to the screech frequency range in the present study. These values are acceptable since the present study focuses on the near-field effects.

Figure 2.11 shows the comparison between the two twin jet configurations (arrowhead-shaped, and V-shaped). In both the cases, the s/h was fixed at 7.4, and the Mach number was maintained at 1.33. The V-shaped configuration coupled symmetrically, and the arrowhead configuration did not show coupling at these conditions. The spectra of these two configurations can be distinguished by the fact that the symmetrically coupled V-configuration shows sharp tones of significant intensities against the multi-peak spectra of the uncoupled arrowhead configuration jets. In the case of the arrowhead configuration, the rise in the screech amplitude with increasing angle is also accompanied by an increase in the broadband shock noise. However, in the case of the symmetrically coupled V-shaped jet, there is no observable increase in the broadband shock associated noise. It may also be seen from the figures that the spectra of the arrowhead configuration are more sensitive to the emission angle as in single jets. This can be reconciled from the fact that when two jets do not couple, their sensitivity to angle remains unaltered.

Figure 2.12 shows the comparison of spectra of the arrowhead and V-shaped twin jets at various emission angles of measurement in the vertical plane. The jets were operated at a higher Mach number of 1.46, at which the V-shaped twin jet coupled anti-symmetrically, as discussed earlier. The following may be observed from these spectra:

- (i) Antisymmetric coupling (V-shaped jets) shows significantly lower amplitudes than arrowhead configuration at all angles.
- (ii) Antisymmetric coupling (V-shaped jets) shows more broadband noise than symmetric coupling (V-shape).

2.7. Broadband shock noise

In order to compare the broadband shock associated noise from each configuration, it was necessary to fix an invariant metric to quantify this noise, while being applicable to all the cases compared. This was achieved using the NASA preferred reliability practice no. PD-ED-1259. A constant bandwidth of 10 kHz was used in each spectra, where the most dominant broadband noise occurred at frequencies higher than the fundamental screech frequency. Further, it was ensured that this band excluded any tones or harmonics. Then, the integrated SPL over this band was calculated. As in the previous sub-section, comparisons have been made for single and the two configurations of the twin jets.

The broadband noise content of the single jet and the twin jets in the V-shaped and the arrowhead configuration are compared in figure 2.13. These plots are for the higher Mach number case ($M_j = 1.46$) where the broadband noise predominates. From figure 2.13, it can be seen that the broadband noise of the twin jets is far greater than that of a single jet. It is to be noted that the V-shaped twin jet configuration corresponds to the antisymmetric coupling, which showed more than the 6 dB lower SPL at the screech tone. Thus, it is clear that a reduction in the tonal amplitude due to the antisymmetric coupling mode does not imply reduced levels in other noise components, an observation that has hitherto gone unreported in the twin jet literature. Thus, coupling should be understood to have a pronounced effect only with respect to screech frequencies and their harmonics. Similarly, a comparison of the broadband shock noise of the V-shaped and arrowhead-shaped twin jet configurations at $M_j = 1.46$ shows that the V-shaped twin jet configuration, that is much noisier than a single jet, was found quieter in comparison with the arrowhead-shaped twin jet configuration. This indicates the possibility that there is a strong interrelationship between the two shock-cells from the two individual jets in the case of coupled twin jets. This would imply that in cases where this interaction between shock-cells is inhibited, as in the case of the arrowhead shape, the two sets of shock cells would act independently, leading to a behavior consistent with the following observations made in the present study:

- (i) Individual jets screech at different frequencies,
- (ii) Shock-associated noise increases with change in configuration from V to A, for the same pressure, mass flow rate and momentum.

In summary, the broadband shock noise levels compare among the three configurations studied as follows: Single Jet < V-shaped < Arrowhead-shaped. This strongly suggests that there could be contrasting differences in shock structures in the three configurations, which could in turn strongly influence their broadband noise emission behavior.

3. STUDY OF COUPLING USING HIGHER-ORDER SPECTRAL ANALYSIS TECHNIQUES

3.1. Time-Series Analyses

While analyzing the experimental data using linear cross spectrum phase at the screech tone, the authors found that there were two modes of coupling, “spanwise-symmetric” and “spanwise-antisymmetric” operating in a co-directed twin jet. All other modes were termed as “uncoupled” based on either or both of the following: (i) absence of a single dominant screech frequency (for example, presence of two dominant screech tones), (ii) no strong phase coherence. Using the three categories (symmetric, antisymmetric, and uncoupled), a coupling map in the parametric space was established, comprising the inter-nozzle spacing and the Mach number, as shown in Figure 3.1. While the jets were “uncoupled” going by the phase metric, they resembled coupled jets from the point of view of frequency locking. This presented a question whether the jets were coupled in non-linear terms. These interesting observations and questions motivated the authors to perform time-series studies. In this section, some of their observations, indicating the extensive role of unsteadiness and nonlinearity in the jet coupling, are highlighted.

Phase plots were generated, where the time series from the two microphone signals were used, and plotted one against the other (see schematic in figure 3.2). It was believed that the shape of the phase space would illuminate the physical understanding. Certain behavior in the phase plots were observed that would not fit in a simple classification such as “symmetrically coupled” or “antisymmetrically coupled”, etc. Some of the phase plots are shown in figure 3.3. The phase difference between the microphones for the case shown in figure 3.3(c) is about 31° (near-symmetric coupling), and that shown in 3.3(k) is about 175° (antisymmetric coupling). As can be seen from the plots, the phase plot of the symmetric coupling case does not look like a $+45^{\circ}$ line, and that of the antisymmetric coupling does not look like a -45° line in the phase space. A closer scrutiny of the power spectra revealed that in order for the symmetric coupling to manifest as a straight line in the phase space, the fundamental frequency should be a few orders of magnitude (at least

2 orders) more powerful than the first harmonic. In cases where the first harmonic had comparable power as the fundamental (same order of magnitude), the phase plot was distorted (eg., Figure 3.3(a)). Nevertheless, the authors were curious about the curved lines in the phase space (figures 3.3(k-n)) corresponding to the antisymmetric coupling, and attempted to simulate them from artificial sinusoids. Although they were partially successful in generating the images, this exercise did not further the authors' understanding of the coupling process. There were multiple ways of producing a certain shape in the phase space. Therefore, the focus of their study was shifted to the time-localized behavior of the twin jets as explained in the next subsection.

3.1.1 Time-Localized Phase Plots and Spectra

Since the phenomenon of twin jet coupling is non-trivial, it is essential to use appropriate diagnostic tools for an enhanced understanding of the same. The authors, therefore, considered the use of time-localized analyses of the time-series signals. Slightly deviating from the conventional waterfall plots of the spectra, they decided to look into the following time localized elements:

- (i). ***Phase plots within each signal:*** The time series of signal $x(t)$ was acquired, and the values in a time sub-interval against those in the adjoining sub-interval were plotted. That is, $\{x(t), t_i \leq t \leq t_i + \tau\}$ was plotted against $\{x(t'), t_i + \tau \leq t' \leq t_i + 2\tau\}$, where t_i is the beginning of the interval. These plots were made for several t_i within a single realization. These plots were expected to reveal the unsteadiness in the phenomenon. It was verified that a combination of sinusoids would result in identical phase plots across intervals as explained above. Therefore, this exercise was performed hoping that it would reveal the changes in the signal for the same flow and geometric conditions. The authors, therefore, assumed that all significant changes in these plots represented instantaneous unsteadiness in the coupling behavior. These phase plots were denoted as “X-X phase plots” for signal X(t).

- (ii). **Phase plots between the two signals:** If the two microphone signals were denoted by $x(t)$ and $y(t)$, $x(t)$ v/s $y(t)$ in the interval $t_i \leq t \leq t_i + \tau$, were plotted. This exercise was also repeated for several t_i as in the previous case. This task was undertaken so as to obtain the nature of coupling between the twin jets. These phase plots were denoted as "X-Y phase plots."
- (iii). **Cross-spectra:** For each sub-interval mentioned above, the cross-spectrum was obtained, to check if the events happening in a particular time interval had a significant effect on the cross-spectrum, and hence the magnitude of coupling.

The following facts were used in analyzing the X-X, Y-Y, and X-Y plots:

- (a) if the signals X and Y were similar, possessing the same frequencies, of comparable magnitudes, the X-X and Y-Y plots would resemble each other.
- (b) Changes in X-X plots across intervals signify that the frequency components were changing within the time series.
- (c) If the dominant frequency possesses substantial power in both signals, while the non-dominant frequency components were changing within the two individual time series, the X-Y plots would not differ significantly in spite of changes in X-X and Y-Y plots.

Several linearly superposed sinusoids and their X-X, Y-Y and X-Y phase plots were constructed to verify the above statements.

The results obtained from the above time-localized studies are shown in Figure 3.4 for Mach number 1.38. It is seen from these results that the cross-power spectrum remains almost constant except for some slight changes at a non-harmonically related frequency greater than the fundamental screech frequency (for example, see labels "P" on figure 3.4(a) and "Q" on figure 3.4(e)). The power at this frequency keeps changing, leading to

changes in X-X phase plots, and Y-Y phase plots. However, it is also clear that since the magnitude of the fundamental is more than an order greater than this non-harmonically related frequency, the X-Y phase plot remains almost the same. A contrasting case is presented in Figure 3.5, for Mach number 1.4. As can be seen from this figure, the cross-spectra as well as the phase plots (X-X, Y-Y, and X-Y) show variations within the sample. It is worth pointing out the relationship between the cross-spectra and the X-Y phase plots. In figure 3.5(a) top left, the cross-spectrum shows a dominant peak, and the side bands are much lower in magnitude. The coupling in this case is closer to anti-symmetric since the X-Y plot shows a -45° band. In the next figure (3.5(b)), it can be seen that a second dominant frequency has gained in magnitude and is comparable to that of the screech tone. This destroys the coupling as can be seen in the adjoining X-Y plot in figure 3.5(b), which looks fuzzy without a clear pattern. At a later time sub-interval, the behavior is similar to 3.5(a). The coupling approaches symmetry in Figure 3.5(d), since the X-Y plot resembles an ellipse. All such observations of transition in the behavior of the phase plots for this case are summarized in Table 3-1, which shows several transitions within short time duration of about 1 second.

The above observations indicate that coupling transitions enhance unsteadiness at certain Mach numbers. Since unsteady pressures should be avoided as far as possible, it is essential to understand and document coupling and its modal transitions. Having discussed the time-localized behavior of twin jet coupling, the authors shifted their attention on documenting the non-linearity of twin jet coupling. The method the authors proposed to use was cross-bicoherence, which was based on third order cumulants. A brief introduction to this tool and the validation of their code is presented in the subsequent section.

3.2. Computation of Cross-Bicoherence

Cross-bicoherence is a third order estimate obtained from two simultaneously acquired time-series signals. The third order quantities like bispectrum and bicoherence result from the Fourier transform of the triple correlation of the time series signals. They are exactly

analogous to the linear spectral methods and rules governing correlation and spectra. An elegant introduction to these methods and their use in the study of high speed jet flows is given in Thomas [30]. Therefore, only the mathematical expression for cross-bicoherence is given below. Cross-bicoherence is the normalized cross-bispectrum. The discrete cross-bispectrum is expressed for an ensemble as,

$$S_{YXX}^{(k)}(f_1, f_2) = Y^{(k)}(f_1 + f_2) X^{(k)*}(f_1) X^{(k)*}(f_2) \quad (3-1)$$

where $X^{(k)}(f)$ and $Y^{(k)}(f)$ are the DFT of discrete time series signals $x(t)$ and $y(t)$. Then, an ensemble average is done to obtain the final estimate of discrete cross-bispectrum.

$$S_{YXX}(f_1, f_2) = \frac{1}{M} \sum_{k=1}^M S_{YXX}^{(k)}(f_1, f_2) \quad (3-2)$$

The cross-bicoherence spectrum is then obtained by normalizing this quantity with the power spectra of the two signals as follows:

$$b_c^2(f_1, f_2) = \frac{|S_{YXX}(f_1, f_2)|^2}{\left(\frac{1}{M} \sum_{k=1}^M |Y^{(k)}(f_1 + f_2)|^2 \right) \left(\frac{1}{M} \sum_{k=1}^M |X^{(k)}(f_1) X^{(k)}(f_2)|^2 \right)} \quad (3-3)$$

The computation of these quantities is simplified by using symmetry properties in the frequency domain. Therefore, referring to Figure 3.6(b), only the region bounded by the two 45° lines in the upper half plane, and that in the lower half plane are unique. Exploiting these observations resulting from the symmetry properties, the computation was restricted to this region. The computation was done in MATLAB 6.5. An example demonstrating the use of cross-bicoherence is presented in the following paragraph.

Referring to equations (3-1), (3-2), and (3-3), the interaction corresponding to a frequency pair (f_1, f_2) was termed either as a “sum interaction” or as a “difference interaction”, depending on whether f_1 and f_2 had the same, or the opposite signs. Sum and

difference interactions between signals and the ability of cross-bicoherence to discriminate between them could be illustrated by generating two sinusoids as follows:

$$f(t) = \sin \omega_1 t + \sin \omega_2 t \quad (3-4)$$

and

$$g(t) = \sin \omega_1 t \sin(\omega_2 t + \varepsilon \text{ rand}(t)) \quad (3-5)$$

where, ω_1 and ω_2 are the circular frequencies, and $\varepsilon \text{ rand}(t)$ - added as a phase component in one of the sinusoids, is a time varying random number with zero-mean and standard deviation ε ($0 \leq \varepsilon \leq 0.1$). The phase randomness simulates noise in experiments that is often referred to as *phase jitter*. These two signals were used as inputs to the program that computed the cross-bicoherence spectrum. The power spectra of the signals are shown in Figure 3.6(a), and cross-bicoherence spectrum is shown in Figure 3.6(b). Note that in this example, the two sinusoids have frequencies of 5 kHz and 8 kHz. It can be seen that the cross-bicoherence spectrum shows two distinct peaks; one at the sum interaction position at (ω_1, ω_2) ($b_c^2(8\text{kHz}, 5\text{kHz}) = 0.9$) and the other at the difference interaction position at $(\omega_1, -\omega_2)$ ($b_c^2(8\text{kHz}, -5\text{kHz}) = 0.9$), indicating the presence of the frequencies $\omega_1 + \omega_2$, and $\omega_1 - \omega_2$, respectively, in the modulated signal. Hence, the advantage of cross-bicoherence is its ability to identify such non-linear interactions, which is not possible with second order methods such as power spectra. For instance, the linear power spectra of $\sin(\omega_1 + \omega_2)t + \sin(\omega_1 - \omega_2)t$, and $2(\sin \omega_1 t)(\sin \omega_2 t)$ would be congruent despite the differences in the time series. In essence, second order spectra obliterate phase information, which could be very important to understand mechanisms in a complex physical process as in the present case (i.e., 2nd order coherence does not consider fixed initial phases between different frequencies).

In the above discussions, it is implicit that the relative phase standard deviation ε between the two modulated signals should be small for the cross-bicoherence to be detectable.

This concept is elucidated by computing the cross-bicoherence for various values of ε in equation (3-5). The variation of the peak cross-bicoherence between the above test signals and the relative phase standard deviation between the modulated signals is plotted in Figure 3.7. This plot shows that the cross-bicoherence was unchanged for small random phase standard deviations, but dropped significantly beyond a phase standard deviation of around $\pi/2$.

The current problem concerned screech wherein the screech tone had relatively substantial amounts of energy relative to the broadband. Therefore, such situations demanded techniques that were capable of detecting non-linearities hidden or submerged under substantial amounts of pure (linear) tones. Therefore the validation of the tool used in these circumstances was essential. Although Walker [31] and Walker and Thomas [29] had successfully used the cross-bicoherence tool in jet screech problem, the authors sought to validate their program since the computational implementation of a technique strongly influenced its efficacy. In order to validate the use of cross-bicoherence in a screech dominated environment, the authors simulated monotonic signals over a noise floor, and superposed them with varying amounts of quadratic terms. This was done by generating two test signals as follows:

$$\begin{aligned} f(t) &= \frac{1}{2}(\sin \omega_1 t + \sin \omega_2 t + \alpha) \\ h(t) &= \frac{1}{2}\{A f(t) + B \sin \omega_1 t \sin(\omega_2 t + \varepsilon)\} \end{aligned} \quad (3-6)$$

where α is a random number in the range $(0 \leq \alpha \leq 0.05)$ simulating the noise floor, and $A + B = 1$. Then, the power spectra of $h(t)$ and the cross-bicoherence spectra between $f(t)$ and $h(t)$ were generated and shown in figure 3.8, for various values of B/A , shown in percentage in the caption. It may be seen that linear spectrum showed the sum and difference frequencies closer to the noise floor, whereas cross-bicoherence spectrum peaked at the respective sum and difference interaction positions. It may be seen from figures 3.8 (d & h) that while the quadratic component had faded away into the noise floor in (d), the cross-bicoherence spectrum in (h) showed the interactions, although at a low coherence (b_c^2 (8kHz, ± 5 kHz) = 0.4), revealing that cross-bicoherence was more

sensitive a tool than power spectrum in revealing small amounts of frequency components. Thus equipped with a validated tool for non-linearity detection, the authors analyzed the twin jet time series data obtained over a parametric range comprising Mach number and inter-nozzle spacing, results of which are presented in the subsequent section.

3.3. Results of Non-linear Spectral Analyses

Time series data were acquired from the two microphones for fifteen Mach numbers, for the six geometric configurations considered in this study. For each set of time series data, the power spectrum was obtained resulting in 180 power spectra. Further, each pair of time series data resulted in a cross-bicoherence spectrum. Therefore, owing to the volume of the data, only a few comparisons are being presented. The main focus is to bring out the manifestation of non-linearity in various situations, and answer the following questions:

- (a) How did the flow and geometrical parameters influence non-linearity?
- (b) Were there patterns in the non-linear interaction set that would enable a classification of interaction types?
- (c) Could the extent of non-linear interactions be classified?

In order to obtain answers for these questions, various cases are presented in the following subsections, each with a specific focus. To begin with, the two twin jet configurations were compared; one that showed coupling (co-directed), and the other that did not couple (contra-directed).

3.3.1. Co-directed and Contra-directed Configurations

Figure 3.9 compares the cross-bicoherence spectra and power spectra for the co-directed and contra-directed twin jets. The extent of non-linearity could be seen from the presence of dots in the cross-bicoherence spectra and their magnitudes. Each peak in the cross-bicoherence spectrum denoted the non-linear interaction between the corresponding frequencies. It was evident that non-linearity was much lower in the contra-directed configuration compared to the co-directed case. Thus, the sparsely populated non-linear spectrum corresponding to the contra-directed configuration was indicative of lower levels of quadratic interaction between various modes. This observation was in agreement with earlier results obtained through linear phase coherence measurements that showed that while the co-directed configuration coupled, the contra-directed configuration did not couple at all. Therefore, it could be concluded that in order for non-linear interactions to occur across the two jets, it is necessary for the shear layers of the two single jets, and the embedded sound sources to be in close proximity, as promoted in the co-directed case. Further, there were non-harmonically related frequencies in both the spectra, suggesting that the presence of non-harmonically related frequencies was not necessarily a cause or an effect of non-linear interactions. In this context, the results concerning the phase dependence of cross-bicoherence may be recollected, wherein it was mentioned that the phase standard deviation between interacting waves should be small to produce noticeable non-linear interactions. In the case of the contra-directed configuration, it could be expected that the sound sources in the two jets were farther apart compared to the co-directed jet, and thus acquired a larger phase standard deviation before any interaction could occur. So, the lack of interactions in the contra-directed case was because of larger phase standard deviation attained before interaction.

The fact that co-directed jets coupled and contra-directed jets did not, along with the fact that symmetric coupling led to geometrically symmetric acoustic fronts as evidenced by earlier phase averaging results (as shown in Chapter 2, §2.4) indicated that shear layers flapped in-phase in the case of symmetric coupling and anti-phase in the case of

antisymmetric coupling. Such synchronous or asynchronous flapping behavior would be consistent with the possibility of fusion and coalescence of shear layers in co-directed jets.

3.3.2. Comparison of Single and Twin Jets

The non-linearity in single jets could be compared against that of twin jets with the aid of two parameters: (i) The number of interactions, and (ii) strength of interactions, as quantified by the cross-bicoherency. The cross-bicoherence spectra for single and twin jets were obtained for the entire Mach number range considered in the present study and the following observations were made: (a) the number of interactions in the single jet was lower than that for twin jets for most of the Mach numbers. At few Mach numbers, they were almost equal, and (b) the strength of the interactions was always greater in the twin jets compared to single jets. This was because in a single jet, the non-linear interactions occurred between screech sources, whereas in a twin jet, screech sources within each component jet interacted among each other apart from interacting with sources in the neighboring jet. Further, in a single jet, the sources were spaced approximately one shock spacing apart. In twin jets, the sources were closer.

A sample comparison is presented in Figure 3.10, showing the cross-bicoherence spectra and linear power spectra of co-directed twin jet and single jet. Note that the power contained in the screech tone was much larger in the twin jet compared to the single jet. Also note that while there were two dominant screech frequencies in the single jet, the coupling led to the existence of one dominant screech tone in the twin jet. Two dominant frequencies implied two independent feedback loops. Coupling eliminated both of them and created a new one. With reference to the cross-bicoherence spectra, the single jet showed almost equal number of interactions compared to the twin jet. However, the interaction strength was greater in the case of twin jet. These observations prove that the presence of an additional jet promoted non-linearity. The common feature between the two cases was that the maximum coherence corresponded to the self interaction of the screech mode. The screech tone self-interacted to produce the first harmonic. The first

harmonic interacted non-linearly with the fundamental to produce the second harmonic in the sum interaction, and the fundamental through a difference interaction. Now, several questions arise: (i) what was the cause and the nature of the self-interaction of the screech tone? (ii) did the first harmonic independently exist and interact non-linearly with the screech tone, or was the non-linear self-interaction of the screech tone, the source of the first harmonic? While the authors are still unable to resolve these issues, they nevertheless place pertinent observations for consideration while attempting to answer the above questions.

3.3.3. Effect of Mach number

Figure 3.11 shows the variation in the linear and the non-linear spectra with increase in fully expanded jet Mach number. The changes in these spectra could be summarized as follows:

- (i). At lower Mach numbers of the screeching regime, there were several clusters of closely spaced interactions. The formation of these clustered interactions could be explained as follows: A frequency much lower compared to the other participating frequencies was essential for the formation of clusters. This low frequency could be an independent mode or could be the resultant of a difference interaction between two closely spaced frequencies. Given that such a low frequency existed, the formation of clusters can be illustrated as in figure 3.12. It may be seen that frequency f_1 interacts with a low frequency Δf , leading to the formation of $(f_1 + \Delta f)$ and $(f_1 - \Delta f)$. This forms two closely spaced points (separated by frequency $2\Delta f$). These resultant frequencies then again interact with the sources like Δf leading to the formation of $(f_1 + 2\Delta f)$ and (f_1) . Thus, several interactions could exist at closely spaced frequencies. If this tendency continued, it would have led to an infinite number of closely spaced points. However, with each interaction the phase mismatch between the participating modes would increase, thus limiting the number of interactions occurring in the cluster. It is clear from the figure that in clustering, the spacing between interactions was about the same as the low frequency Δf . This

raised an interesting question whether the low frequency essential for clustering existed independently, or was a resultant of a non-linear interaction. A close-up view of a cluster is shown in Figure 3.13. The sequence of events forming this cluster can be described as follows: Frequencies f_1 and f_2 interacted in a sum interaction to produce the mode (f_1+f_2) , (S1 in figure 3.13), and in a difference interaction to produce the mode (f_1-f_2) , (D1 in figure 3.13). This is represented by $(S1, D1)$; $b_c^2(f_1, f_2) = 0.7$, $b_c^2(f_1, -f_2) = 0.7$. The mode (f_1-f_2) participated with mode f_2 and produced a sum mode f_1 with a $b_c^2(f_1-f_2, f_2) = 0.7$, and a difference mode f_1-2f_2 with a $b_c^2(f_1-f_2, -f_2) = 0.5$. This mode f_1-2f_2 underwent a sum interaction with f_2 to yield f_1-f_2 with a $b_c^2(f_1-2f_2, f_2) = 0.6$. The earlier mentioned resultant mode (f_1+f_2) , (S1 in figure 3.13) interacted with f_2 in a difference mode yielding the mode f_1 , with the $b_c^2(f_1+f_2, -f_2)$ being 0.5. The sequence of these interactions has been presented in a binary-tree-like structure in Figure 3.14, which describes the hierarchy of modal evolutions. It was interesting to note that as one came down the tree, the cross-bicoherence magnitudes kept decreasing, pointing out to the fact that the phase relationship diminished with each successive interaction.

- (ii). As Mach number increased, clustering was dominant, except at the Mach number (1.33) that showed strongest symmetric coupling, where clustering tended to decrease (see figure 3.11(c)). Beyond the symmetric coupling point, clustering again increased till Mach number 1.4, where the coupling switched to antisymmetric. In fact, clustering phenomenon was at a maximum at this “coupling-transition” Mach number.
- (iii). At the antisymmetrically coupled Mach numbers, the clustering phenomenon did not occur, and interactions occurred that mainly involved the screech frequency and its first harmonic.

Thus, from the above observations, it may be stated that the twin jet coupling underwent a marked variation in non-linear coupling behavior, with Mach number. It should be pointed out that the clusters observed in the bicoherence spectra were not due to the

numerical implementation effects such as FFT length, number of averages, etc. This was verified by using various combinations of FFT length and number of averages, overlap between records, etc., wherein it was found that clustering phenomenon was real and not due to numerical errors and manifestations.

In order to bring out the various aspects discussed, the details of some major interactions corresponding to figure 3.11(a), are presented in table 3-2. It can be seen that the strongest interactions ($b_c^2 = 0.8$) involved the fundamental or the first harmonic as one of the participating frequencies. To clarify this concept, consider the following example: Referring to the first column (in Table 3-2), interaction No.6 also involved the fundamental frequency. However, the coherency was 0.7. This is because, 15.4 kHz is the resultant of interaction No.3. Therefore, interaction No.6 is the second generation of interactions leading to a lower value of coherence.

The authors also looked into the possibility of the coupling-transition Mach number being related with the bevel angle. The bevel angle in the present case was 30° , and thus the bevel plane made an angle of 60° with the flow direction. The authors examined whether the coupling-transition Mach number had a wave angle ($\sin^{-1}(1/M)$) matching the bevel geometry. This did not seem to be the case, with respect to fully expanded Mach number, although a possibility of such a relationship with a transformed Mach number was not ruled out.

3.3.4. Effect of Inter-Nozzle Spacing

Figure 3.15 compares the effect of inter-nozzle spacing on the non-linear interactions in co-directed twin jet configurations. As can be seen from the figures, the cross-bicoherence spectra showed localized clusters in each case. The cluster size grew as inter-nozzle spacing was increased. The interactions clustered around three main zones concerning: (1) interactions of the fundamental and its neighboring frequencies with lower frequencies, (2) self interaction of the fundamental frequency (and its neighborhood) with themselves, (3) difference interaction between the neighborhood of

the second harmonic and the neighborhood of the fundamental. There were other prominent zones, but the aforementioned zones contained high levels of cross-bicoherence. It should be pointed again that the linear spectra were qualitatively similar to one another. Therefore, it appeared that an increase in inter-nozzle spacing promotes non-linearity. However, there had to be a limiting case, since as $s/h \rightarrow \infty$, logically, the phase correspondence would be lost, and hence the interactions would lose strength, and the cross-bicoherence would decrease and tend to zero. This was partly verified by obtaining the cross-bicoherence spectrum at an inter-nozzle spacing of $s/h = 11.2$ and Mach number 1.32, wherein the interaction density dropped significantly, and the peak cross-bicoherence was low (0.6) (see figure 3.16). From these results it was also obvious that the non-linearity should peak somewhere in between an s/h of 7.9 and 11.2.

Another comparison bringing out the effect of inter-nozzle spacing is presented in figure 3.17, for a slightly higher Mach number of 1.46. The clusters seen in figure 3.15 were no longer seen in this figure since the necessary low frequency, or closely separated frequencies did not exist in the spectra. Therefore, the interactions were restricted to the self-interaction of the fundamental screech frequency. Another contrasting observation was the presence of dots (interactions) along horizontal and vertical lines at positions corresponding to the fundamental frequency. These are marked on figure 3.17(e) as “A” and “B”. These interactions indicate that at these Mach numbers, the most desired participating frequencies for non-linear interactions are the fundamental and the first harmonic, as elaborated in the next subsection.

3.3.5. Actively Participating Modes

The observation of horizontal trail ‘A’ in figure 3.17(e) seems to suggest that the common frequency pertaining to those interactions (obtained by extending the line to intersect y-axis) emerged from a strong source. For the generation of a trail (like line ‘A’) to exist, the following conditions must be met: (i) the other participating mode (frequency) should have had a strong phase relationship with the common frequency explained above. In case the phase relationship was weak, the non-linear coupling did not

occur. In case the other mode was weak, the strength of the fundamental mode could be strongly overpowering to produce a non-linear coupling. These types of interactions generally produced difference interactions such that the combined mode was split into the two original modes. This can be seen from figure 3.17(e), and explained as follows: (i) the fundamental screech mode was extremely dominant, it got involved in a nonlinear sum interaction with even weaker modes, (ii) the resultant nonlinear mode did not become a dominant mode owing to a weak phase relationship, or lower magnitudes. Hence, such resultant modes could be termed as “unstable” modes. (iii) Such resultant unstable modes readily participated with the fundamental mode to produce the fundamental screech frequency. This is a possible explanation for the screech frequency being observed as the *most-desired resultant frequency*. Since, the sum and difference interactions were equivalent to modulation and demodulation operations in a signal processing sense, it may be possible to figuratively view the jet column to be behaving like a modulator/demodulator of the various modes, leading to the production of the participating frequencies themselves.

Further, in most of the cross-bicoherence spectra in figure 3.17, there was a trail of interaction zones tending to form a -45° line in the cross-bicoherence spectrum (marked in figure 3.17(g) as “C”). Such lines in the cross-bicoherence spectrum indicated that the resultant frequency corresponding to the line was the most desired. In all these cases, the fundamental frequency seemed to be the most desired resultant frequency from the non-linear interactions. That is, the presence of a trail like pattern indicated that there were numerous interactions along the line. However, all those interactions resulted in the “most desired frequency.” Examples of these rectilinearly aligned interactions are shown in Figure 3.18.

3.3.6. New Metrics Defined

In order to view all the observations in a common perspective, the authors have developed two new metrics. The first, termed as “*Interaction density*” (I_c), is the number of peaks in the cross-bicoherence spectrum above a certain threshold value. In this study,

threshold values of 0.3, and 0.4 have been used. The threshold is indicated in the subscripts.

Figure 3.19 shows the variation of interaction density with Mach number for all the configurations studied, for threshold values of 0.3 and 0.4. Observations made using interaction density are consistent with the earlier discussions, and can be summarized as follows: (i) the interaction density of co-directed twin jets were much higher compared to arrowhead shaped jet, (ii) the single jet displayed intermediate values, and (iii) the interaction density for the co-directed twin jets showed a sharp increase around Mach number 1.4. This Mach number is the one at which a coupling shift occurred from symmetric to antisymmetric, as detailed in the previous chapter. Therefore, there seems to be a strong correspondence between these two observations. Further, our earlier studies had concluded based on linear phase measurements that coupling existed only when the inter-nozzle spacing was $s/h = 7.3$. However, the present results show that non-linear interactions were similar at higher spacings, and in fact, tended to increase with spacing. This seems to indicate that although there was no evidence of linear coupling at higher spacings, there seemed to be a strong non-linear coupling at higher spacings. One interesting observation was that this behavior of interaction density was the same for the two values of bicoherence threshold considered. This enhances the authors' confidence in the new metric that we have developed.

In order to consider the effect of inter-nozzle spacing and Mach number on the interaction density, the interaction densities of co-directed twin jets were averaged at each Mach number using four inter-nozzle spacings of $s/h = 7.3, 7.5, 7.7$, and 7.9 . This second metric is termed as the "*Average Interaction density*". The average interaction densities so obtained, are plotted against Mach number as shown in figure 3.20(a & b). These two curves correspond to cross-bicoherence threshold values of 0.3, and 0.4, respectively. From these plots, it is clear that the non-linearity sharply increased at around a Mach number of 1.4, where linear phase coherence showed a switch from symmetric to anti-symmetric coupling. Thus, it may be conjectured that a coupling mode switch was accompanied by an increase in the extent of non-linearity. Plots 3.20 (c and d)

show the average interaction densities, calculated by averaging the interaction densities over all Mach numbers for a certain inter-nozzle spacing. These graphs show the effect of inter-nozzle spacing considering the entire Mach number range. The plots show that there was a monotonic increase in the interaction density with inter-nozzle spacing, and the observations were similar for both cross-bicoherence threshold values considered. This corroborates the previous observation that an increase in inter-nozzle spacing promoted non-linear interactions among the sound sources (up to the maxima location).

It was pointed out by Thomas and Chu [26] that the planar shear layer showed a preference for difference interactions than sum interactions. Based on the metrics defined above, we looked at the distribution between sum and difference interactions in twin jets. Like shear layers, twin jets also seemed to prefer difference interactions. We observed that except for few single jet cases, the difference interactions dominate sum interactions in all the configurations and Mach numbers studied ($I_{c,diff} > I_{c,sum}$).

4. CONCLUSIONS

The coupling phenomenon of jets exhausting from twin jets of single beveled geometry has been studied in great detail in the course of this project. Two possible twin jet configurations, namely the arrowhead-shaped configuration and V-shaped configuration were compared. Linear and non-linear techniques were used to study the jets and attempts were made to quantify the interaction that occurred between them. In the process the authors obtained some interesting results and additionally, came up with some new metrics, hitherto unused, in order to characterize the coupling phenomenon. Studies focused at the closest spacing and dynamic tests were run at higher inter-nozzle spacings. The key results are summarized below:

1. The authors were able to demonstrate coupling between twin supersonic jets exhausting from nozzles of single beveled geometry. For the nearest inter-nozzle spacing ($s/h = 7.4$), the V-shaped twin jets coupled in a symmetric mode at the lower Mach numbers and in an antisymmetric mode at the higher Mach numbers. In contrast, the arrowhead (A-shaped) configuration did not show coupling at all spacings and Mach numbers covered in this study.
2. The symmetric coupling produced higher tonal peaks than those produced by single jets and the antisymmetric coupling lead to a reduction in the tonal peaks than the single jets. The augmentation and the reduction were both greater than the 6 dB that one would expect through source doubling/halving for tones. Phase averaged measurements in the near field confirm symmetric coupling in the case of $M_j=1.33$ and antisymmetric coupling at $M_j=1.46$.
3. Dynamic tests run for the nozzles at their closest inter-nozzle spacing showed the existence of both coupling modes at non-harmonically related frequencies for the midrange of pressures tested. The dynamic spectra acquired by moving the nozzles apart while running the jets at a fully expanded Mach number of 1.33 showed that the

nozzles coupled in a symmetric mode until about $s/h = 9.7$. After this they decoupled and no further phase locked coupling was seen.

4. The measured screech frequencies seemed to agree well with the wave guide modes proposed by Tam et. al. [33]. The screech frequencies of the symmetrically coupled V-shaped twin jet corresponded to the higher order waveguide modes ($n = 3$), while those of antisymmetric coupling corresponded to modes between $n=1$ or $n=2$.
5. Coupled jets had the same tones and harmonics dominant at all emission angles, while the spectra were sensitive to direction for single and uncoupled (A-shaped) twin jets.
6. The broadband shock associated noise has a strong dependence on the configuration, and hence possibly the shock-structures and their inter-relationships. Studies at Mach 1.46 revealed that the coupled twin jet in V-configuration emitted lower broadband shock noise followed by the uncoupled twin jet in the A-configuration.
7. Co-directed twin jets apparently uncoupled beyond a certain inter-nozzle spacing using second order methods, show non-linear coupling at higher spacings as revealed by non-linear spectra.
8. Time-localization studies revealed that unsteadiness increases when coupling mode transitions are involved. This should be considered in design of flow situations.
9. Two patterns of the cross-bicoherence spectrum were observed, one in which an array of dots dominate the spectrum, indicating interactions between close frequencies, and the other in which the dots tending to form straight lines appear in the spectrum. This case indicated the preference of the fundamental frequency as a participant in the nonlinear interactions, as well as a resultant frequency of the interactions.

10. A new metric has been defined, termed as the “interaction density”, based on the number of peaks in the cross-bicoherence spectrum, and seems to be a relevant parameter to quantify nonlinear coupling.
11. Another metric, the “average interaction density” increases sharply around a Mach number that showed a transition between symmetric to antisymmetric coupling in linear phase coherence studies. Therefore, modal transitions in coupling can be believed to be accompanied by a large amount of non-linear interactions.
12. The average interaction density increases monotonically with inter-nozzle spacing for the range of spacings considered in the present study.
13. There are more number of difference interactions than sum interactions.

Acknowledgements

This work was funded by the US Air Force Office of Scientific Research (AFOSR) with Dr. John Schmisser as Program Manager.

5. LIST OF THESES, PAPERS AND PUBLICATIONS FROM THIS PROGRAM

- [1] P. Panickar, "Coupling of twin jets from nozzles having single beveled exits," Masters' Thesis, Illinois Institute of Technology (2003).
- [2] P. Panickar, K. Srinivasan, G. Raman, "Interactions of Twin Jets from Nozzles of Spanwise Oblique Geometry", American Institute of Aeronautics and Astronautics Paper 2003-1197 (2003).
- [3] P. Panickar, K. Srinivasan, G. Raman, "Aeroacoustic features of coupled twin jets with spanwise oblique shock-cells," accepted for publication in the Journal of Sound and Vibration.
- [4] K. Srinivasan, P. Panickar, G. Raman, B-H. Kim, D.R. Williams, "Study of supersonic twin jet coupling using higher order spectral analysis," American Institute of Aeronautics and Astronautics Paper 2003-3871 (2003).
- [5] P. Panickar, K. Srinivasan, G. Raman, "Acoustic coupling of twin jets from single-beveled nozzles," American Institute of Aeronautics and Astronautics Paper 2004-0006 (2004).

CHAPTER 7. FIGURES

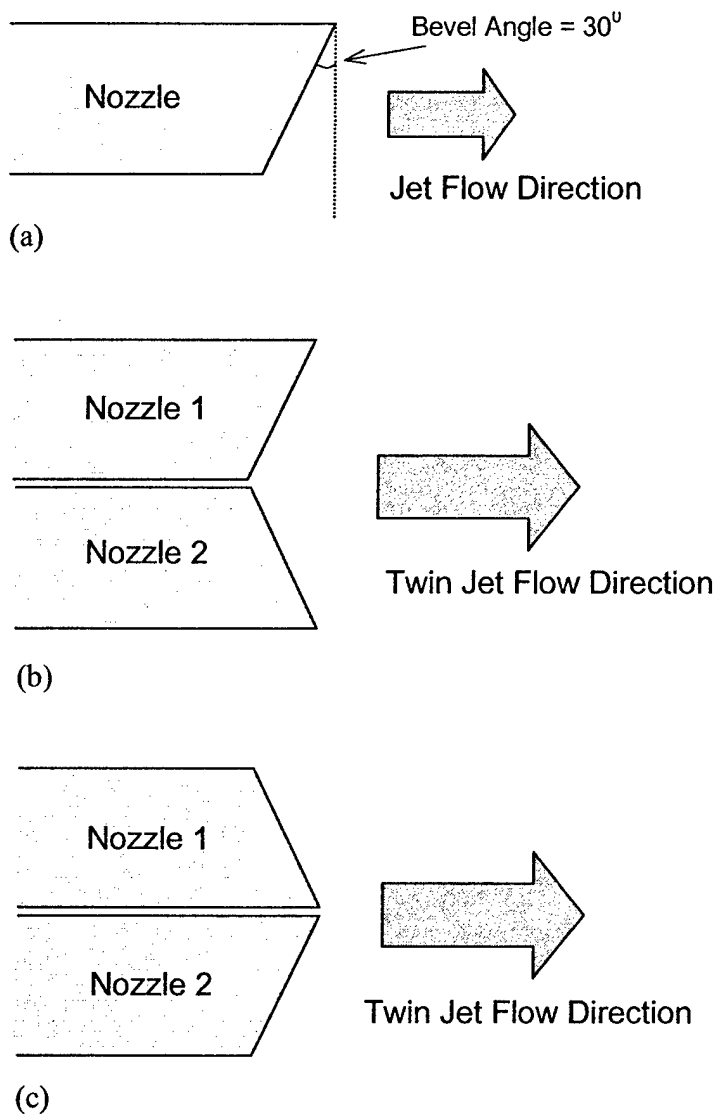
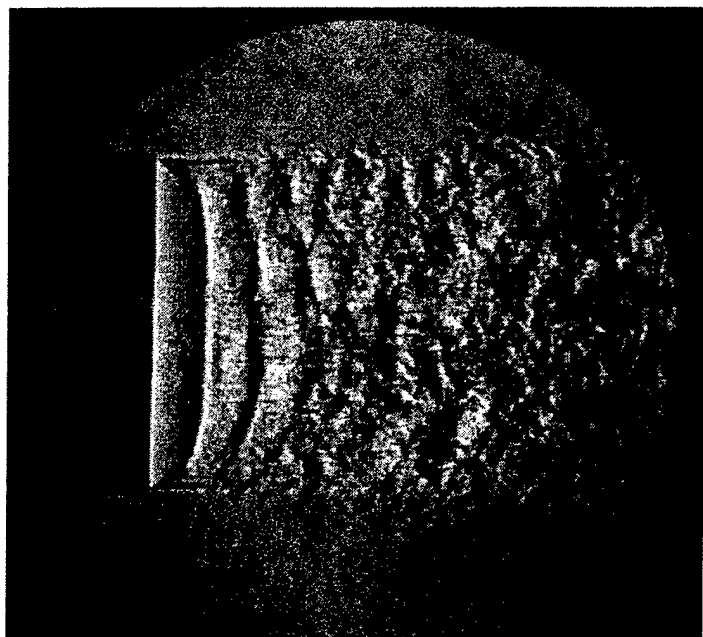
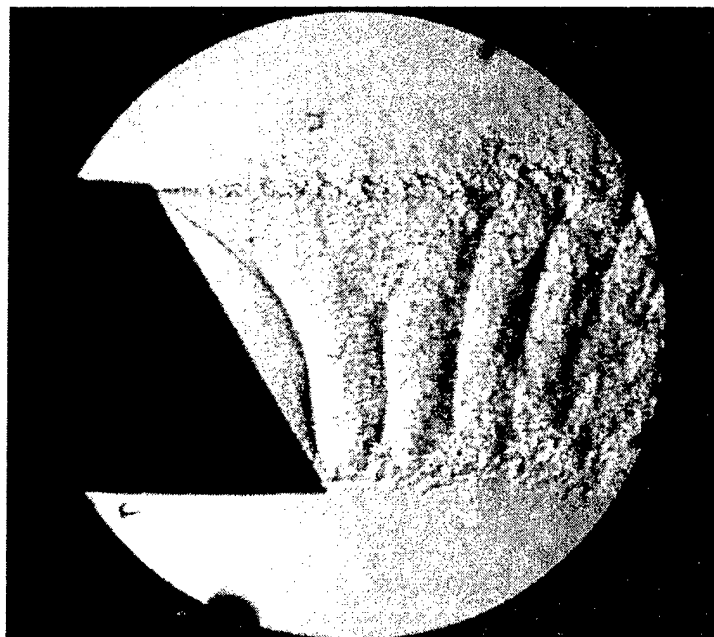


Figure 1.1. Schematic diagrams showing single and twin jet configurations. **(a).** Single jet, **(b).** Twin Jet: V-shaped configuration (co-directed), **(c).** Twin Jet: Arrowhead-shaped configuration (contra-directed).



(a)



(b)

Figure 1.2. Spark-schlieren photographs of a jet comparing shock containing jets from uniform and spanwise beveled nozzles (from Raman [25]). (a). Uniform exit (b). Single beveled exit. Note the spanwise oblique shock cell structure.

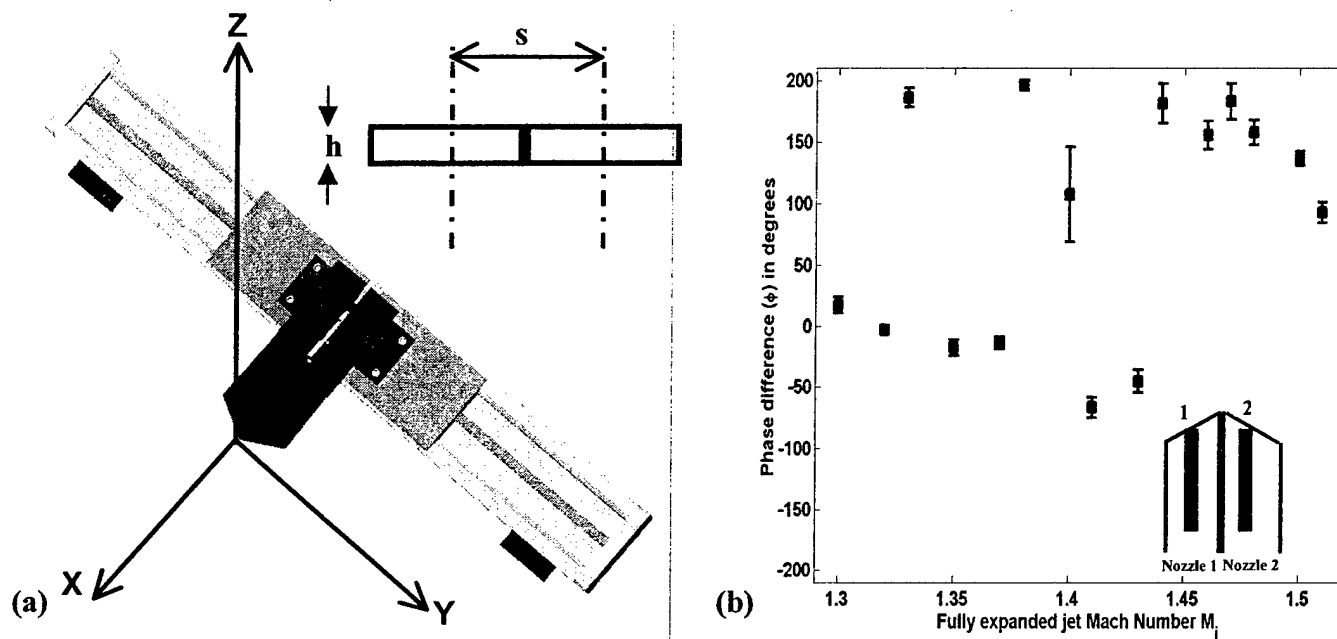
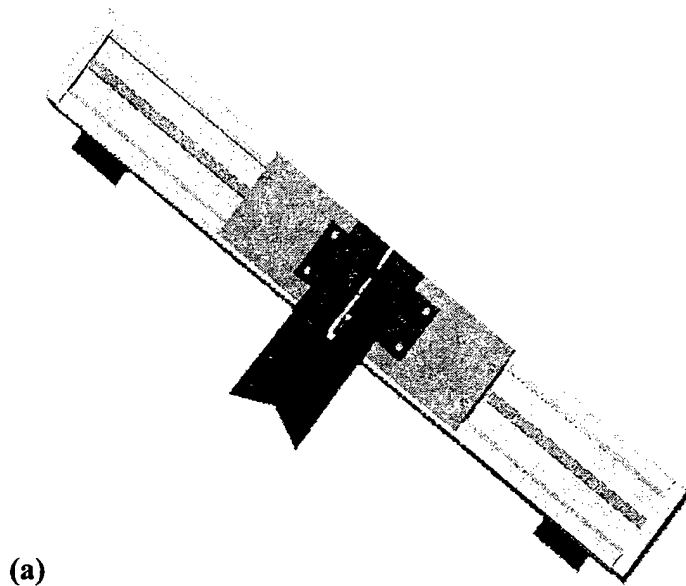
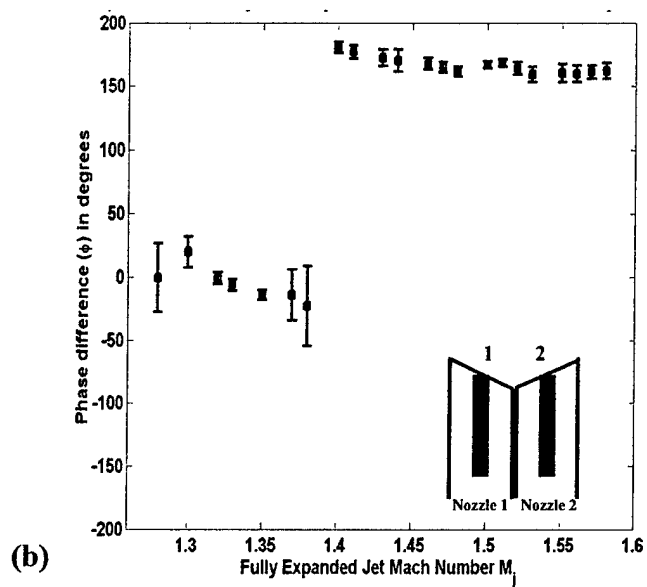


Figure (2.1). Twin jet in the arrowhead or A-shaped configuration and spanwise phase associated with it (a). A-shaped twin jet configuration of the two single beveled nozzles, along with the coordinate axis setup, and nozzle dimension nomenclature used during the experimental study (b). Spanwise phase angle between the two jets as measured by microphones 1 and 2. The microphone locations are on the spanwise center of the individual nozzle as shown by the black rectangular strips in the schematic. This configuration showed **no coupling** as is evident from the phase chart.



(a)



(b)

Figure (2.2). Twin jet in the V-shaped configuration and spanwise phase associated with it (a). Schematic of V-shaped configuration of the two single beveled nozzles (b). Spanwise phase angle between the two jets as measured by microphones 1 and 2. The microphone locations are on the spanwise center of the individual nozzle as shown by the black rectangular strips in the schematic.

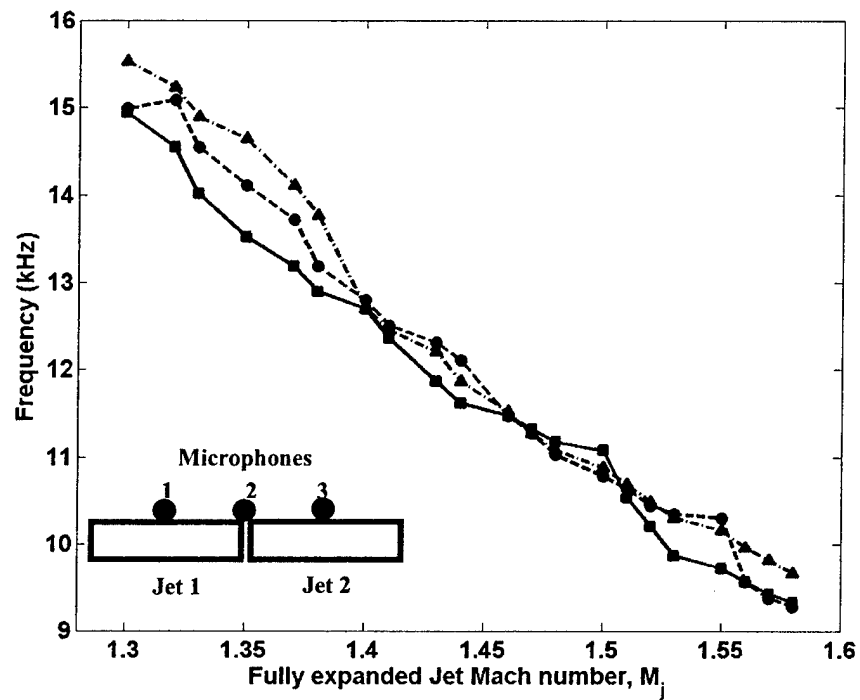


Figure 2.3. Frequency characteristics of Single Beveled Nozzles at various fully expanded Mach Numbers. The data was taken using microphone 1 for jet 1 operating individually, microphone 3 for jet 2 operating individually and microphone 2 for the twin jet operation. (—■—) Jet 1, (—●—) Jet 2, (—▲—) twin jet configuration

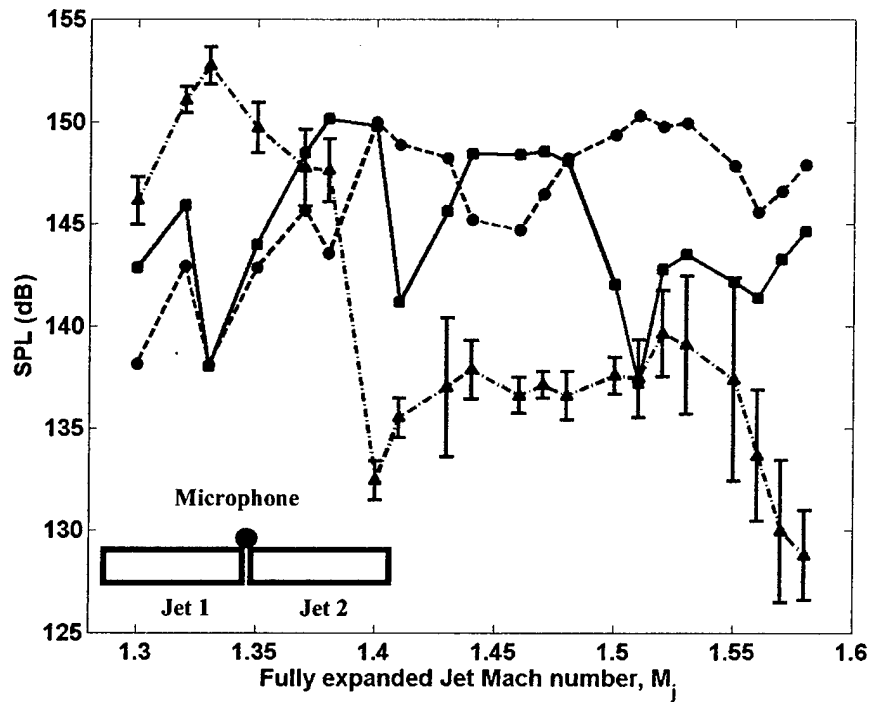


Figure 2.4. SPL characteristics of Single Beveled Nozzles at various fully expanded Mach Numbers. Note the augmentation in dB levels for the twin jet case at lower M_j and the suppression in the dB levels at medium and high M_j . The data was taken using microphone 1 for all the 3 cases. (—■—) Jet 1, (—●—) Jet 2, (—▲—) twin jet configuration

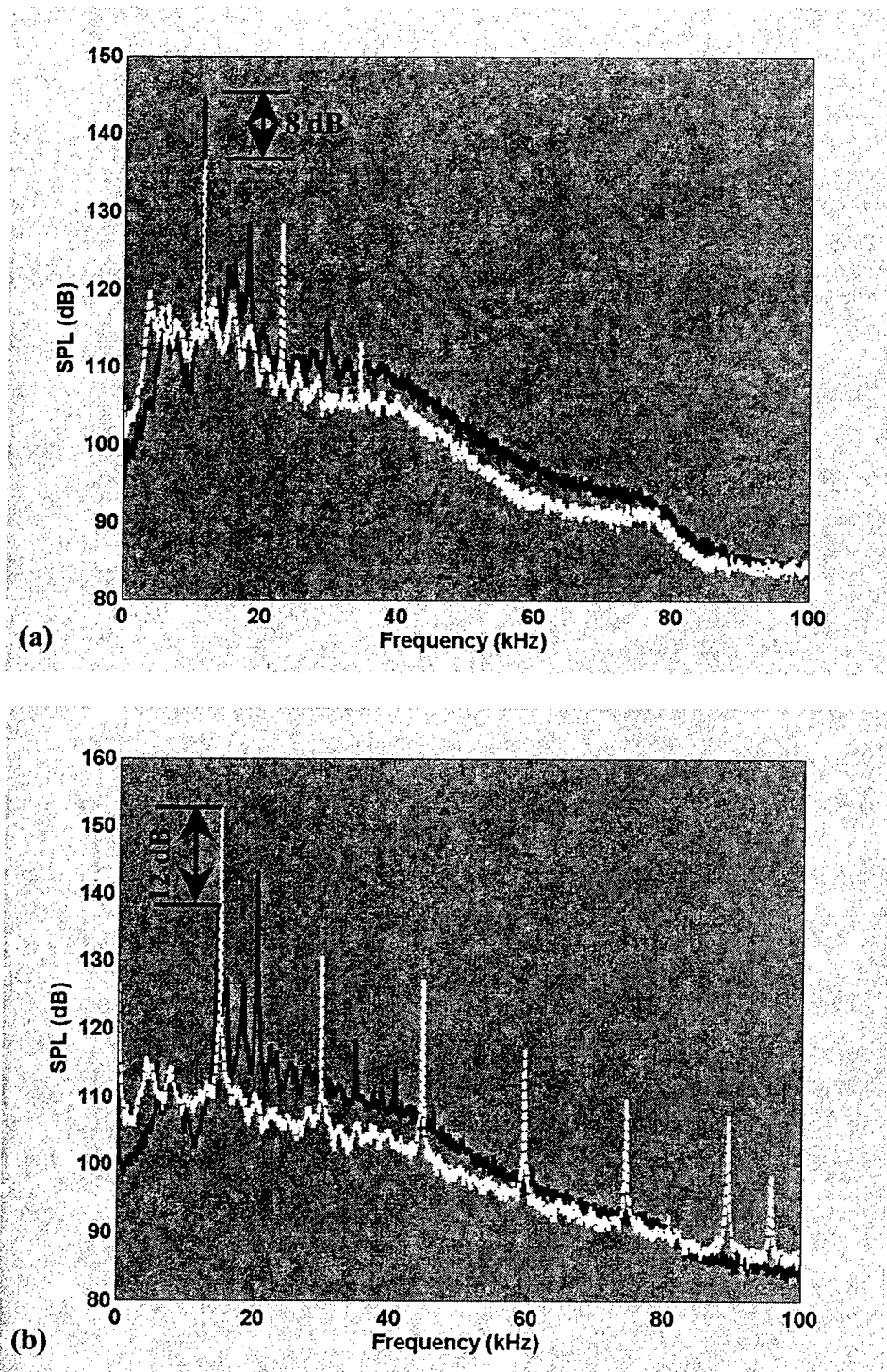


Figure 2.5. Spectra illustrating the coupling modes in V-shaped twin jets. (a). Antisymmetric coupling at a fully expanded jet Mach number $M_j = 1.46$ (b). Symmetric coupling at a fully expanded jet Mach number $M_j = 1.33$. Note the difference in amplitude levels for the twin jet case as compared to the individual jets. (black) Spectra for single jet. (white) Spectra for twin jet configuration

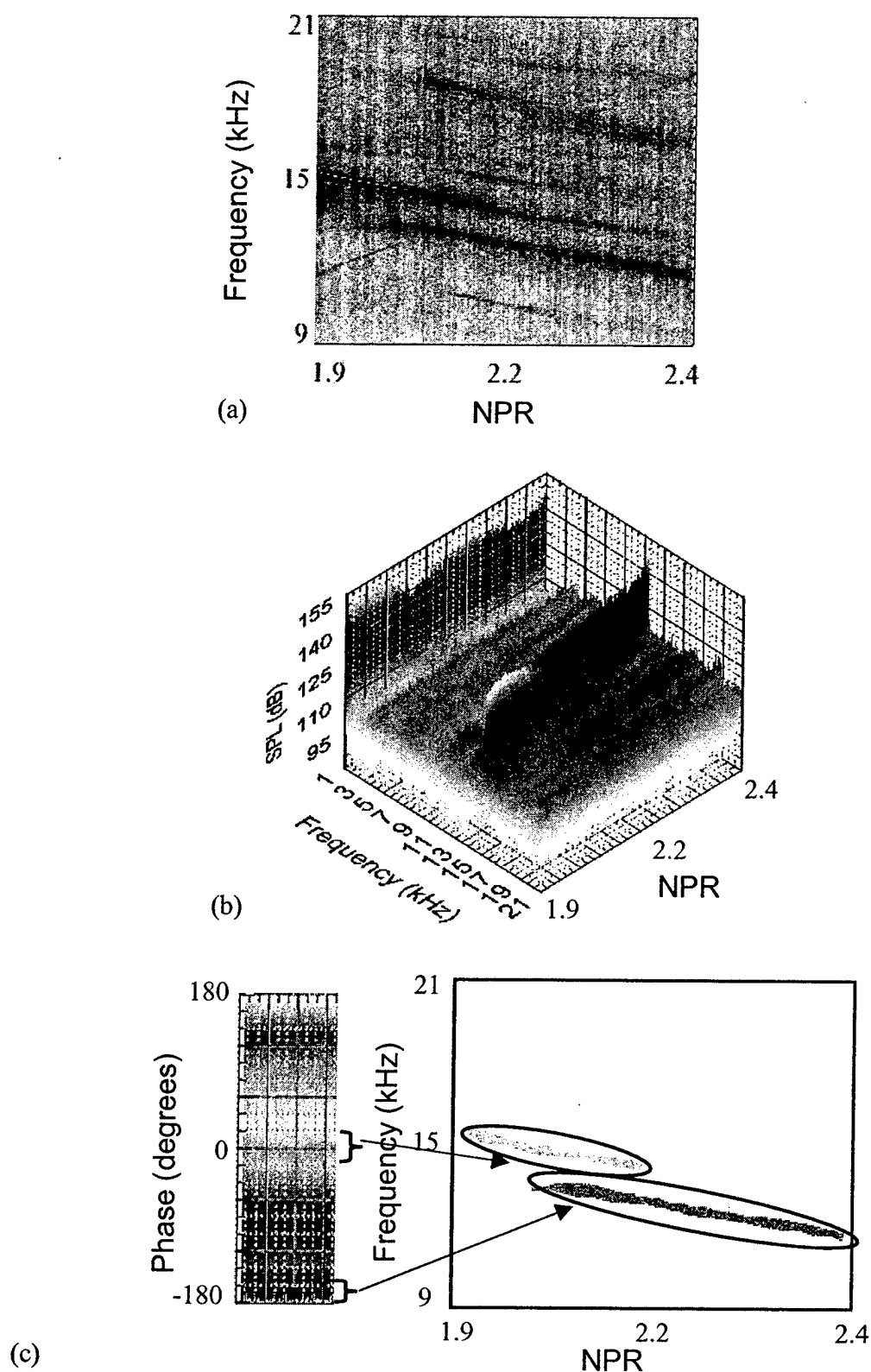


Figure 2.6. Continuous instantaneous spectra for nozzles acquired while the internozzle distance remained fixed at $s/h = 7.4$ and the pressure changed continuously. The two modes of coupling can be seen simultaneously at the intermediate pressures at non-harmonically related frequencies. (a). Two dimensional representation of spectra showing screech frequency variation with change in NPR. The plot shows constant SPL contours. (b). Three dimensional continuous instantaneous spectra. (c). Phase variation with change in the NPR. The color bar on the left shows the phase variation and the plot on the right shows contours of constant phase.

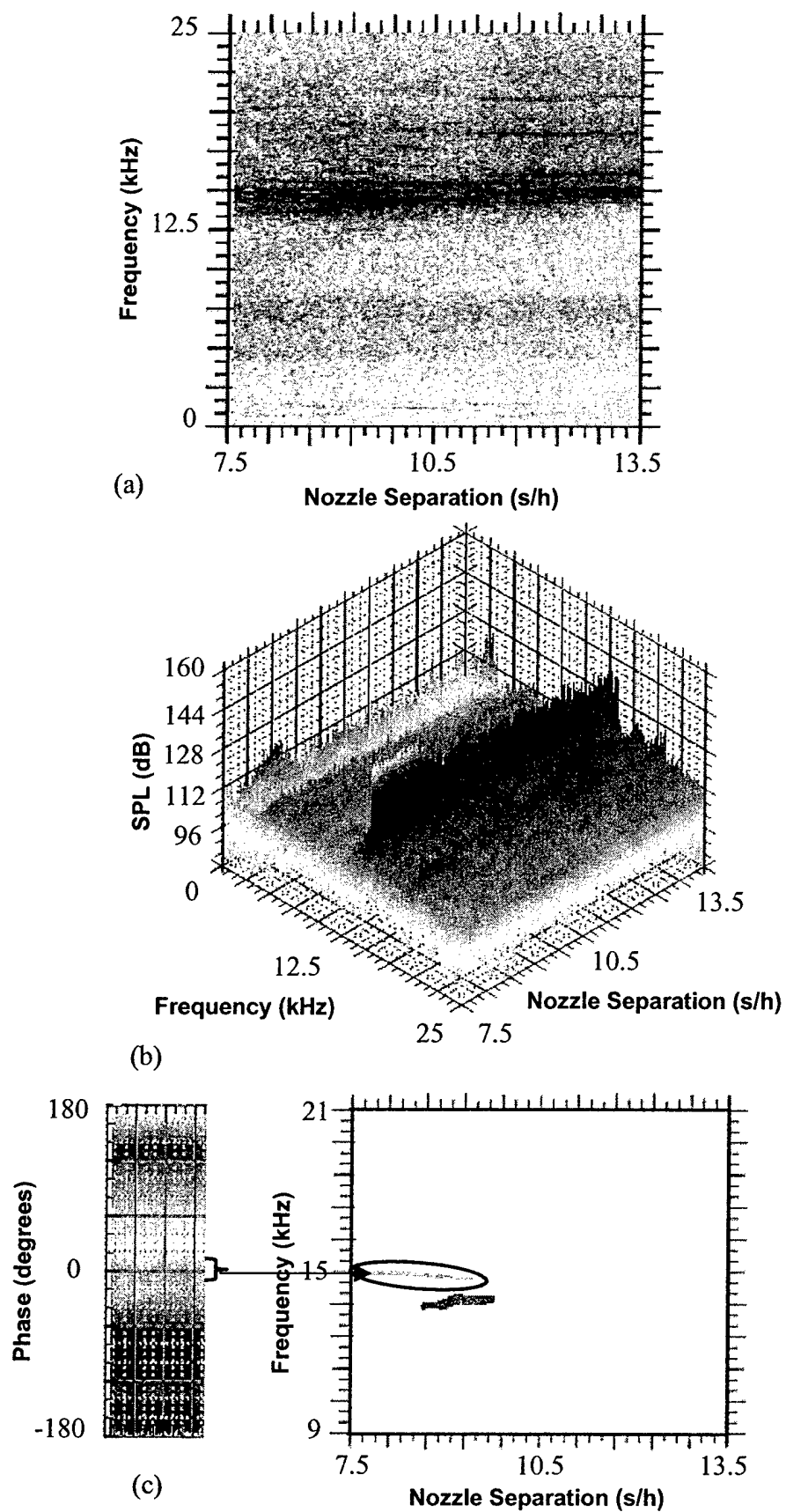


Figure 2.7. Continuous instantaneous spectra for nozzles acquired while the internozzle distance changed continuously and the exit jet Mach number remained fixed at 1.33. (a). Two dimensional representation of spectra showing screech frequency variation with change in the internozzle separation. (b). Three dimensional continuous instantaneous spectra. (c). Phase variation with change in the nozzle separation. The color bar on the left shows the phase variation and the plot on the right shows contours of constant phase.

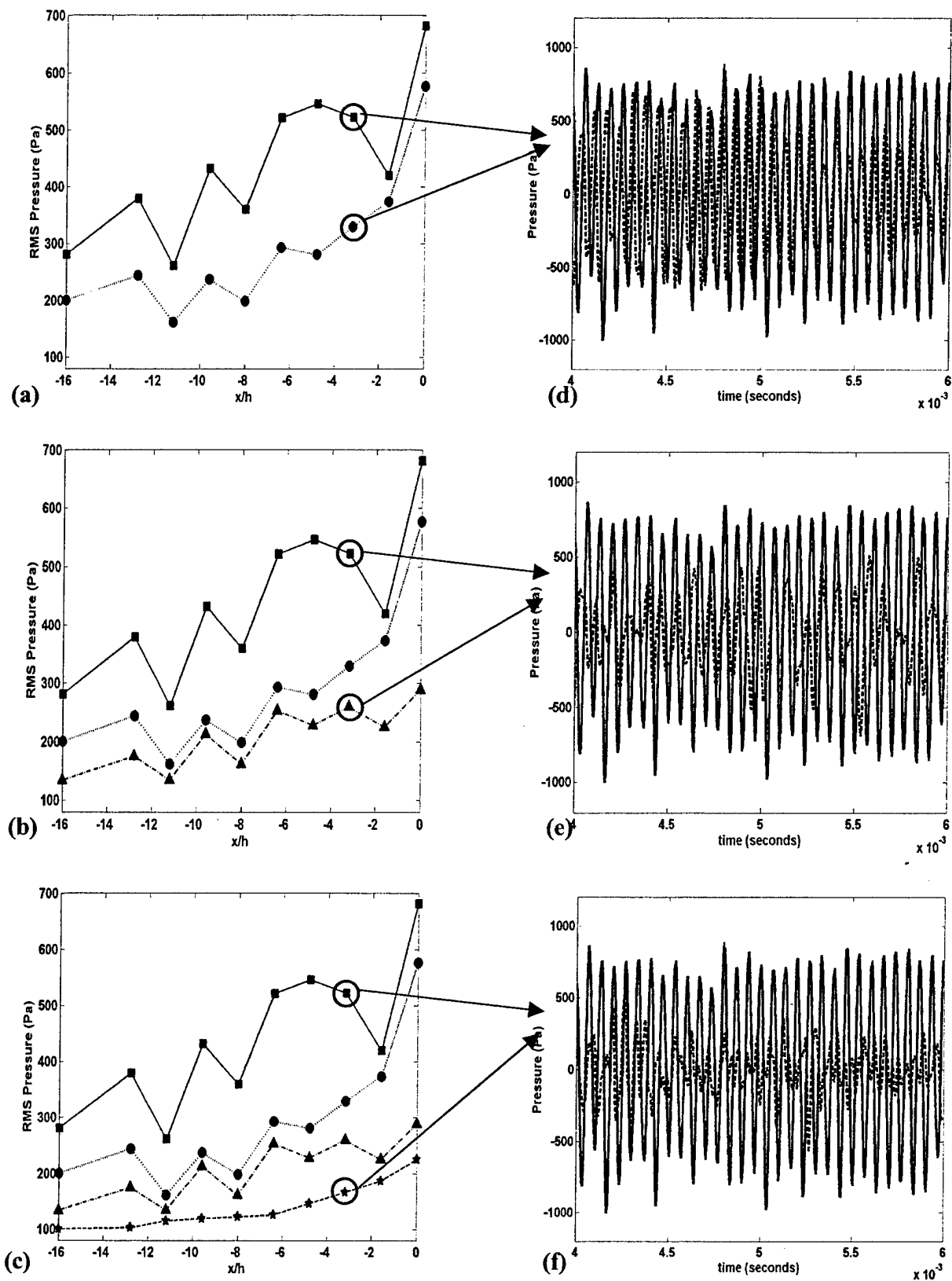


Figure 2.8. Inter-nozzle rms sound pressure distribution. (a), (b) and (c) show the distribution of the rms pressure in the internozzle region for the various operating conditions. (—■—) coupled jets $M_j = 1.33$, (·····○·····) uncoupled jets $M_j = 1.33$, (---▲---) coupled jets $M_j = 1.46$, (—*—) uncoupled jets $M_j = 1.46$ (d), (e), (f) show the timeseries data at the operating conditions circled in the graph. The solid curves (—■—) are for the coupled case at $M_j = 1.33$ and the dashed curves (---▲---) are for the uncoupled case at $M_j = 1.33$, the coupled case at $M_j = 1.46$, and the uncoupled case at $M_j = 1.46$ respectively. Data taken keeping $y/h = 0$ and $z/h = 4$.

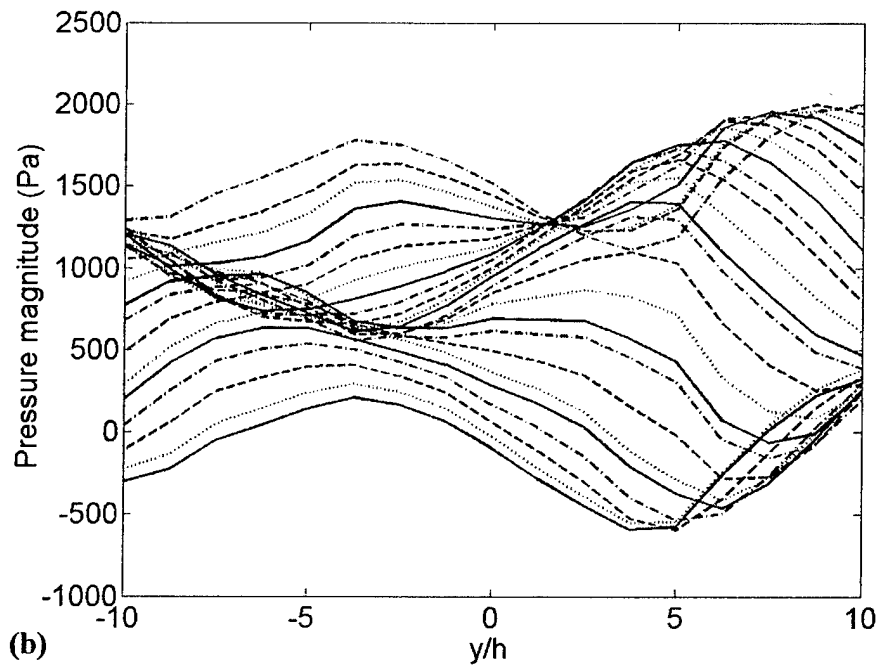
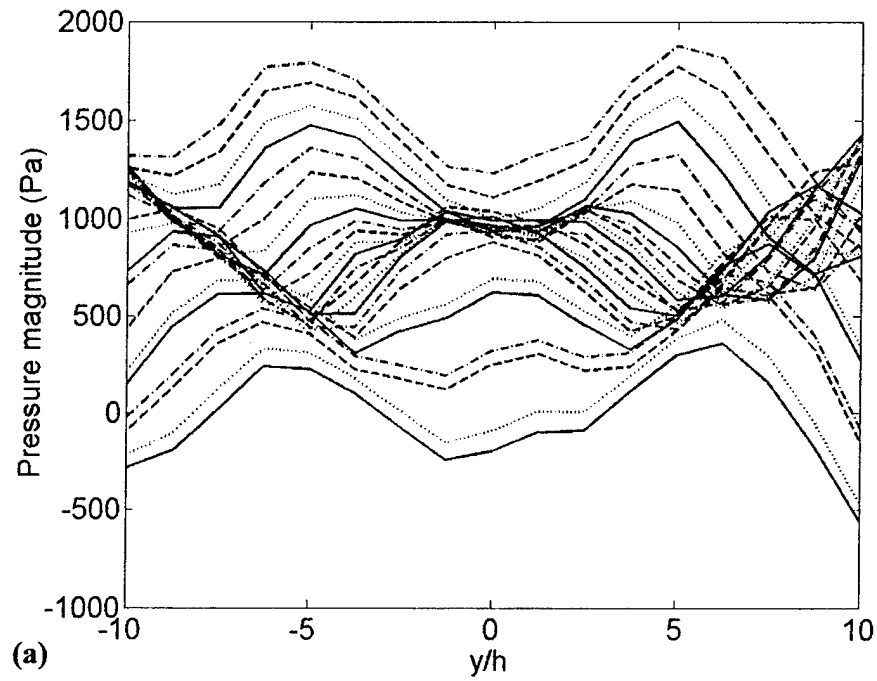


Figure 2.9. Phase averaged sound pressure values for the twin nozzles. The values are averaged on either side of the Y-axis keeping the X and Z coordinate fixed. **(a).** Operating condition $M_j = 1.33$. Note the symmetry about $y/h = 0$ indicating symmetric coupling. **(b).** Operating condition $M_j = 1.46$. Note the antisymmetry about $y/h = 0$ indicating antisymmetric coupling. Successive curves are offset by 70 Pa and a phase difference of 15° . Line codes repeat every 60° .

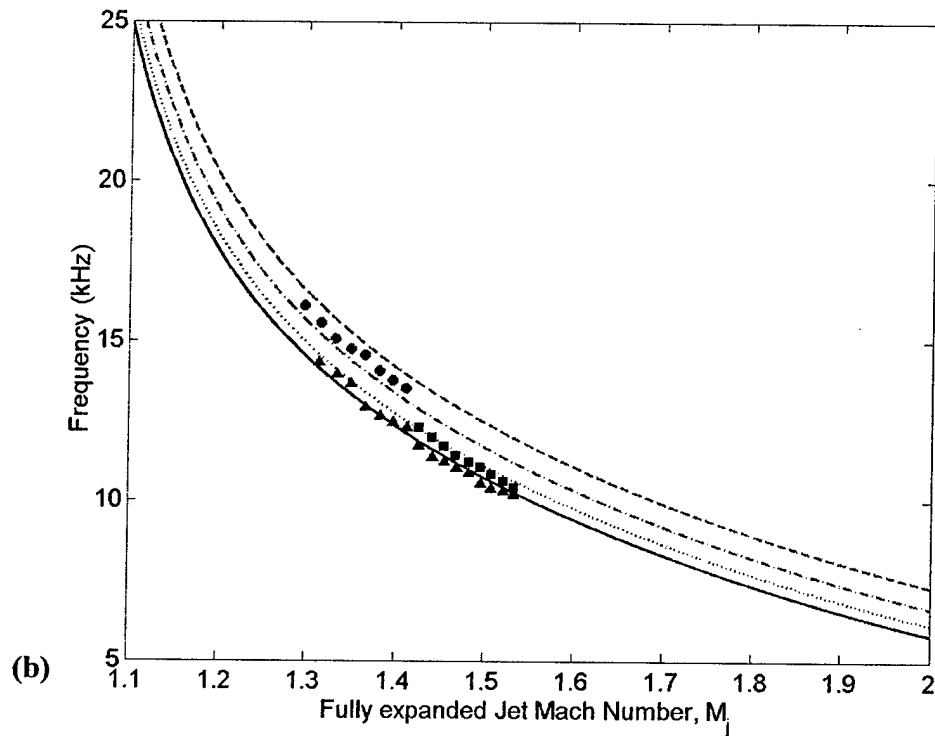
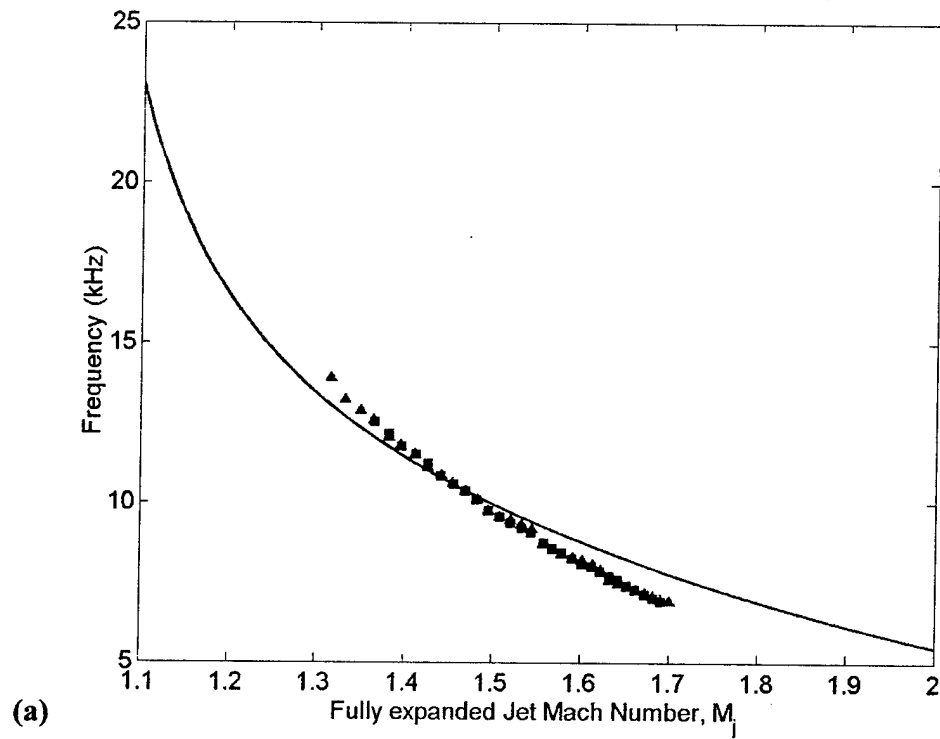


Figure 2.10. Screech frequency data compared to Tam's waveguide theory. (a). Screech frequency vs. fully expanded jet Mach Number for an aspect ratio 7 rectangular exit jet. (—) curve for lowest waveguide mode ($n = 1$), (\blacktriangle) single rectangular jet, (\blacksquare) twin rectangular jets (b). Screech frequency vs. fully expanded jet Mach number for the single beveled jets used in this study. Curves show waveguide modes (—) $n = 1$, (.....) $n = 2$, (- · - ·) $n = 3$, (- - -) $n = 4$. (\blacktriangle) single jet (\bullet) twin jets symmetrically coupled, (\blacksquare) twin jets antisymmetrically coupled.

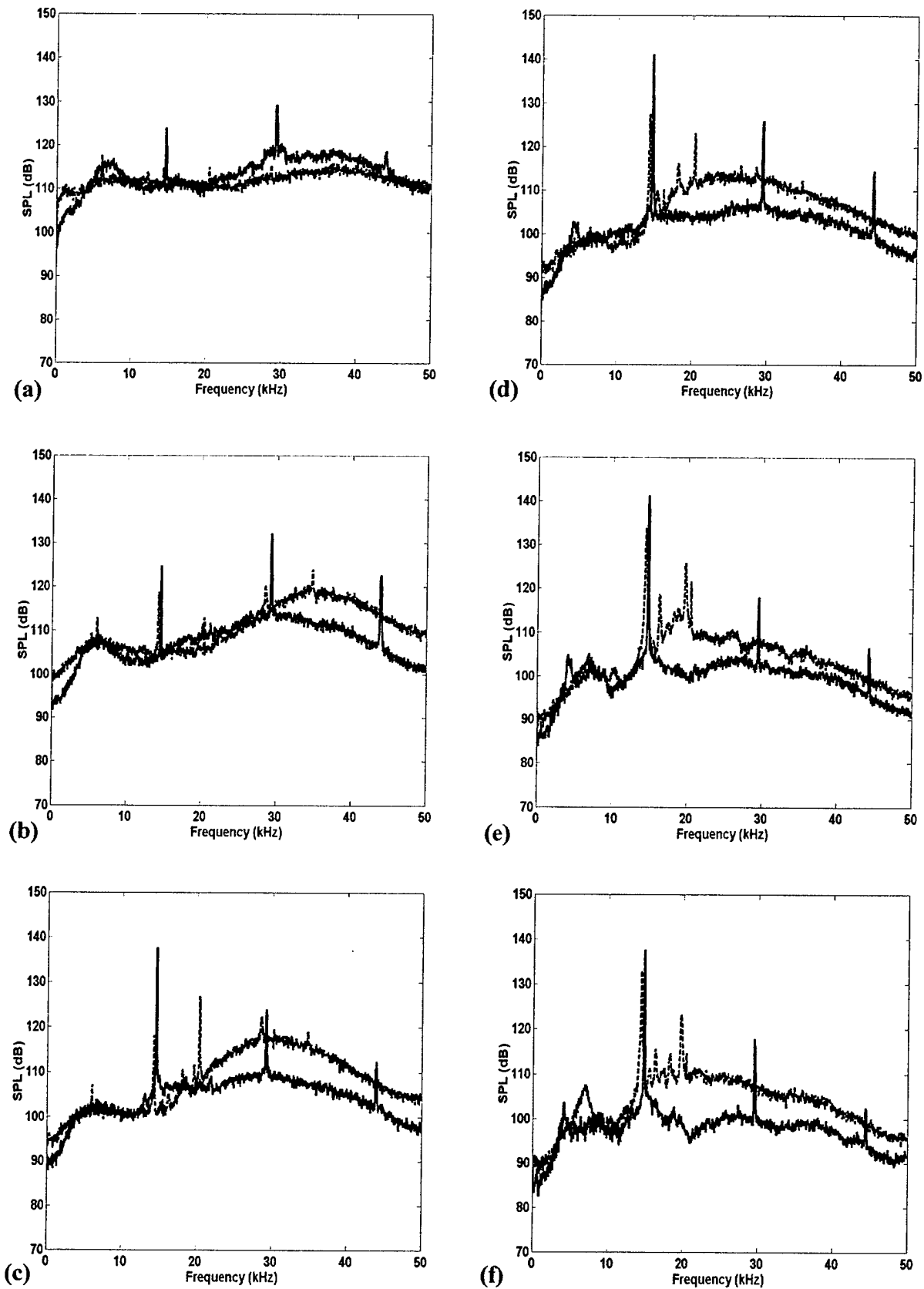


Figure 2.11. Comparison between twin jet spectra for various angles at an arc radius of $r/h = 22.5$ in the vertical plane (XZ plane depicted in Figure 3(a)) for the arrowhead and the V-shaped configurations at $M_j = 1.33$ at $s/h = 7.4$ (a) 50° (b) 70° (c) 90° (d) 110° (e) 130° (f) 150° . Solid curves (—) are for the 'V'-shaped configuration and the dashed curves (---) are for the Arrowhead configuration.

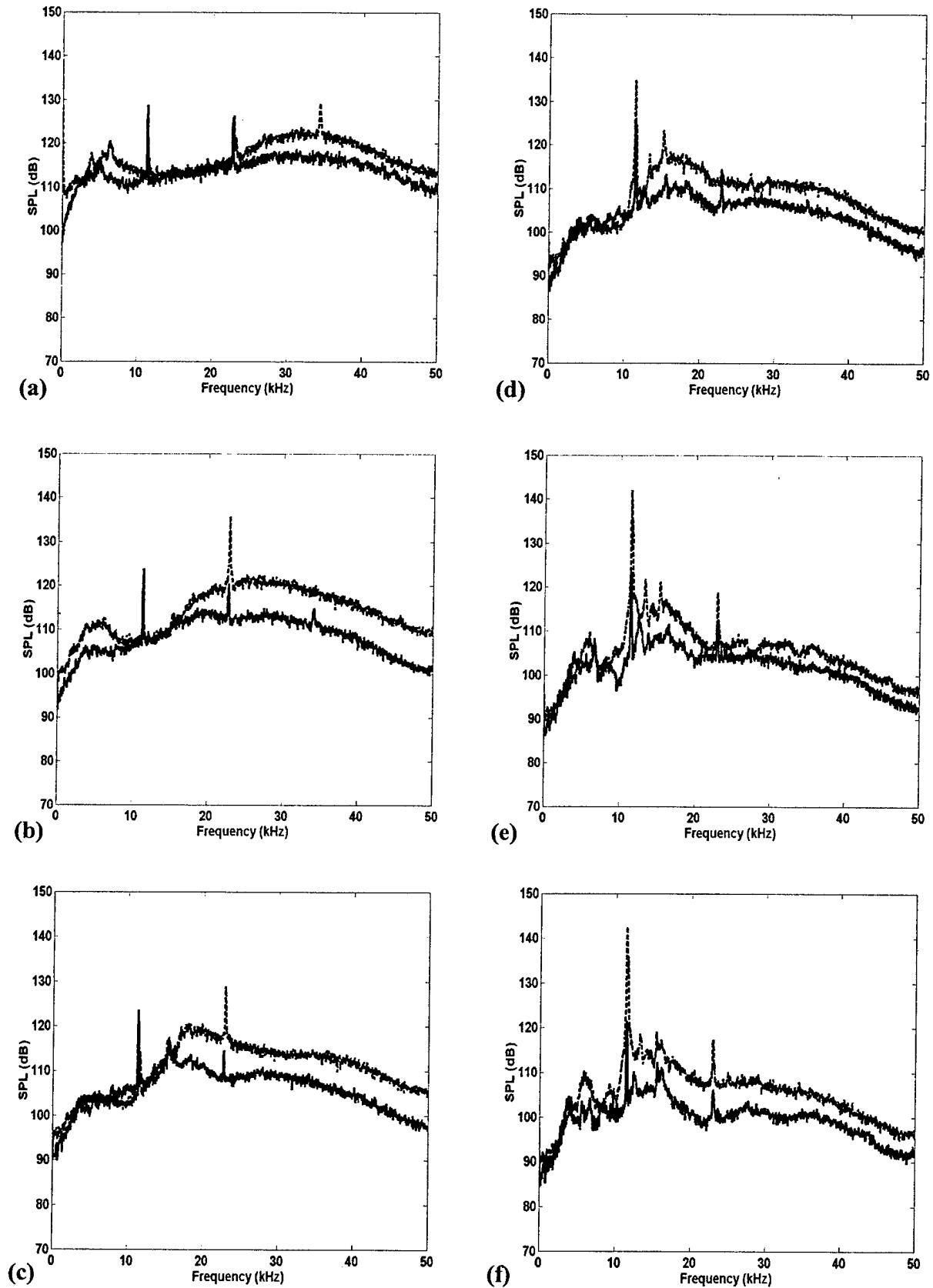


Figure 2.12. Comparison between twin jet spectra for various angles at an arc radius of $r/h = 22.5$ in the vertical plane (XZ plane depicted in Figure 3(a)) for the arrowhead and the V-shaped configurations at $M_j = 1.46$ at $s/h = 7.4$ (a) 50° (b) 70° (c) 90° (d) 110° (e) 130° (f) 150° . Solid curves (—) are for the 'V'-shaped configuration and dashed curves (---) are for the Arrowhead configuration.

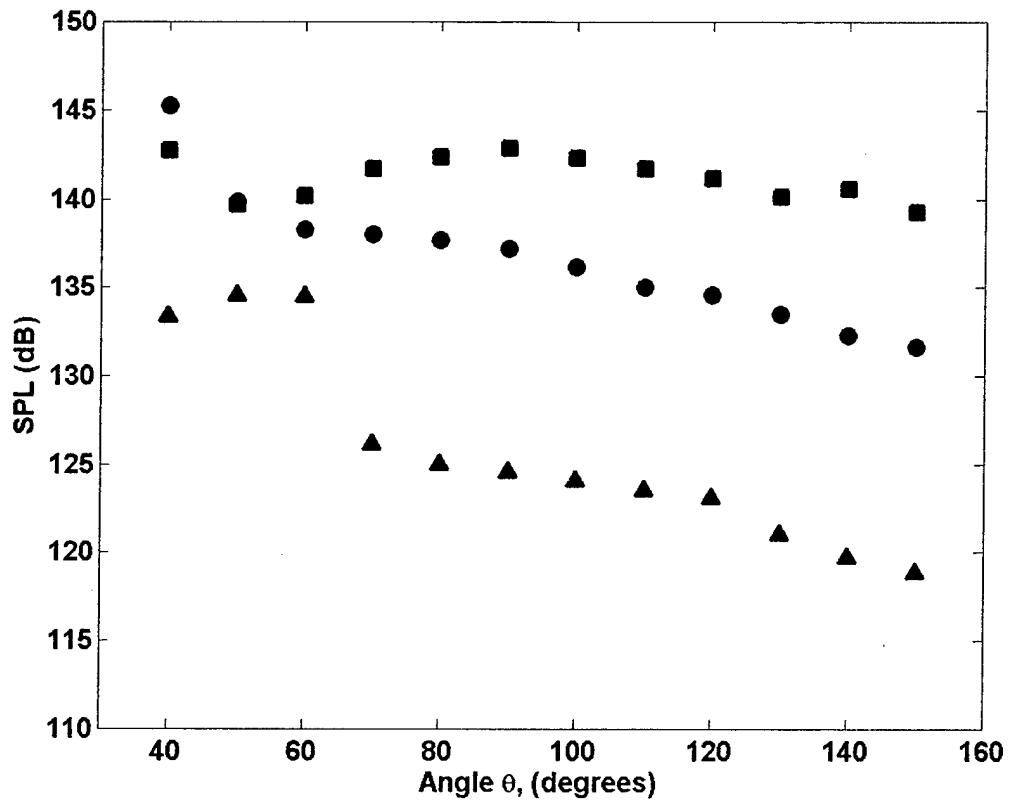


Figure 2.13. Broadband shock noise characteristics of single and twin jets at $M_j = 1.46$, $s/h = 7.4$, and arc radius of $r/h = 22.5$. (▲) Single jet, (●) twin jets in the V-shaped configuration, and (■) twin jets in the arrowhead configuration. θ is the angle measured with respect to the jet exit axis on the XZ plane depicted in Figure 3(a).

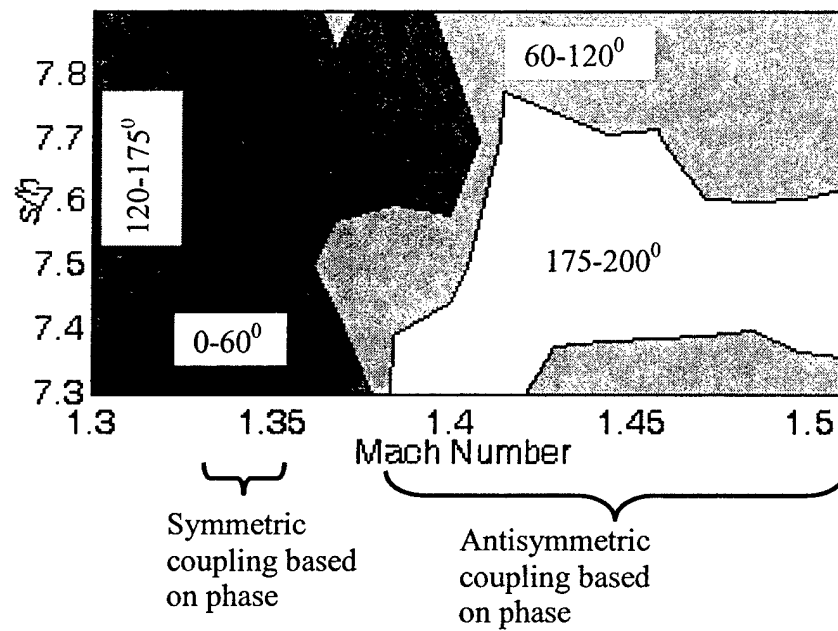


Figure 3.1. Contour map showing the coupling zones in the parametric space comprising Mach number and inter-nozzle spacing based on the phase difference at the screech tone. Phase difference shown in degrees.

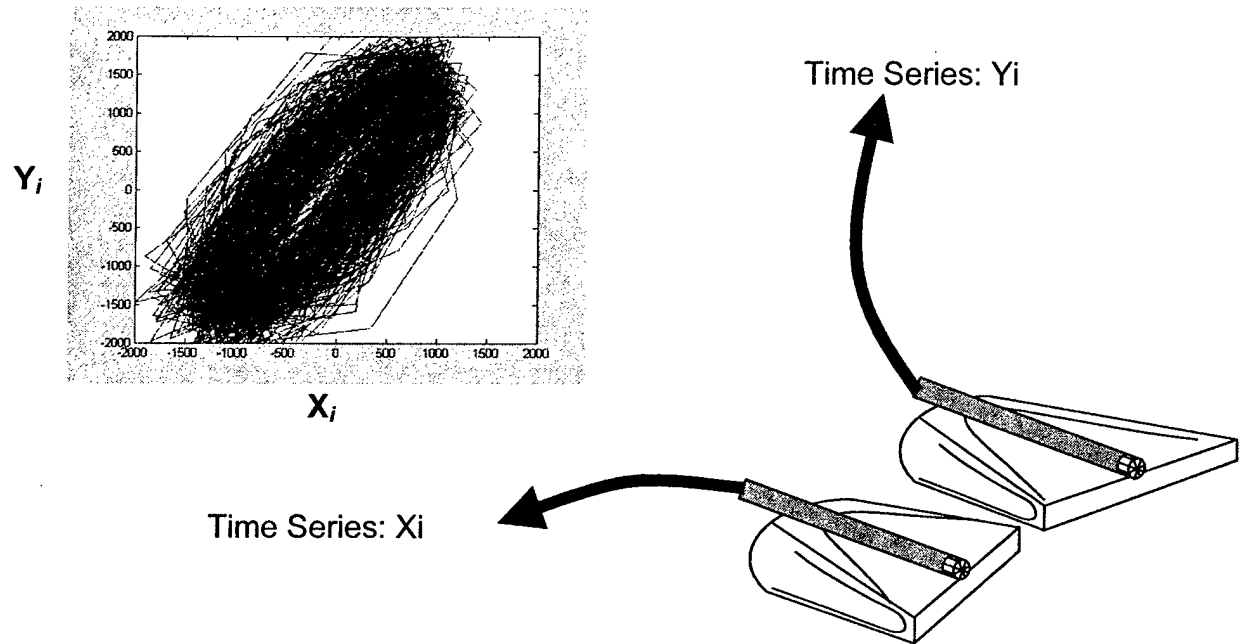


Figure 3.2. Schematic of phase plot

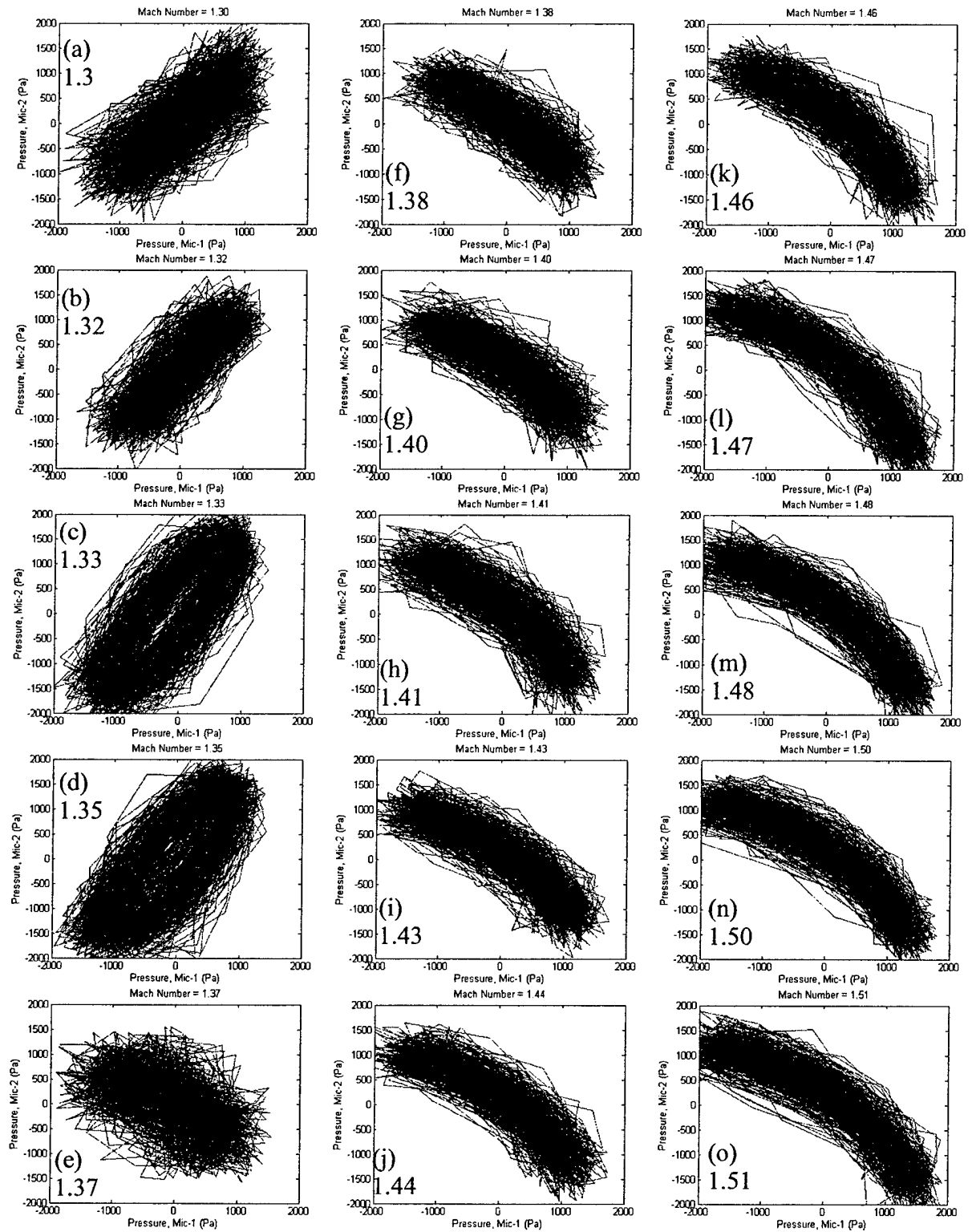


Figure 3.3. Phase plots between the two microphone signals at various Mach numbers, for the co-directed twin jet at $s/h = 7.3$. Mach numbers are shown in each plot.

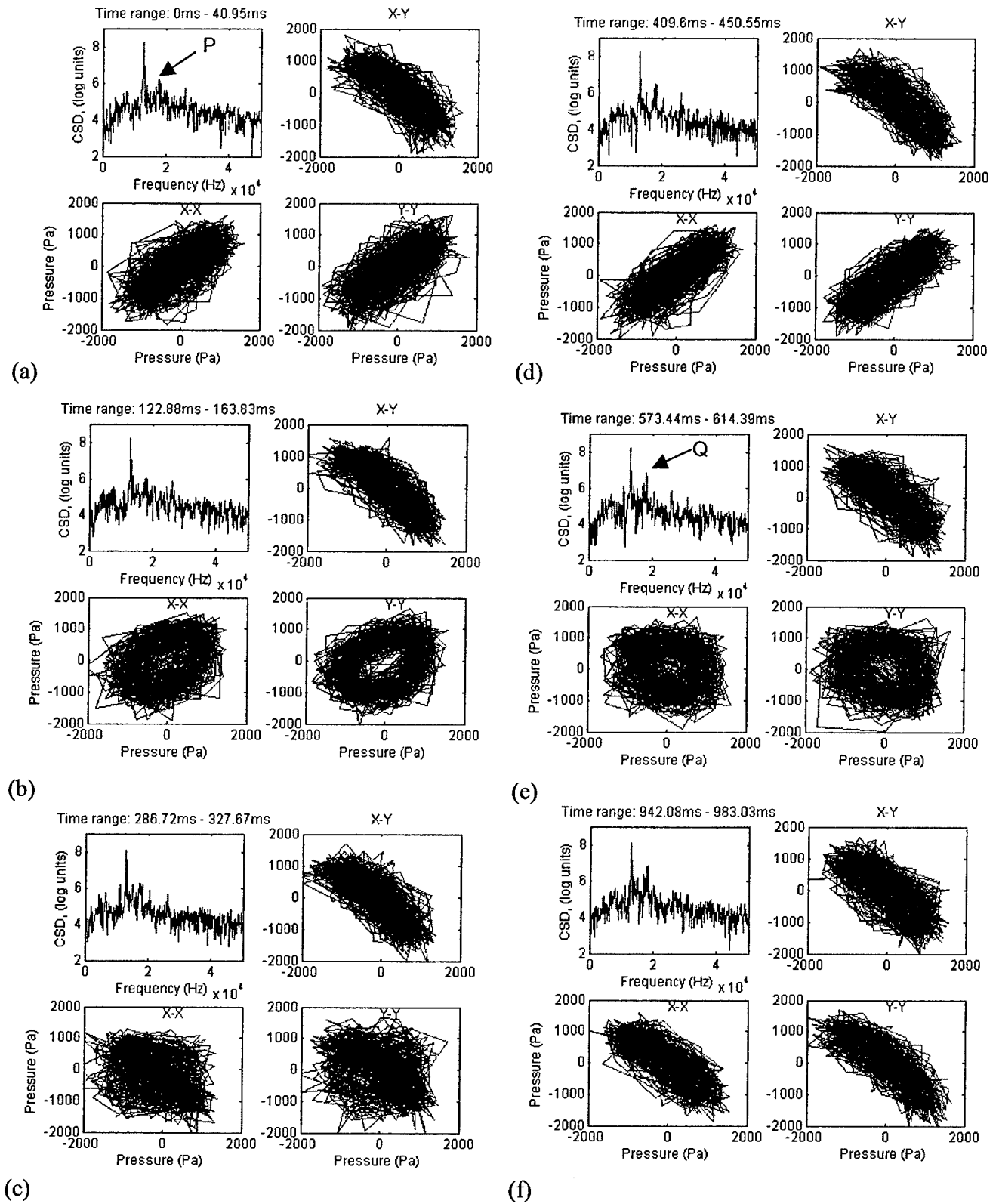
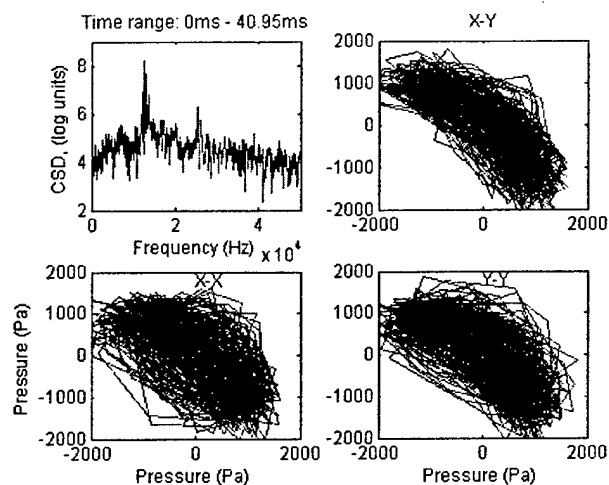
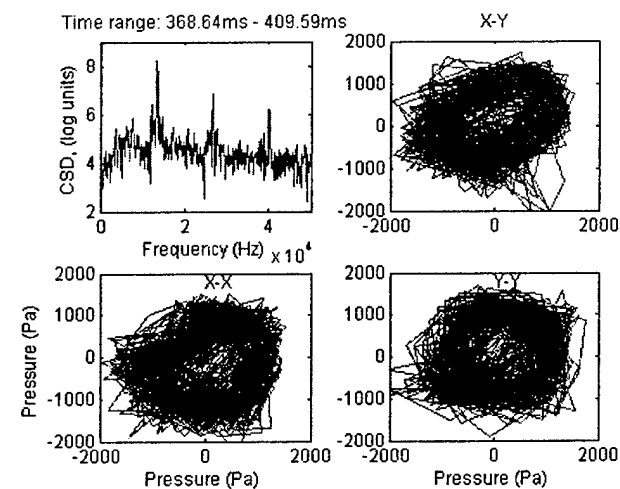


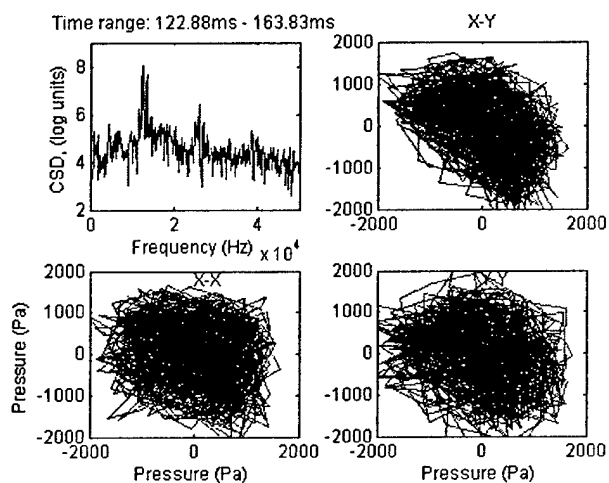
Figure 3.4. Cross power spectra, X-Y phase plots, and X-X phase plots, and Y-Y phase plots of microphone signals at Mach No. 1.38 for the co-directed twin jet configuration at $s/h = 7.3$. The time interval of the data is shown on top of the cross-spectrum.



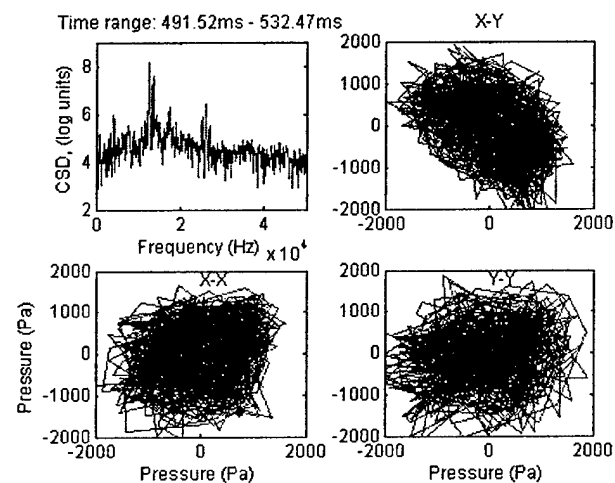
(a)



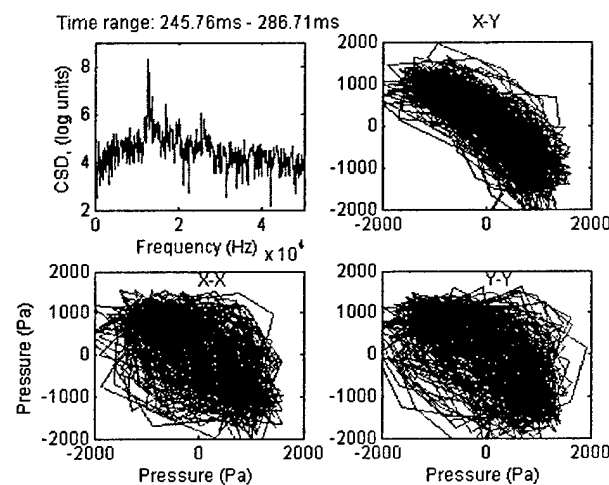
(d)



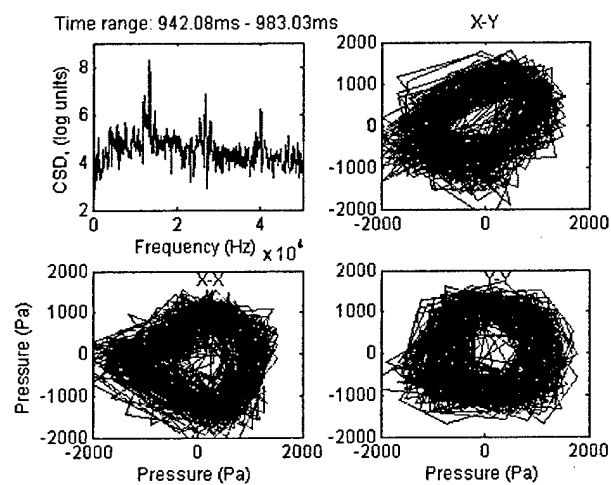
(b)



(e)



(c)



(f)

Figure 3.5. Cross power spectra, X-Y phase plots, and X-X phase plots, and Y-Y phase plots of microphone signals at Mach No. 1.4 for the co-directed twin jet configuration at $s/h = 7.3$. The time interval of the data is shown on top of the cross-spectrum.

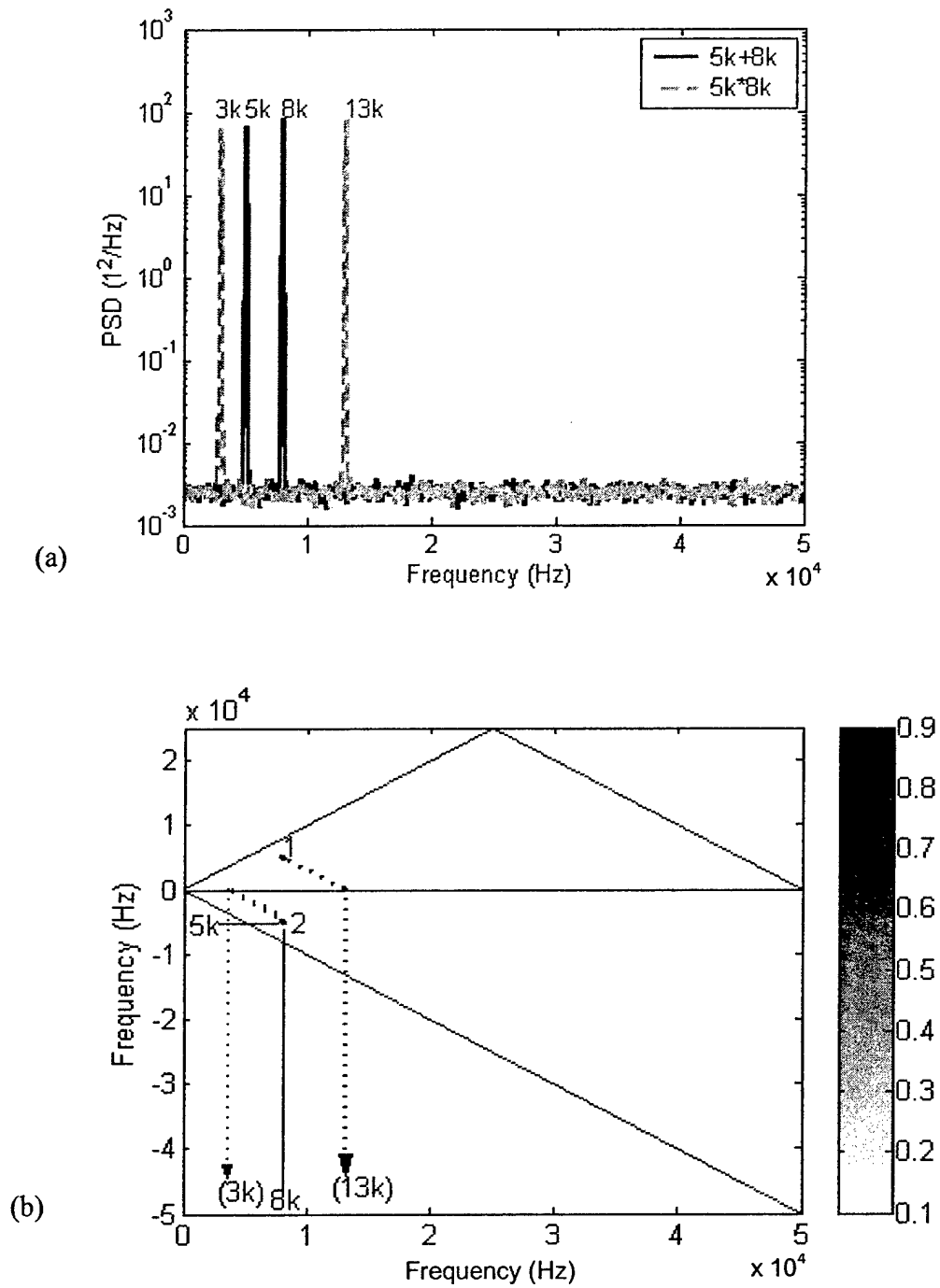


Figure 3.6. (a) Power Spectra of the test signals. (b) Cross-Bicoherence plot.

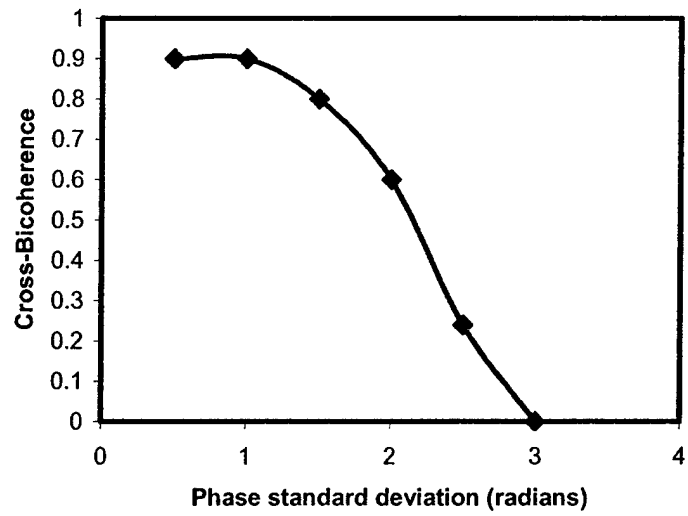


Figure 3.7. Sensitivity of cross-bicoherence to phase standard deviation between modulated test sinusoids.

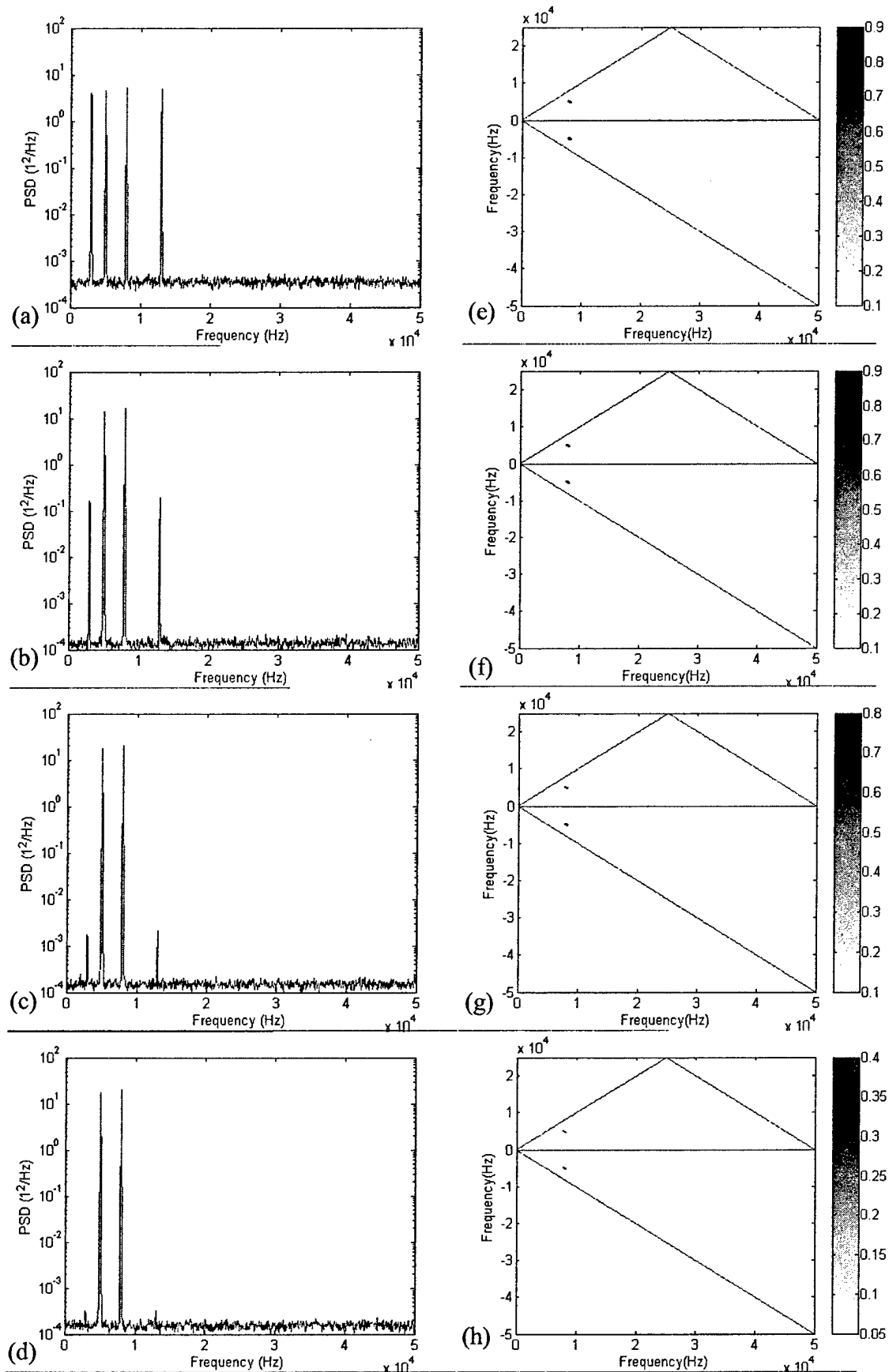


Figure 3.8. Comparison of sensitivity of second order and third order statistics to the relative magnitude of non-linear component: (a,e: 50%), (b,f: 10%), (c,g: 1%), (d,h: 0.5%)

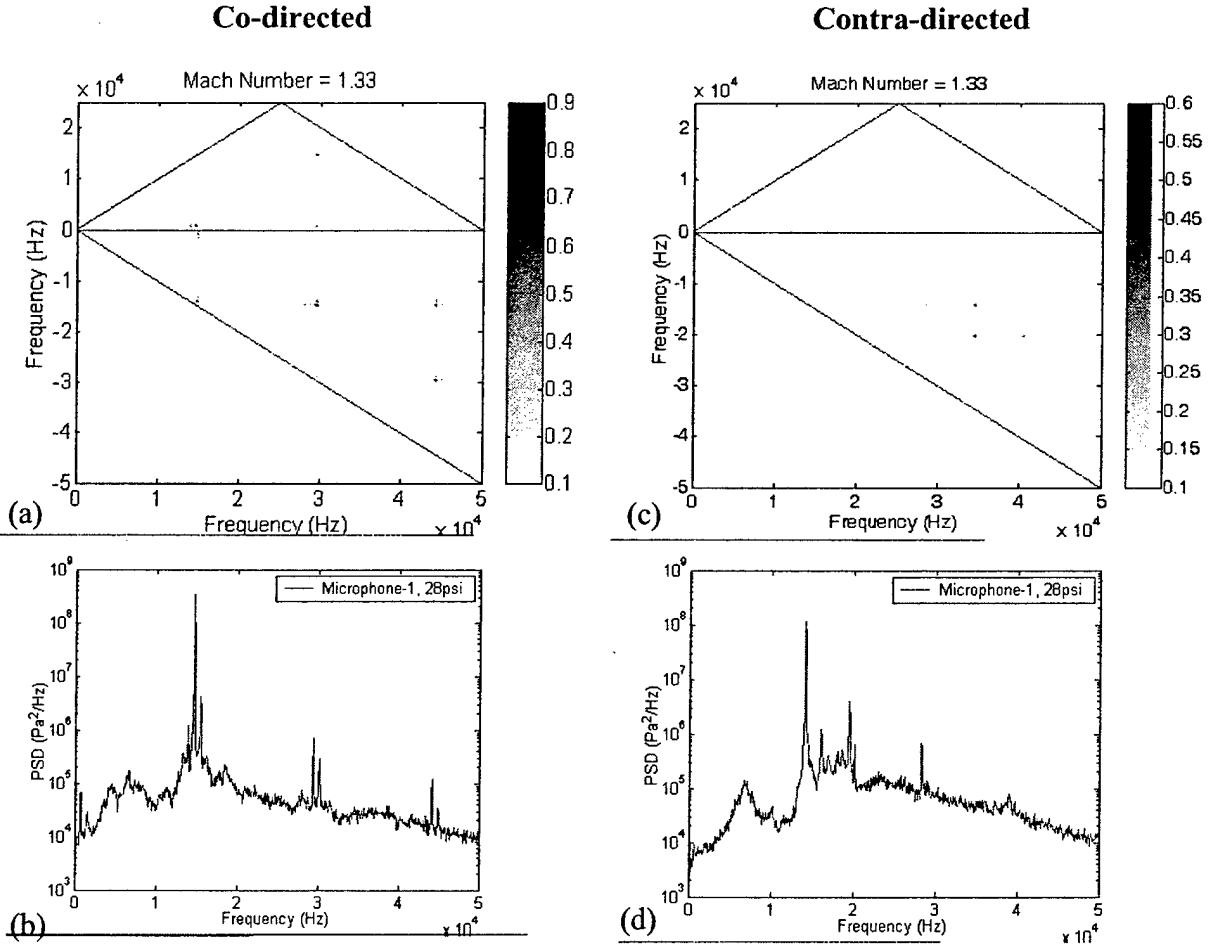


Figure 3.9. Cross-bicoherence and spectra of twin jets at $M_j = 1.33$, $s/h = 7.3$ for co-directed and contra-directed configurations. (a) Cross-bicoherence spectrum for co-directed, (b) Power spectrum for co-directed, (c) Cross-bicoherence spectrum for contra-directed, (d) Power spectrum for contra-directed.

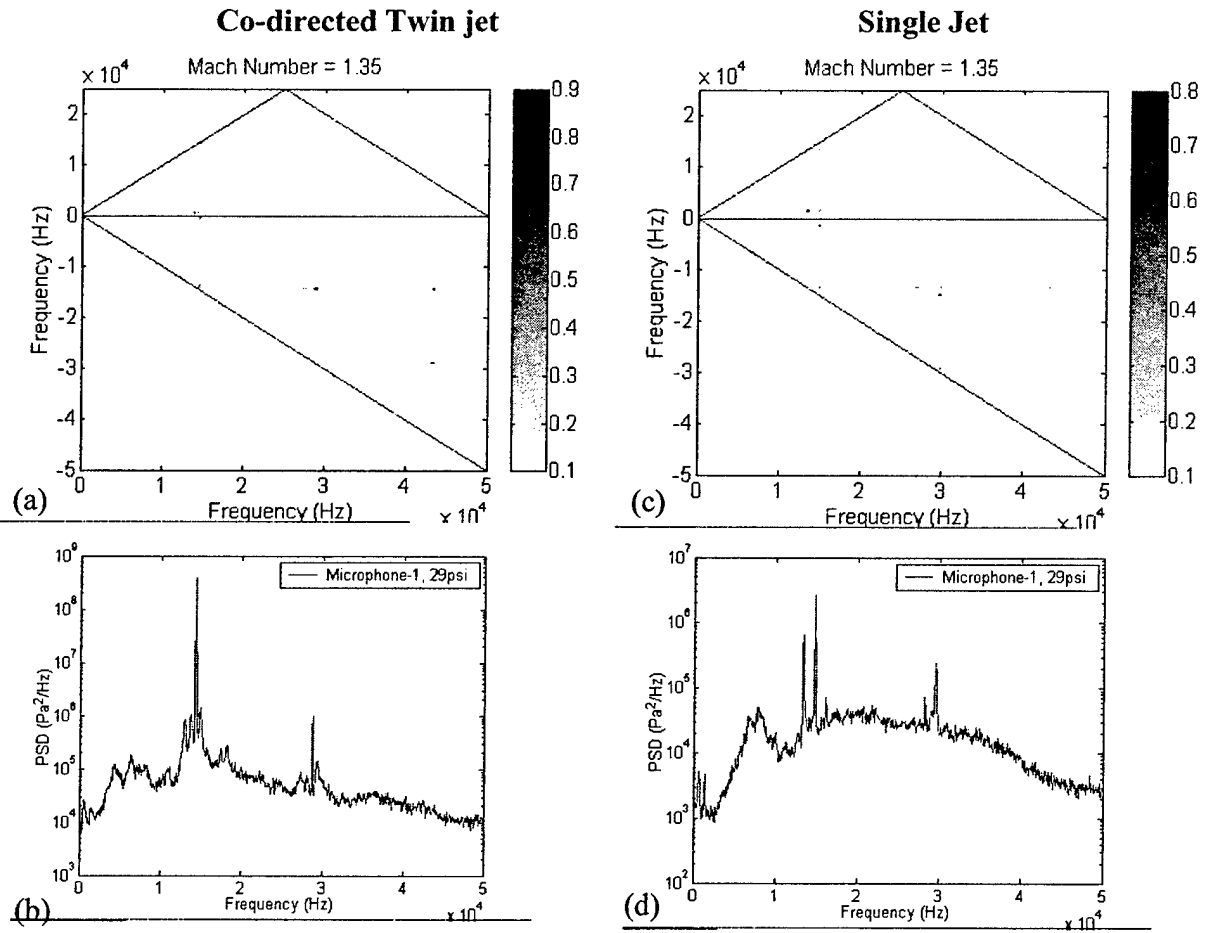


Figure 3.10. Comparison of cross-bicoherence spectra and power spectra of co-directed twin jet and single jet. $M_j = 1.35$, Twin jet spacing: $s/h = 7.3$

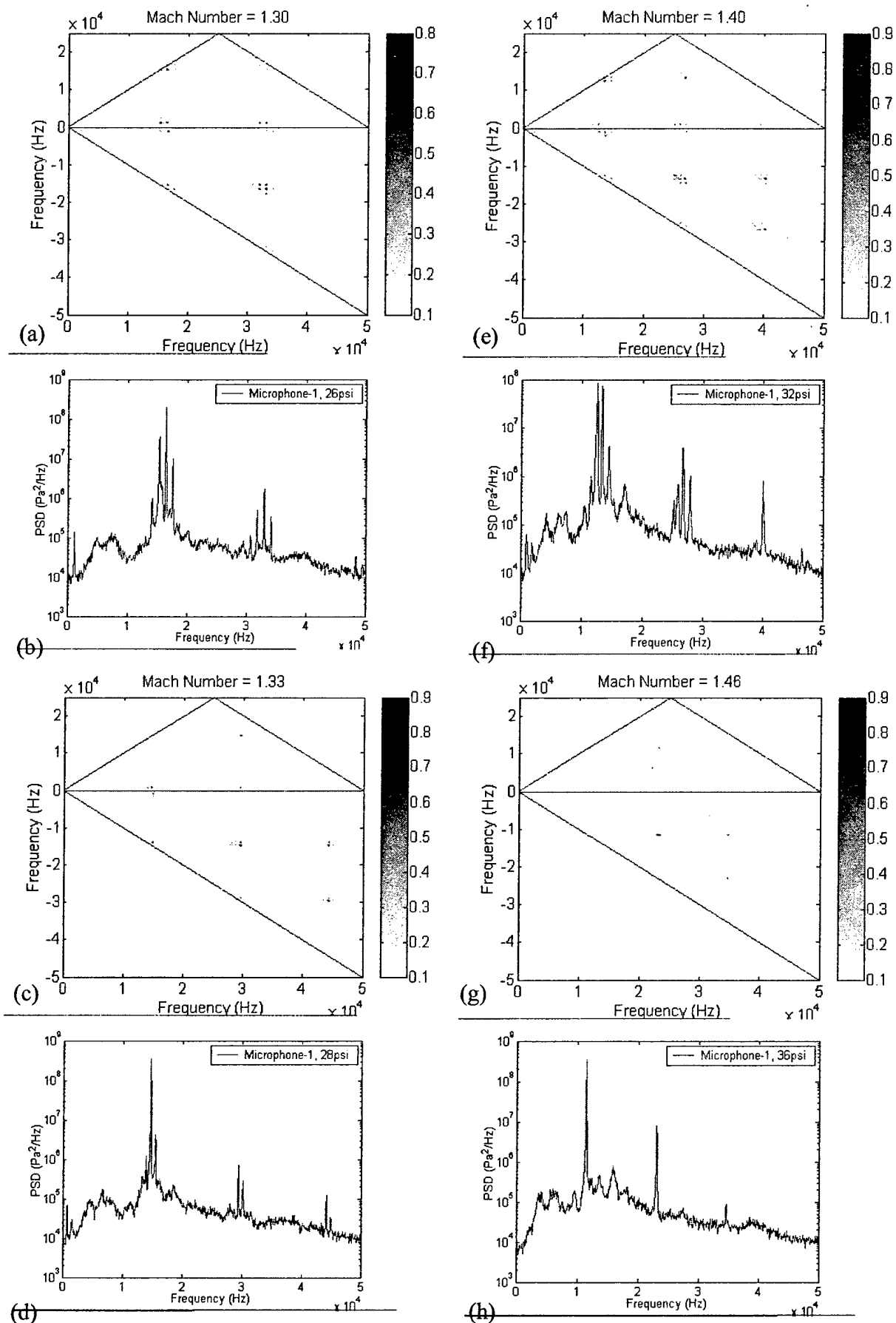


Figure 3.11. Cross-bicoherence and linear spectra of co-directed twin jets at $s/h = 7.3$, at various Mach numbers; (a, b: 1.3), (c, d: 1.33), (e, f: 1.40), and (g, h: 1.46).

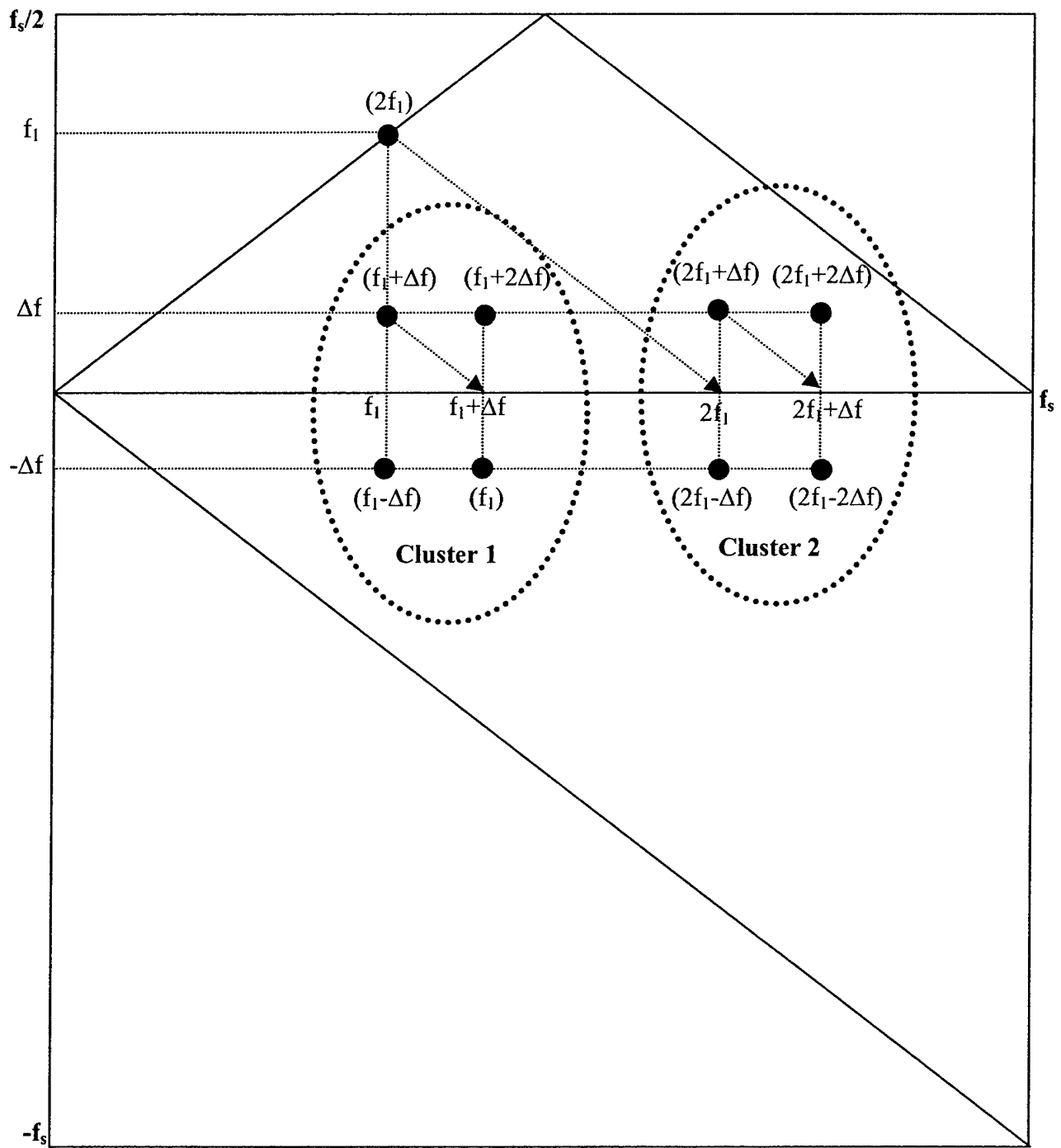


Figure 3.12. Depiction of the clustering phenomenon. Frequencies within parentheses denote resultant frequencies, and those without parentheses denote participating frequencies. The dotted ellipses are shown to indicate clusters.

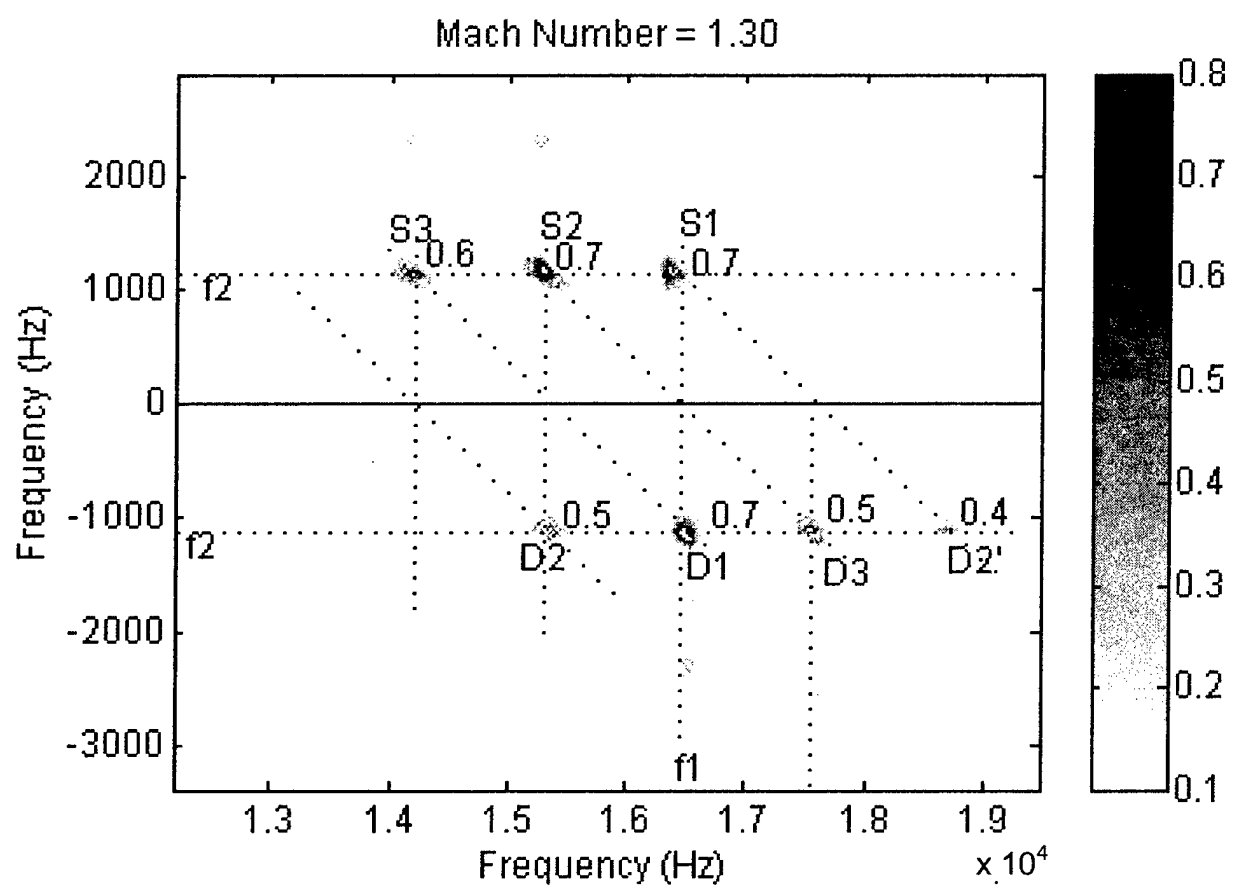


Figure 3.13. Close-up view of a cluster illustrating the sequence of interactions building it.

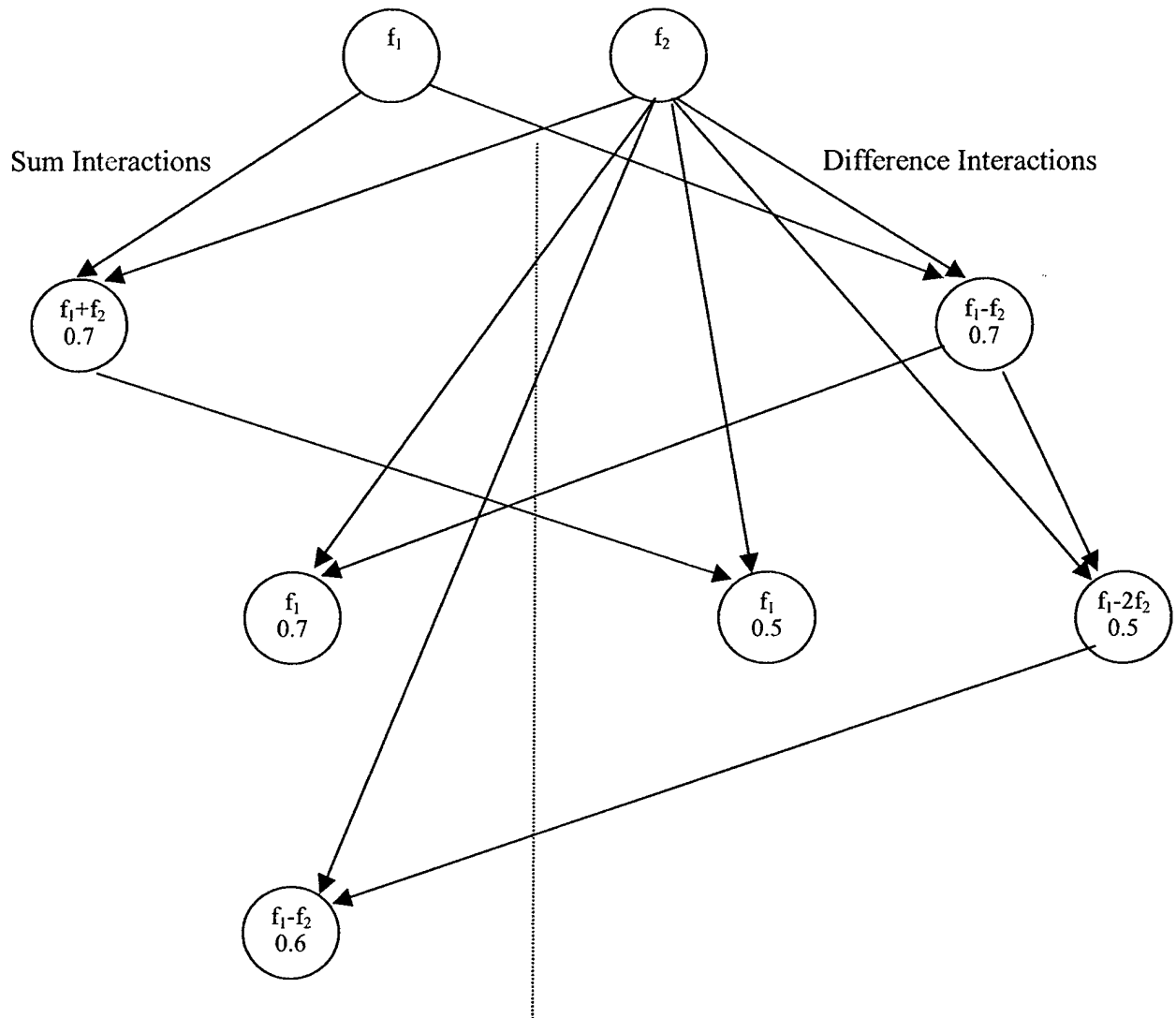


Figure 3.14. : Details of the evolution of non-linear interactions shown in Figure 3.13(b). Left hand side of the illustration shows sum interactions while the right side shows difference interactions. The modes resulting from the interactions are shown inside the circles, and the cross-bicoherence values are mentioned below them.

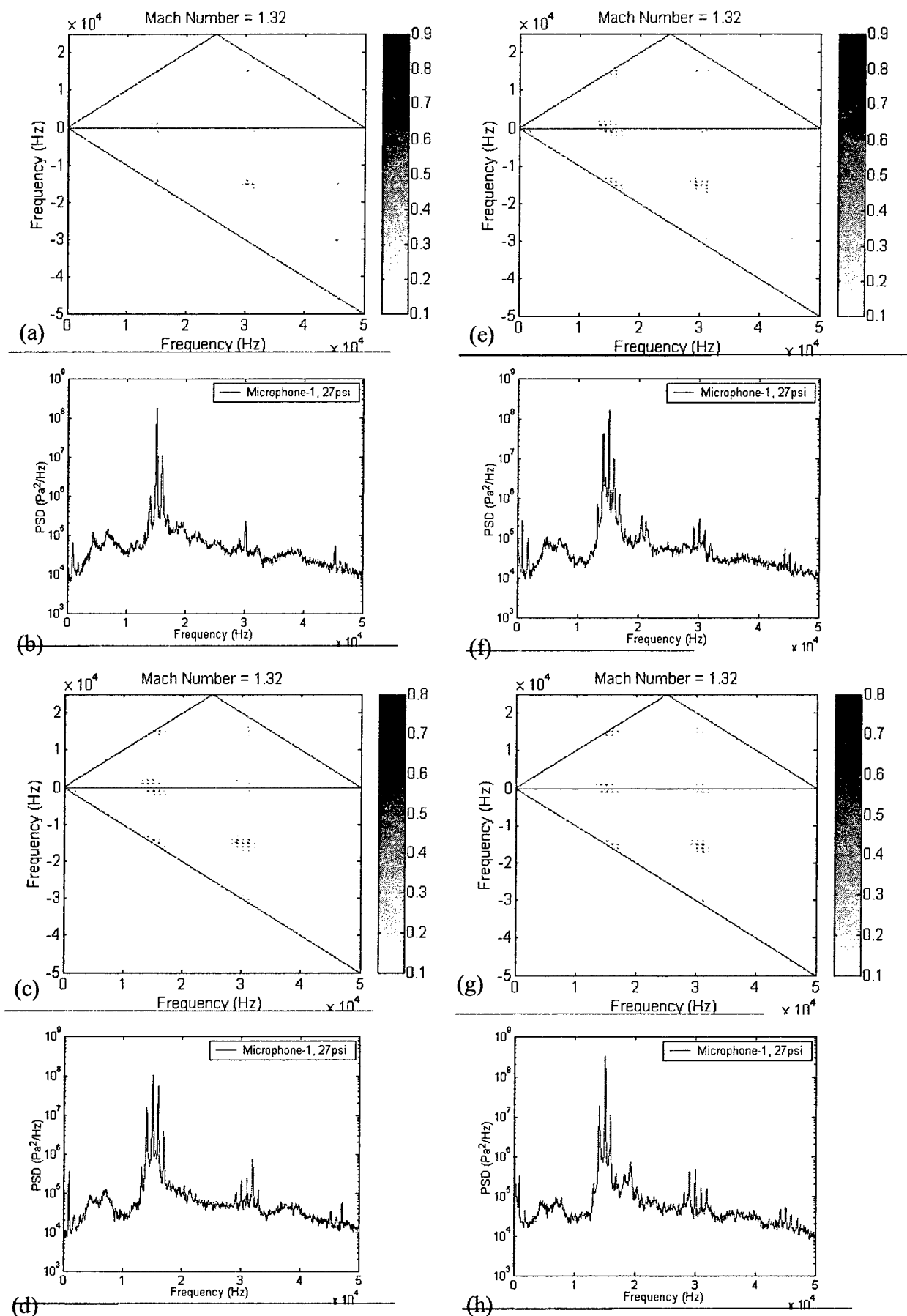


Figure 3.15. Cross-bicoherence and spectra of co-directed twin jets at $M_j = 1.32$, for various internozzle spacings. (a,b): $s/h = 7.3$, (c,d): $s/h = 7.5$, (e,f): $s/h = 7.7$, (g,h): $s/h = 7.9$

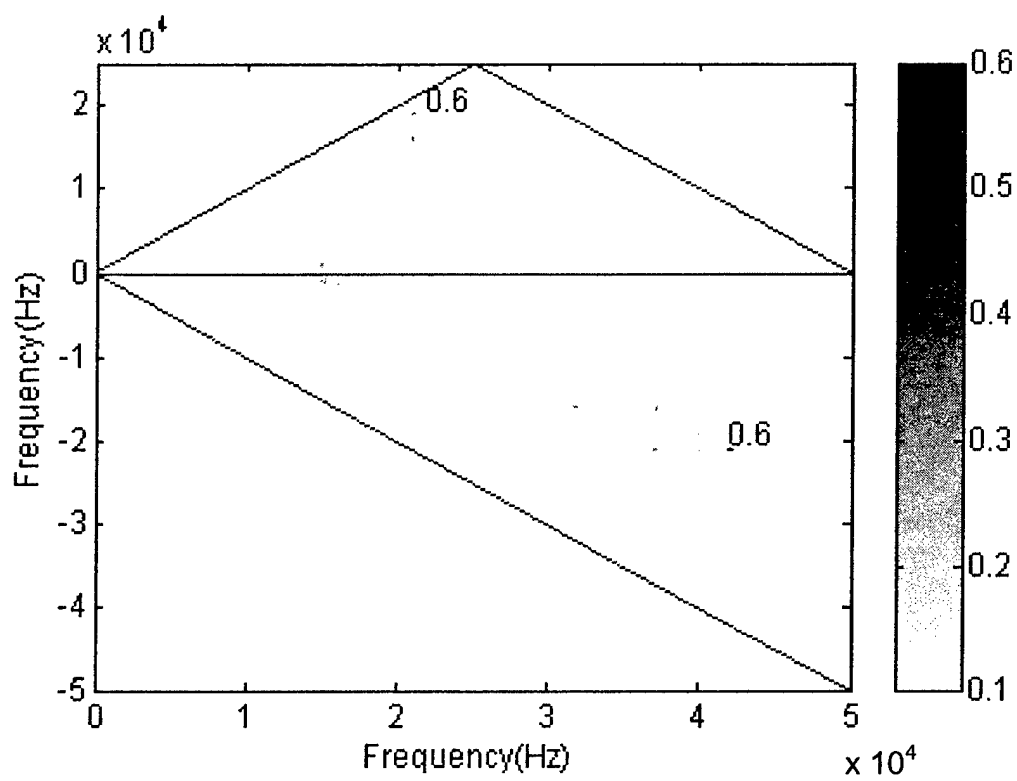


Figure 3.16. Cross-bicoherence spectrum of co-directed twin jets at $M_j = 1.32$, at internozzle spacing $s/h = 11.2$. Except those marked, all other interactions had a coherency of 0.3 or less.

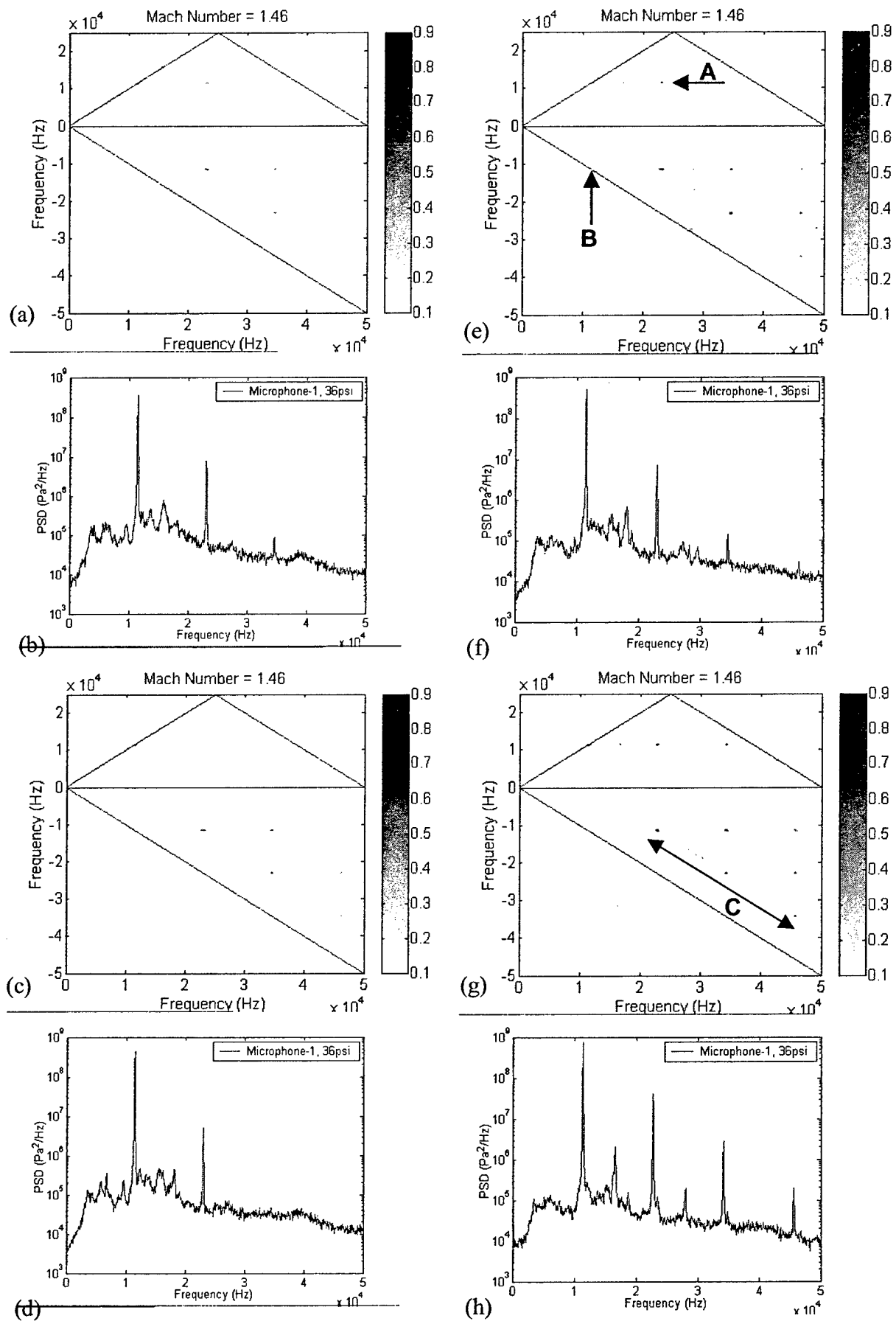


Figure 3.17. Cross-bicoherence and spectra of co-directed twin jets at $M_j = 1.46$, for various internozzle spacings.
(a,b): $s/h = 7.3$, (c,d): $s/h = 7.5$, (e,f): $s/h = 7.7$, (g,h): $s/h = 7.9$

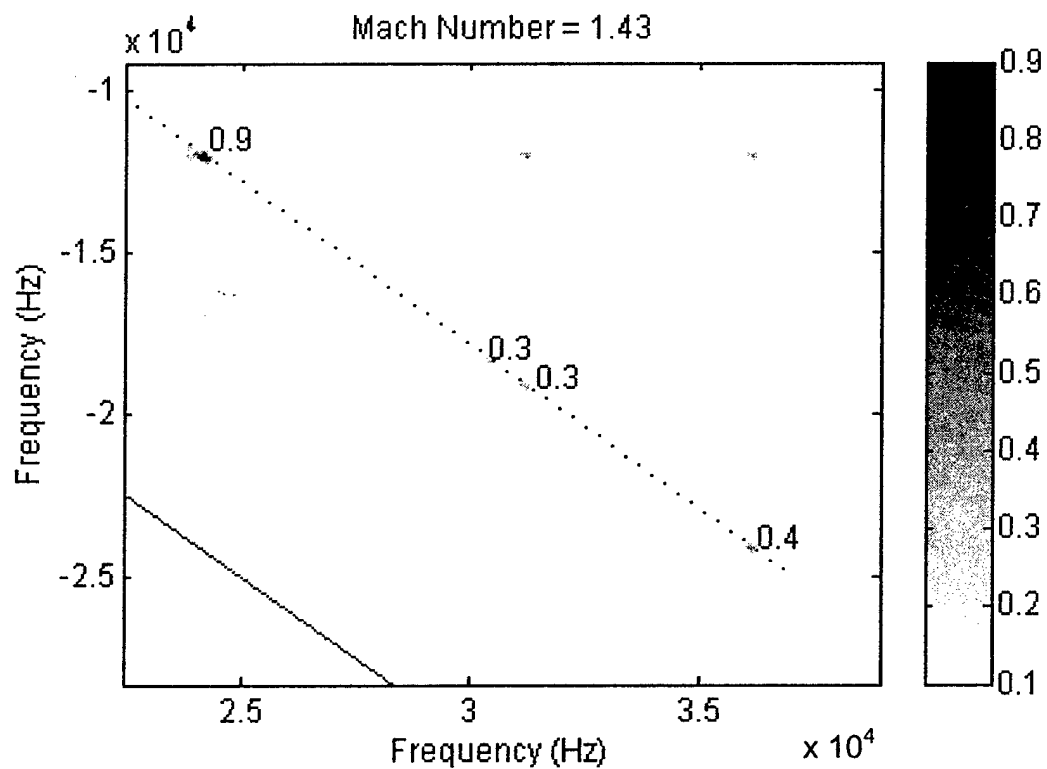
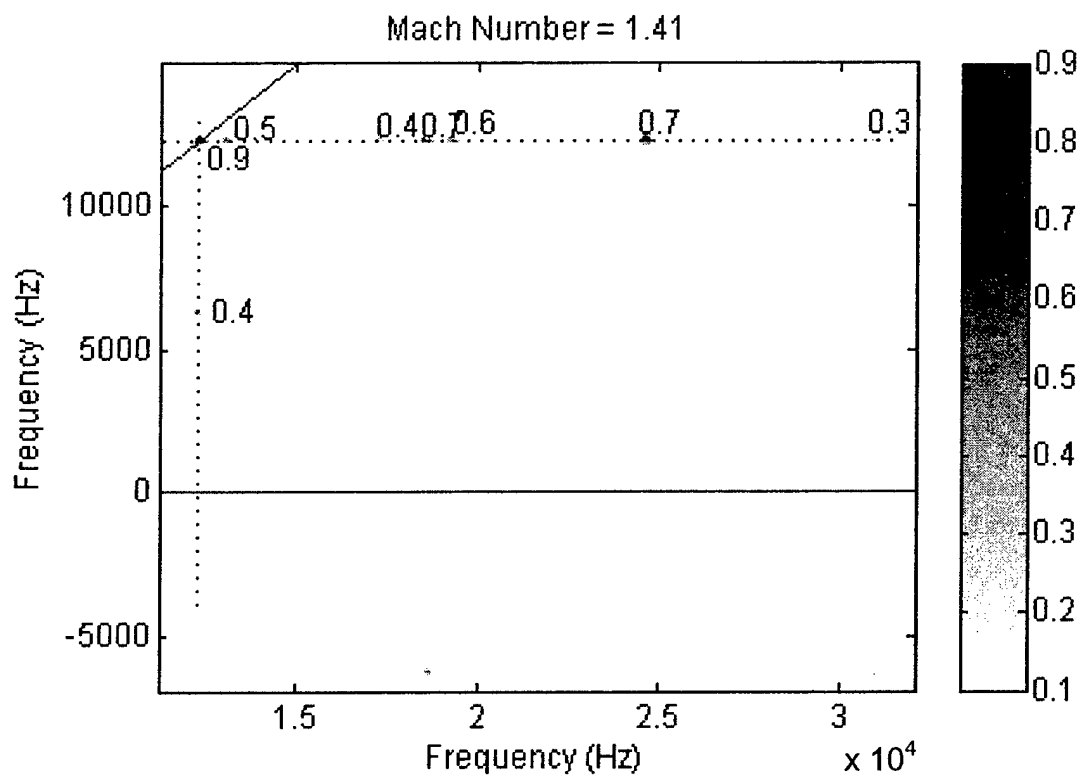


Figure 3.18. Close-up views of rectilinearly aligned interactions. The dotted line in (a) denotes the most active participating frequency, and the dotted line in (b) denotes the most desired resultant frequency.

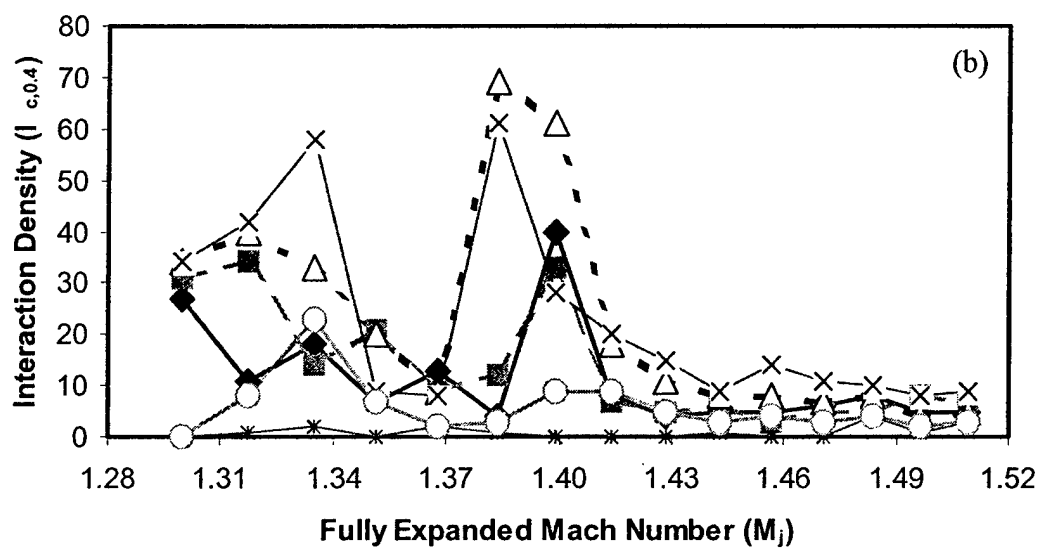
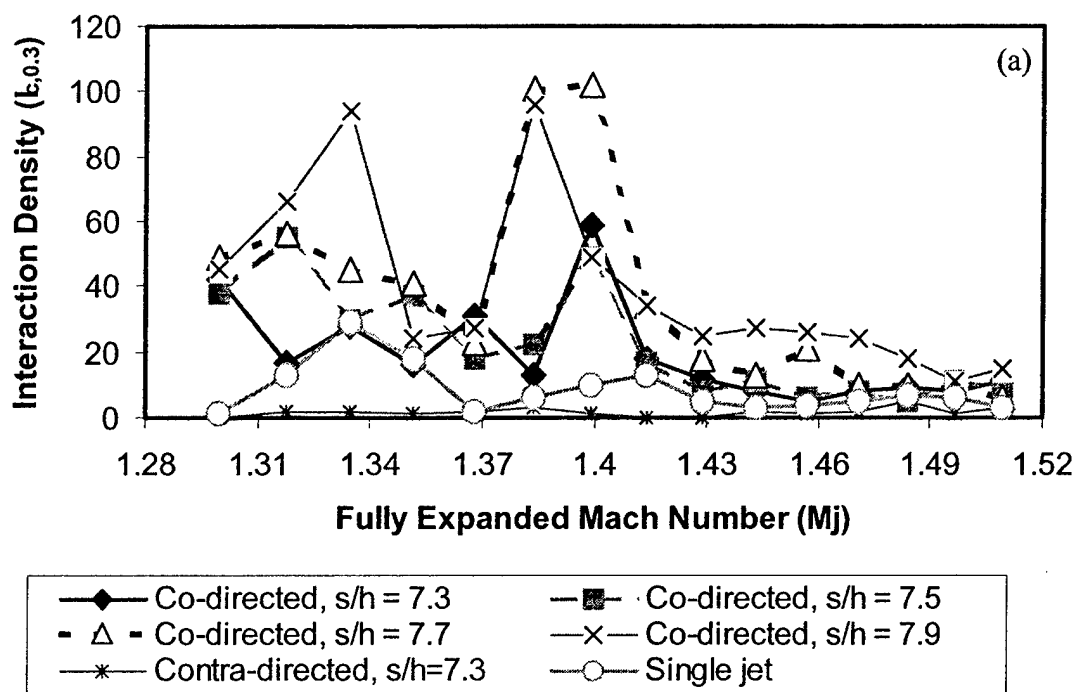


Figure 3.19. Interaction density variation with Mach number. (a) Threshold 0.3. (b) Threshold 0.4.

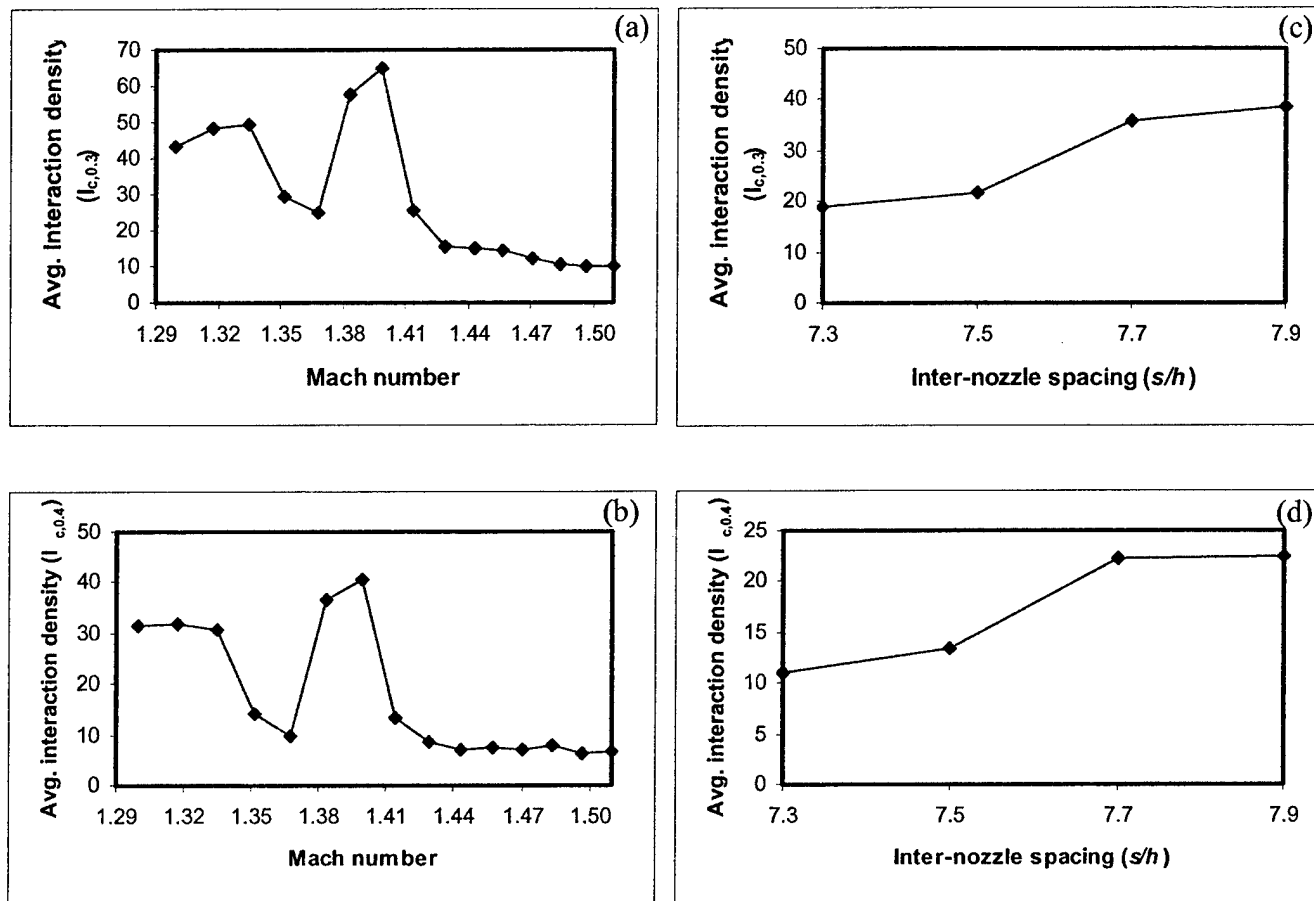


Figure 3.20. Variation of average interaction density with Mach number and inter-nozzle spacing. (a,c) Cross-bicoherence Threshold 0.3, (b,d) Threshold 0.4.

BIBLIOGRAPHY

- [1] P. Panickar, "Coupling of twin jets from nozzles having single beveled exits," Masters' Thesis, Illinois Institute of Technology (2003).
- [2] P. Panickar, K. Srinivasan, G. Raman, "Aeroacoustic features of coupled twin jets with spanwise oblique shock-cells," accepted for publication in the Journal of Sound and Vibration.
- [3] K. Srinivasan, P. Panickar, G. Raman, B-H. Kim, D.R. Williams, "Study of supersonic twin jet coupling using higher order spectral analysis," American Institute of Aeronautics and Astronautics Paper 2003-3871 (2003).
- [4] P. Panickar, K. Srinivasan, G. Raman, "Acoustic coupling of twin jets from single-beveled nozzles," American Institute of Aeronautics and Astronautics Paper 2004-0006 (2004).
- [5] A. Powell, "On the mechanism of choked jet noise," Proceedings of the Physical Society of London B66 (1953) 1039-1056.
- [6] G. Raman, "Supersonic jet screech: Half-century from Powell to the present," Journal of Sound and Vibration 225 (1999) 543-571.
- [7] D.E. Berndt, "Dynamic pressure fluctuations in the inter-nozzle region of a twin-jet nacelle, Society of Automotive Engineers," Warrendale, PA Society of Automotive Engineers Technical Paper Series 841540 (1984).
- [8] J.M. Seiner, J.C. Manning, M.K. Ponton, "Dynamic pressure loads associated with twin supersonic plume resonance," American Institute of Aeronautics and Astronautics Journal 26 (1988) 954-960.
- [9] C.K.W. Tam, J.M. Seiner, "Analysis of twin supersonic plume resonance," American Institute of Aeronautics and Astronautics Paper 87-2695 (1987).
- [10] P.J. Morris, "Instability waves in twin supersonic jets," Journal of Fluid Mechanics 220 (1990) 293-307.
- [11] R.W. Wlezien, "Nozzle geometry effects on supersonic jet interaction," American Institute of Aeronautics and Astronautics Paper 87-2694 (1987).
- [12] L. Shaw, "Twin-jet screech suppression," Journal of Aircraft 27 No.8 (1990) 708-715.

- [13] J.S. Lilley, "The design and optimization of propulsion systems employing scarfed nozzles," *Journal of Spacecraft and Rockets* 23 (1986) 597.
- [14] R.W. Wlezien, V. Kibens, "Influence of nozzle asymmetry on supersonic jets," *American Institute of Aeronautics and Astronautics Journal* 26 (1988) p.27.
- [15] E.J. Rice, G. Raman, "Mixing noise reduction for rectangular supersonic jets by nozzle shaping and induced screech mixing," *American Institute of Aeronautics and Astronautics Paper* 93-4322 (1993); also *National Aeronautics and Space Administration Technical Memorandum* 106364 (1993).
- [16] E.J. Rice, G. Raman, "Supersonic jets from beveled rectangular nozzles," *American Society of Mechanical Engineers Paper No.* 93-WA/NCA-26 (1993); also *National Aeronautics and Space Administration Technical Memorandum* 106403 (1993).
- [17] E.J. Rice, "Jet mixer noise suppressor using acoustic feedback," *United States Patents* 5,325,661 and 5,392,597 (1995).
- [18] J.-H. Kim, M. Samimy, "On mixing enhancement via nozzle trailing edge modifications in high speed jets," *American Institute of Aeronautics and Astronautics Journal* 38 No.5 (2000) 935-937.
- [19] C. Kerechanin, M. Samimy, J.-H. Kim, "Effects of nozzle trailing edges on acoustic field of a supersonic rectangular jet," *American Institute of Aeronautics and Astronautics Journal* 39 No.6 (2001) 1065-1070.
- [20] G. Raman, R.R. Taghavi, "Resonant interaction of a linear array of supersonic rectangular jets: an experimental study," *Journal of Fluid Mechanics* 309 (1996) 93-111.
- [21] G. Raman, R. Taghavi, "Coupling of twin rectangular supersonic jets," *Journal of Fluid Mechanics*, 354 (1998) 123-146.
- [22] R.R. Taghavi, G. Raman, "Interaction of twin rectangular supersonic jets in various configurations," *American Society of Mechanical Engineers Fluids Engineering Division Summer Meeting*, Washington D.C. FEDSM98-5243 (1998).
- [23] G. Raman, "Coupling of twin supersonic jets of complex geometry," *Journal of Aircraft* 36 No. 5 (1999) 743-749.
- [24] G. Raman, "Screech tones from rectangular nozzles with spanwise oblique shock-cell structures," *Journal of Fluid Mechanics* 330 (1997) 141.

- [25] G. Raman, "Shock-induced flow resonance in supersonic jets of complex geometry," *Physics of Fluids* 11 No.3 (1999) 692-709.
- [26] F.O. Thomas, H.C. Chu, "" (1991)
- [27] F.O. Thomas, H.C. Chu, "Experiments on the nonlinear stages of excited and natural planar jet shear layer transition," *Experiments in Fluids* 14 (1993) 451-467.
- [28] F.O. Thomas, H.C. Chu, "Nonlinear Wave Coupling and Subharmonic Resonance in Planar Jet Shear Layer Transition", *Physics of Fluids (A)* 5 No.3 (1993) 630-646.
- [29] S.H. Walker, F.O. Thomas, "Experiments Characterizing Nonlinear Shear Layer Dynamics in a Supersonic Rectangular Jet Undergoing Screech," *Physics of Fluids* 9 2562-2579.
- [30] F.O. Thomas, "Applications of Advanced Data Analysis Techniques to High Speed Jets", In "High Speed Jet Flows", Editors, Morris, P.J., McLaughlin, D.K., and Raman, G., Taylor and Francis, NY, 2003 (in press).
- [31] S.H. Walker, "" (1997)
- [32] D.E. Zilz, R.W. Wlezien, The sensitivity of near-field acoustics to the orientation of twin two-dimensional supersonic nozzles, *American Institute of Aeronautics and Astronautics Paper* 90-2149 (1990).
- [33] C.K.W. Tam, H. Shen, G. Raman, Screech tones of supersonic jets from beveled rectangular nozzles, *American Institute of Aeronautics and Astronautics Paper* 97-0143 (1997).
- [34] C.K.W. Tam, N.N. Reddy, Prediction method for broadband shock associated noise from supersonic rectangular noise, *Journal of Aircraft* 33 No.2 (1996) 298-303.
- [35] C.K.W. Tam, The shock-cell structure and screech tone frequencies of rectangular and non-axisymmetric supersonic jets, *Journal of Sound and Vibration*, 121 (1988) 135-147.
- [36] G. Raman, E.J. Rice, "Instability Modes Excited by Natural Screech Tones in a Supersonic Rectangular Jet," *Physics of Fluids* 6 No. 12 (1994) 3999-4008.